Superfluid Effective Field Theory: From Theory to Numerics

Júlio Oliveira
Mestrado em Física
Departamento de Física e Astronomia
2023

Orientador
João Manuel Parente Viana Lopes, Professor Auxiliar,
Faculdade de Ciências da Universidade do Porto

Coorientador
João Penedones, Associate Professor,
École polytechnique fédérale de Lausanne

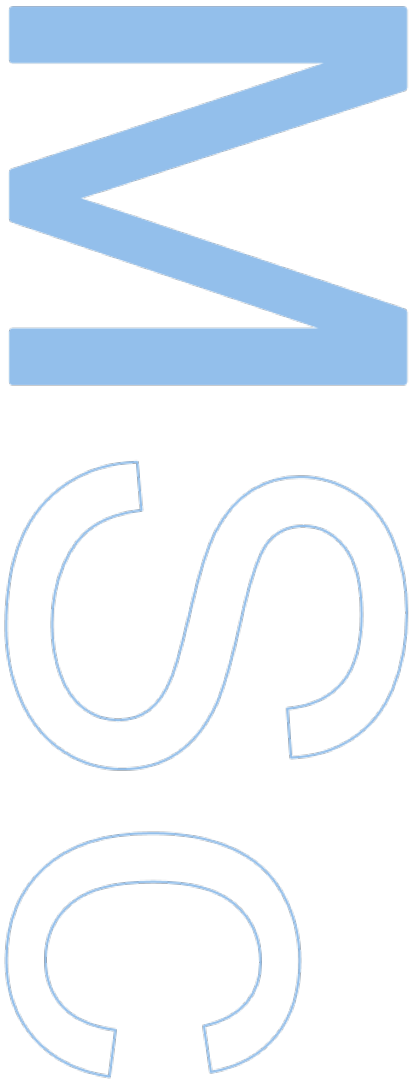

U.PORTO

FACULDADE DE CIÊNCIAS
UNIVERSIDADE DO PORTO

MCS

[This page was intentionally left blank]

To my mother

[This page was intentionally left blank]

"You could give Aristotle a tutorial. And you could thrill him to the core of his being. Aristotle was an encyclopedic polymath, an all time intellect. Yet not only can you know more than him about the world. You also can have a deeper understanding of how everything works. Such is the privilege of living after Newton, Darwin, Einstein, Planck, Watson, Crick and their colleagues. I'm not saying you're more intelligent than Aristotle, or wiser. For all I know, Aristotle's the cleverest person who ever lived. That's not the point. The point is only that science is cumulative, and we live later."

Richard Dawkins

[This page was intentionally left blank]

Acknowledgments

A master's thesis is a culmination of five intense years of hard-work, great parties and a little luck. Overall, it is an experiment about intense exposure to physics, to life and I am grateful to have been a part of it. This is a tribute to those who made this experiment successful.

First, I wish to thank my supervisor, Prof. João Viana Lopes, for all the fruitful scientific discussions and for the valuable advices that I will carry in journeys to come. I am also grateful to my co-supervisor, Prof. João Penedones, for presenting me with the theme of this thesis and for providing important insight into the problem. I would also like to thank one of my closest collaborator, José Matos, whose ideas were crucial to the success of this work and for always being available to help me. Still in the context of this work, I would like to thank Prof. Gabriel Cuomo for the enriching discussions. At last, I wanna thank João Vilas Boas for teaching me some useful aspects of the software Mathematica; António Antunes for the discussions about QFT and João Pedro Pires for the useful discussions and advices on writing.

Regarding the numerical portion of this thesis, I am very grateful to the computational facilities at Grid FEUP and the cluster time provided by INCD funded by FCT and FEDER under project 01/SAICT/2016 nº 022153 and the grants 2021.09830.CPCA and 2022.15885.CPCA of the Advanced Computing Projects.

I would also like to thank those who are not directly involved in this thesis. This are some of the names of those who made the last five years a wonderful human experience: Ana Cacho, Anselmo Falorca, Diogo Pinheiro, Helena Silva, Luís Afonseca, João Pinho, David Lima, Tiago Gonçalves, Patricia Soares, Nicolau Sobrosa, Raul Liquito. Also to Diogo Pimenta and Jorge Fernandes for the many meals shared in restaurants throughout Porto, I hope this tradition continues for years to come. Finally, to my grandmother, Irene, for making the best cozido à Portuguesa and tripas à moda do Porto.

A special thanks to my Counter-Strike partners who have been there since way back and kept me sane in the middle of covid: Diogo "Tista" Batista, João "Morgan" Mogrão, Filipe "Keledyn" Pereira, Marcos "Márcio" Freitas, Ricardo "Groot" Martins and Henrique "Noxter" Martins.

The last round of acknowledgments is dedicated to some of those who have inspired me: Prof. Leonard Susskind, Prof. Richard Feynman, Prof. David Tong. Al Pacino, Robert De Niro, Martin Scorsese, Dave Chappelle, George Carlin, Nas, David Bowie, Sade, Marvin Gaye and Ms. Lauryn Hill.

[This page was intentionally left blank]

Abstract

Conformal field theories (CFTs) are providing new and promising tools to study both phase transitions in a non-perturbative fashion as well as quantum gravity via the Anti-de Sitter (AdS)/CFT correspondence [1]. CFTs are fixed points of the renormalization group flow which encode the universal properties of second-order phase transitions.

Local physical observables in CFTs are described by a set of dimensionless numbers, called CFT data, *i.e.* the conformal dimensions and operator product expansion (OPE) coefficients [2–4]. For a CFT in the strongly coupled regime, the spectrum of low dimension operators often lacks an organizational principle, making it impossible to compute it analytically. In that case, and in order to compute the CFT data, one has to resort to novel numerical approaches such as bootstrap or Monte-Carlo.

A decade ago, it was discovered that some sectors associated with large quantum numbers are amenable to a perturbative description. Most notably, the large spin sector of a CFT, where the CFT data can be computed through an expansion in inverse powers of spin [5–8]. More recently and relevant to this thesis, Hellerman *et al.* and others [9, 10] used an expansion, dubbed large charge expansion, in inverse powers of the charge associated with an internal symmetry to compute the CFT spectrum of charged operators. Hellerman *et al.* considered a CFT invariant under an internal $U(1)$ symmetry group, for which the state-operator correspondence implies that an operator with large $U(1)$ charge is associated with a finite density state and they argued that, in the simplest case, the finite density state has a superfluid nature. Two years later, Monin *et al.* [10] were able to describe the large charge states via an universal effective field theory (EFT) description for a Goldstone mode of the superfluid. Such description allowed for the systematic calculation of correlation functions and consequently the CFT data.

The universal nature of the superfluid EFT makes it a candidate description for the large charge sector of many theories. However, in contrast with the large spin expansion, a rigorous proof of the validity of the superfluid description is lacking. Therefore, it is important to check its prediction in theories where the calculations can be made. With this thesis, we seek to provide evidence for the usefulness of the superfluid EFT in the strongly coupled three dimensional $O(2)$ model via Monte-Carlo calculations.

[This page was intentionally left blank]

Resumo

As teorias de campo conforme (CFT) têm ganho popularidade na comunidade científica porque permitirem estudar transições de fase de uma forma não perturbativa, bem como, serem possíveis candidatas a uma teoria de gravitação quantica através da correpondência Anti-de Sitter (AdS)/CFT [1]. Uma CFT corresponde a um ponto fixo no fluxo do grupo de renormalização, que entre várias informações, contêm a propriedades universais características de transições de fase de segunda ordem.

Numa CFT, as observáveis físicas são descritas por um conjunto de quantidades adimensionais chamadas CFT Data, por exemplo, a dimensão conforme. Quando uma CFT é fortemente acoplada, o seu espetro perde organização o que inviabiliza qualquer tipo de cálculo analítico. Nesse caso, é necessário recorrer a novos métodos como "bootstrap" e Monte-Carlo.

Há uma década e de forma engenhosa, descobriu-se que, em alguns limites associados a números quanticos elevados, certas CFTs recuperavam o tratamento perturbativo. Por exemplo, no limite em que o "spin" é elevado, é possível calcular a CFT data através de uma expansão em potências do inverso do spin [5–8]. Recentemente, Hellerman *et al.* e outros físicos [9, 10] proposeram que usar uma expansão similar para a carga associada a uma simetria interna. Primeiramente, Hellerman *et al.* consideraram uma CFT com invariância $U(1)$ e sabendo que a um operador de carga elevada está associado um estado de densidade finita, os autores argumentaram que este seria realizado numa fase superfluida. Dois anos mais tarde, Monin *et al.* [10] foram capazes de descrever os estados de densidade finita através de uma teoria efetiva universal (EFT) cujo grau de liberdade é um modo de Goldstone. Com essa descrição os autores conseguiram calcular, de uma forma sistemática, as funções de correlação e, consequentemente, a CFT Data.

A universalidade da EFT torná-la-ia uma candidata a explicar vários fenómenos físicos. Contudo, e em contraste com a expansão em spin, não há uma prova matématica que valide a descrição de superfluido. Sendo assim, é extremamente importante verificar se as previsões desta teoria são corroboradas por cálculos em modelos mais palpáveis. E é com esse intuito, esta tese propõe encontrar evidencia que corrobore a EFT. Nesse sentido, iremos usar métodos de Monte-Carlo para estudar o modelo $O(2)$ em três dimensões.

[This page was intentionally left blank]

Contents

List of Figures

[This page was intentionally left blank]

Chapter 1

Introduction

In 1911, Heike Kamerlingh Onnes was studying the properties of materials at very low temperature, when he noticed that the resistance of mercury goes to zero when the temperature is below 4.2 K. This was the first experimental observation of superconductivity. It took forty years for Bardeen, Cooper and Schrieffer to develop the first microscopic theory of superconductivity, called BCS theory. However their theory was received with some contention because it was not gauge invariant. This problem was solved by Anderson. He showed that the gauge symmetry is restored when one takes into account other modes, now called Goldstone and Higgs modes. A couple years later, Peter Higgs used a similar mechanism to suggest a new particle called the Higgs boson, which explained how some particles became massive at low-energies. This story is a great example about how the study of phase transition can connect different areas of physics, reflecting a deeper principle called universality. By universality or universality classes we mean that at the critical point (in the case of mercury when the temperature is equal to 4.2 K) most microscopic details do not contribute to the emergent macroscopic properties of the system. For example, the specific heat of certain gases and magnetic susceptibility in some magnets behave similarly as a function of temperature. Even today, we are still unsure why universality exists. Polyakov [11] suggested that, at the critical point, the system acquires extra symmetries, making it invariant under the conformal group. Although not rigorously proven, Polyakov's idea has led to remarkable advancements. Conformal field theory predicts conformal dimensions, which is the quantity that controls the behavior of specific heat and magnetic susceptibility with temperature.

The use of conformal field theory (CFT) to study phase transitions started to gain traction after El-Showk *et al.* [12] devised a method to find bounds for the conformal dimensions of the lowest parity positive operator, Δ_ϵ, and lowest parity negative operator, Δ_σ, for a CFT with $\mathbb{Z}_2$ symmetry[1]. Their method, called bootstrap, will be briefly explained in Section 2.6. As shown in Fig. 1.0.1 a), they concluded that not all values of the conformal dimension are allowed, in fact, only those that lay on the blue region generate consistent CFT's. In particular, the 3D Ising model lives on the red region, at the kink. The authors also tried, although unsuccessful, to extend this study for operators beyond the lightest operators. In 2016, Kos *et al.* [13] improved on the work done by El-Showk *et al.* and were able to compute the conformal dimensions Δ_σ and Δ_ϵ with unprecedented accuracy, their results are displayed in Fig. 1.0.1 b). These two papers carry an important lesson, the conformal dimensions and OPE coefficients are not independent numbers, *i e.*, once you fix Δ_ϵ , Δ_σ can only take values in the certain region where certain self consistent conditions are true.

[1] In this case parity means that under a $\mathbb{Z}_2$ symmetry the positive parity operators transform as $\epsilon \to \epsilon$ and negative parity operators transform as $\sigma \to -\sigma$.

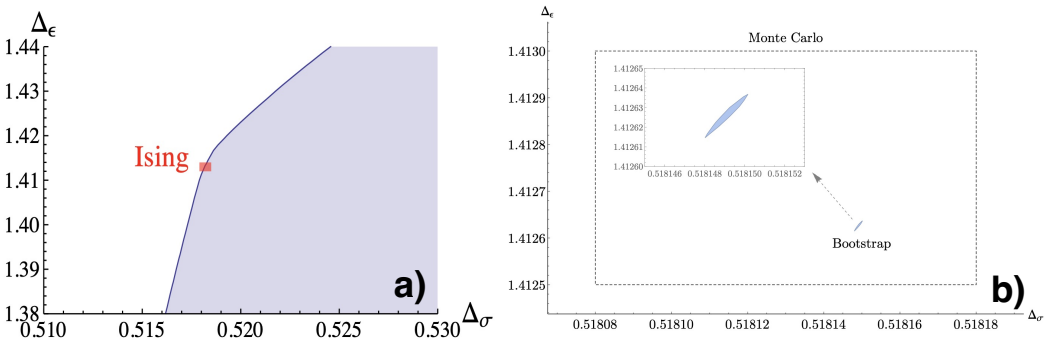

Figure 1.0.1: a) The blue region correspond to the values of Δ_ϵ and Δ_σ allowed by symmetry, taken from [12]; b) Precision measurements of the region of allowed conformal dimensions in the Ising model, taken from [13], four years later.

In a nutshell, the reason why bootstrap fails beyond the lightest operator is related to the nature of the spectrum. The spectrum of a weakly coupled theory is usually organized in terms of quantum number. For example, in condensed matter, the dispersion relation of a non-interacting system is always a function of the momentum, $\boldsymbol{k}$. However, if the theory is highly interactive, we often cannot easily organize the spectrum as a function of a known quantum numbers, and we say that a CFT is strongly coupled.

Remarkably, Alday *et al.* [7] discovered that in the large spin sector of certain strongly coupled theories, it is possible to recover the organizational principle of the spectrum. More concretely, the CFT data can still be computed via an expansion in inverse powers of spin, which supports the recently rigorously proven analytical properties of the CFT data as a function of spin [14, 15].

The success of the large spin expansion inspired Hellerman *et al.* [9] to propose the large charge expansion, where the charge is associated with an internal symmetry. In their article, they argued that, the operator associated with a large charge corresponds to a state with finite charge-density in a superfluid phase. Using that argument, they could draw qualitative results for the conformal dimension of charged operators. Later, aiming to formalize the arguments by Hellerman *et al.* in a more applicable fashion, Monin *et al.* used a saddle point approach that allowed for the systematic calculation of correlation functions. In this thesis, we will review the approach pioneered by Monin *et al.* [10] that is able, using geometrical arguments, to describe a universal CFT with $U(1)$ symmetry from the dynamics of a massless mode, called Goldstone mode. That description allows for the systematic calculation of the correlation functions of operators with large $U(1)$ charge and therefore the CFT data.

Unfortunately, and in contrast with the large spin expansion, even when a model is specified there is no rigorous proof of the validity of the large charge expansion. So, it is of paramount importance that we use models were the calculations are possible, in order to verify the predictions from the superfluid description. The main objective of this thesis is to provide that evidence by studying the highly coupled three dimensional $O(2)$ model using Monte-Carlo methods.

Thesis Outline

In this thesis we will walk through the theoretical aspect of the superfluid effective field theory and the numerical tools used to verify it. The Chapters 2, 3, 4, 5 focus on the theoretical aspects of the thesis,

- **Chapter 2**: This chapter is dedicated to theories that exhibit conformal invariance. In particular, we discuss how the symmetries of the conformal group constrained the form of n-point correlation function and how any conformal field theory can be described by a set of numbers called CFT Data. At the end, we outline a bootstrap method that can provide bounds on the CFT Data;
- **Chapter 3**: We start this chapter by making a brief review of some important concepts in differential geometry. Then, we use the complex scalar theory to illustrate the idea behind non-linearly realized symmetries, Goldstone modes and Higgs modes. Through the rest of the chapter we focus on a procedure, called coset construction, that provides a systematic method of construction Lagrangians with non-linearly realized symmetries. In the last section, we use the coset construction to build the superfluid effective action;
- **Chapter 4**: In this chapter, we use a toy model, the rigid rotor model, to motivate the use of perturbation theory around large quantum numbers. Next, we use perturbation theory around large charge and the superfluid effective action from chapter 3 to predict a portion of the CFT Data;
- **Chapter 5**: This chapter is solely about the $O(2)$ model and its properties. First, we use the lattice version of the $O(2)$ model to display an example of a topological phase transition, the BKT transition. Then, we discuss an alternative description of the $O(2)$ model, on the dual lattice, in terms of integer degrees of freedom and how to express the correlation function of charged operators in that representation.

Chapters 6, 7, 8, 9 will be dedicated to the numerical tools and results obtained using those tools,

- **Chapter 6**: In the first section of this chapter, we present the Monte-Carlo method as a solution to the problem of evaluating a sum/integral over an high dimensional space. Then, we spend some time outlining the general structure of the algorithm and adapting it to the specific task of computing correlation functions. After that, we will justify why our method, the continuous-time update, is superior to the often used metropolis-update;
- **Chapter 7**: This chapter revolves around the finite-volume effects, stochastic errors and lattice errors. After analyzing each of the latter mentioned, we devise a strategy that minimizes those errors;
- **Chapter 8**: The focus of this chapter will be to showcase the results obtained using the measurement strategy outlined in chapter 7. Furthermore, we will analyze and extract physical conclusions from those results;
- **Chapter 9**: In this chapter we wrap up the results from the analysis in chapter 8, together with the mentioning of other results that were obtained in the course of this thesis. Finally, we propose other measurements that would provide further evidence for the superfluid effective field theory.

Chapter 2

Overview of Conformal Field Theory

In this Chapter, we will introduce relevant concepts in conformal field theory, in particular those that are directly related to the study of second-order phase transitions. This chapter is based on the following set of books and lecture notes [2–4, 16, 17]. However, if we consider a certain aspect to be more clearly explained in one of the references, we will mention it.

2.1 Why do we care about Conformal Field Theory?

The short answer is that CFTs describe the universal properties of second order phase transitions. **Phase transition** is the name given to a sudden change in matter. A day to day example would be the boiling of water when exposed to a heat source. During a phase transition, a large number of particles (water) behaves collectively in a way that none of the individual particles (water molecules) can, resulting in a discontinuous change of its macroscopic properties. Furthermore, it looks as if, near the critical temperature, T_c, certain macroscopic properties, for example the heat capacity of water, $C(T)$, diverge like

$$C(T) \sim \frac{1}{|T - T_c|^{0.11008\ldots}}. \tag{2.1.1}$$

The exponent that characterizes this divergence is called a **critical exponent**. Turns out that one can relate the exponents which characterize the divergence of the heat capacity of many gases and the susceptibility of some magnets . Meaning that the majority of the microscopic details do not influence the macroscopic behavior. This is called **universality**.

Many of the ideas described in the previous paragraph were developed in the context of a model of magnet called Ising model. The Ising model is a cubic lattice model composed of N sites. Each site, i, is associated with a degree of freedom called spin, S_i, that is either -1 or $+1$. The Hamiltonian or energy of the system is given by

$$H(\{S_i\}) = -J \sum_{\langle i,j \rangle} S_i S_j, \tag{2.1.2}$$

where $\langle i, j \rangle$ means that the spins only interact with their nearest neighbors and J characterizes the strength and type of interaction between neighboring spins. If $J > 0$, then the spins want their neighbors to have the same sign whereas, if $J < 0$, the spins want their neighbors to have different signs[1]. The phase transition in the Ising model is characterized by an **order parameter**, the total magnetization, m, given by $\frac{1}{N}\sum_i S_i$. Below a critical temperature, m is ± 1 and above the critical temperature the total magnetization is 0.

[1] For simplicity we will work with J equal to 1.

According to the mean field approximation, for small m the free energy admits the following expansion

$$f(m) \equiv \frac{F(m)}{N} + T\log 2 \approx \frac{1}{2}(T-6)m^2 + \frac{1}{12}Tm^4 + \ldots \tag{2.1.3}$$

A physical system evolves towards the minimal of $f(m)$, that state is formally known as equilibrium. As showcased in Fig. 2.1.1, above the critical temperature the system has a total magnetization of 0, whereas below the critical temperature, $f(m)$ has two global minima at $m = m_0/N$ and $m = -m_0/N$.

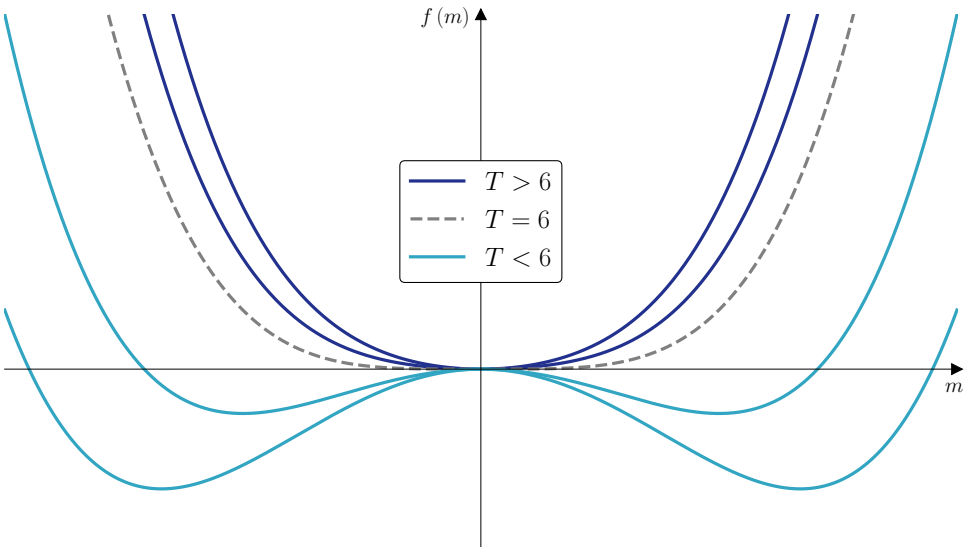

Figure 2.1.1: Free energy $f(m)$ as a function of m for different temperatures

The Hamiltonian in Eq. 2.1.2 has $\mathbb{Z}_2$ global symmetry, which, in practice, means that H is invariant under $S_i \to -S_i$ for all spins or, in other words, changing the magnetization from m to $-m$. Above the critical temperature, the ground-state of the system remains invariant under $\mathbb{Z}_2$ because changing the sign of all the spins results in the same magnetization, $0 \to -0$. Below the critical temperature, despite $f(m)$ being invariant under $\mathbb{Z}_2$, the equilibrium state is not. As an example, suppose that the system is in a state with magnetization m, if one changes the signs of all the spins, the magnetization becomes $-m$ resulting in a different state. When this happens we say that the symmetry has been **spontaneously broken**. Usually, when a global symmetry is spontaneously broken, the equilibrium state becomes degenerate and the symmetry plays the role of mapping the different states. For example, in the Ising model the $\mathbb{Z}_2$ symmetry maps the state with magnetization equal to $-m$ into the state with magnetization to m and vice-versa.

In the limit where the system has a large amount of sites, we can think of it as being described by the density of magnetization $m(\boldsymbol{x})$, from the expansion of $F(m)$ around small m we know that

$$F[m(x)] = \int d^3\boldsymbol{x}\left\{\frac{1}{2}\alpha_2(T)m^2 + \frac{1}{4}\alpha_4(T)m^4 + \frac{\gamma(T)}{2}\nabla m\cdot\nabla m + \ldots\right\}, \tag{2.1.4}$$

where $\gamma(T)$ is an unknown coefficient, $\alpha_2(T) \approx (T - T_c)$ and $\alpha_4(T) \approx \frac{T}{3}$. For simplicity, we will redefine m to be equal to $m_{\text{GS}} + \phi(\boldsymbol{x})$, where m_{GS} corresponds to the equilibrium magnetization density[2] and $\phi(\boldsymbol{x})$ is a field that characterizes the thermal fluctuations around equilibrium.

[2] $m_{\text{GS}} = \begin{cases} 0 & T \geqslant T_c \\ \pm m_0 & T < T_c \end{cases}$ and from the equation of motion $m_0 = \sqrt{-\frac{\alpha_2}{\alpha_4}}$

Ignoring powers of ϕ greater than 2, the free energy can be written as a function of $\phi(\boldsymbol{x})$

$$F[\phi(\boldsymbol{x})] = F[m_{\text{GS}}] + \int d^3\boldsymbol{x}\left\{\frac{1}{2}\gamma(T)\nabla\phi\cdot\nabla\phi + \frac{1}{2}\alpha_2'(T)\phi^2 + ...\right\}, \tag{2.1.5}$$

where $\alpha_2'(T) = \alpha_2(T) + 3\alpha_4(T)m_{\text{GS}}$. We can compute the correlation function, $C(\boldsymbol{x}-\boldsymbol{y})$, from the path integral

$$C(\boldsymbol{x}-\boldsymbol{y}) = \int \mathcal{D}\phi\, e^{\beta F[\phi]}\phi(\boldsymbol{x})\phi(\boldsymbol{y}). \tag{2.1.6}$$

Without going into too much detail, after manipulating the path integral we arrive at the following expression

$$C(\boldsymbol{x}-\boldsymbol{y}) = \frac{1}{\gamma}\int \frac{d^3\boldsymbol{k}}{(2\pi)^2}\frac{e^{-i\boldsymbol{k}\cdot(\boldsymbol{x}-\boldsymbol{y})}}{\boldsymbol{k}\cdot\boldsymbol{k}+1/\xi^2}, \tag{2.1.7}$$

where $\xi^2 \equiv \frac{\gamma}{\alpha_2'}$ is the **correlation length**. The integral in Eq. 2.1.7 cannot be solved exactly with the exception of two limiting cases, $|\boldsymbol{x}-\boldsymbol{y}| \gg \xi$ and $|\boldsymbol{x}-\boldsymbol{y}| \ll \xi$, where it has the value

$$C(\boldsymbol{x}-\boldsymbol{y}) \backsim \begin{cases} \frac{1}{|\boldsymbol{x}-\boldsymbol{y}|} & |\boldsymbol{x}-\boldsymbol{y}| \ll \xi \\ \frac{e^{-|\boldsymbol{x}-\boldsymbol{y}|/\xi}}{|\boldsymbol{x}-\boldsymbol{y}|} & |\boldsymbol{x}-\boldsymbol{y}| \gg \xi \end{cases}. \tag{2.1.8}$$

The correlation length is proportional to some positive power of $\frac{1}{T-T_C}$, meaning that at the critical temperature of a second order phase transition the correlation length is infinite. Therefore at the critical temperature $|\boldsymbol{x}-\boldsymbol{y}|$ is always much smaller than ξ and the correlation function is

$$C(\boldsymbol{x}-\boldsymbol{y}) \backsim \frac{1}{|\boldsymbol{x}-\boldsymbol{y}|}. \tag{2.1.9}$$

Intuitively, when the correlation between two regions of space is infinite the system loses its typical length scale, it becomes scale invariant. The fact that the correlation function is $\frac{1}{|x-y|}$ suggests that when $x \to \lambda x$ the fields transform like $\phi \to \lambda^{-1/2}\phi$ and $\frac{1}{2}$ is called the **classical scaling dimension** of the field ϕ. Therefore, at a critical temperature, the system is invariant under translations, rotations and scaling transformations. Moreover, it was conjectured by Polyakov [11] that the system with these properties is also invariant under the so called special conformal transformations, making it invariant under the conformal group[3].

[3] Although every piece of evidence points towards this conjecture being true, it still lacks a mathematical rigorous proof

2.2 Conformal Group

Quantum field theories are invariant under the Poincaré group, local translations and rotations. A conformal field theory is invariant under the conformal group. The conformal group is composed by the set of coordinate and Weyl transformation , $x^\mu \to \tilde{x}^\mu(x^\mu)$ on $\mathbb{R}^d$, such that the metric[4] is preserved up to a local rescaling, $\Omega(x)$,

$$g^{\mu\nu}(x) \to \tilde{g}^{\mu\nu}(\tilde{x}) = \Omega(x)\, g^{\mu\nu}(x)\,. \tag{2.2.1}$$

For a dimension greater than two, the conformal group is composed by only four families of transformations,[5]

$$\begin{aligned}
\tilde{x}^\mu &= \alpha x^\mu && \text{Dilations}\\
\tilde{x}^\mu &= \Lambda^\mu_{\ \nu} x^\nu && \text{Rotations}\\
\tilde{x}^\mu &= x^\mu + a^\mu && \text{Translations}\\
\tilde{x}^\mu &= \frac{x^\mu + b^\mu x^2}{1 + 2b^\mu x_\mu + b^2 x^2} && \text{Special conformal transformations}
\end{aligned} \tag{2.2.2}$$

where $\alpha \in \mathbb{R}$, $a^\mu, b^\mu \in \mathbb{R}^d$, $\Lambda^\mu_{\ \nu} \in SO(d)$ parametrize those transformations. Although special conformal transformations (SCT) looks exotic, they are a combination of an inversion, a translation by b^μ and another inversion[6]. By studying how each transformation acts on a general function, we are able to arrive at a differential representation for the generators of the infinitesimal transformation D, P_μ, K_μ, $L_{\mu\nu}$,

$$\begin{aligned}
D &= -ix\cdot\partial && \text{Dilation}\\
P_\mu &= -i\partial_\mu && \text{Rotations}\\
K_\mu &= -i\left(2x_\mu x\cdot\partial - x_\mu\partial^2\right) && \text{Translations}\\
L_{\mu\nu} &= -i\left(x_\mu\partial_\nu - x_\nu\partial_\mu\right) && \text{Special conformal transformations}
\end{aligned} \tag{2.2.3}$$

The set of generators spawns an algebra, known as the conformal algebra, whose non-trivial commutators are

$$\begin{aligned}
[D, P_\mu] &= iP_\mu, & [D, K_\mu] &= -iK_\mu,\\
[P_\mu, L_{\nu\rho}] &= i\left(\eta_{\mu\nu}P_\rho - \eta_{\mu\rho}P_\nu\right), & [K_\mu, L_{\nu\rho}] &= i\left(\eta_{\mu\nu}K_\rho - \eta_{\mu\rho}K_\nu\right),\\
[K_\mu, P_\nu] &= 2i\left(\eta_{\mu\nu}D - L_{\mu\nu}\right) & [L_{\mu\nu}, L_{\rho\sigma}] &= i\left(\eta_{\nu\rho}L_{\mu\sigma} \pm \text{ permutations}\right).
\end{aligned}$$

Because $[M_{\mu\nu}, D]$ is zero, the irreducible representations of the conformal group will be classified in terms of the eigenvalues of $M_{\mu\nu}$, the spin, and the eigenvalues of D, the conformal dimensions. For that reason, we will want to construct a quantum field theory whose states are organized in terms of the conformal dimensions and spin. Furthermore and as we will see in the following section, in the irreducible representation labeled by the eigenvalues of $M_{\mu\nu}$ and D, the translation and SCT generators act as creation and annihilation operators, respectively.

[4] Although understanding the metric is not needed for the comprehension of this chapter, it will be explained in Section 3.1.2.

[5] In two dimensions, the global conformal transformations are also given by Eq. 2.2.2, but the conformal group is also composed of local transformation which involve derivatives.

[6] The inversion is defined as $x^\mu \to \frac{x^\mu}{x^2}$. Then, we perform a translation by b^μ, $\frac{x^\mu}{x^2} + b^\mu$. After that, we invert once again, $\frac{x^\mu}{x^2} + b^\mu \to \frac{x^\mu x^{-2} + b^\mu}{x^{-2} + 2b^\mu x_\mu x^{-2} + b^2}$. At the end of the three transformations, $x^\mu \to \frac{x^\mu + b^\mu x^2}{1 + 2b^\mu x_\mu + b^2 x^2}$.

2.3 Foliation and Radial Quantization

The usefulness of conformal symmetry only becomes apparent when we define the states and their evolution in this new quantum theory. That will require understanding foliation and how it can be used to build the Hilbert space.

Foliation [2] is the operation of slicing a D dimensional spacetime into several non-intersecting $D-1$ surfaces, whose union is the whole space. Despite not being mentioned in most textbooks, this process is a crucial in the construction of the Hilbert space for a QFT. Consider a $1+1D$ spacetime, the widely used choice is to foliate the spacetime using surfaces of equal time, $t=$ const. Then, for each surface with $t=\tau$, one associates a Hilbert space, $\mathcal{H}_\tau$. Most calculations in QFT require computing the overlap between a state $|\Psi_{\text{out}}\rangle$ and a state $|\Psi_{\text{in}}\rangle$. If the states live in the same Hilbert space, then the overlap is $\langle\Psi_{\text{out}}|\Psi_{\text{in}}\rangle$. However, if they live on different Hilbert spaces, namely $\mathcal{H}_t$ and $\mathcal{H}_{t+\Delta t}$, we must find an unitary operator, U, connecting the two Hilbert spaces, such that the overlap can be computed through $\langle\Psi_{\text{out}}|\,U\,|\Psi_{\text{in}}\rangle$. It is at this point that the choice of foliation plays a major role, depending on the choice of foliation, U may be trivial or not. Because we chose the foliation to be equal time surfaces, the operator U will be the time evolution operator, $U=e^{iP_t\Delta t}$, where $P_t=\frac{1}{i}\frac{\partial}{\partial t}$.

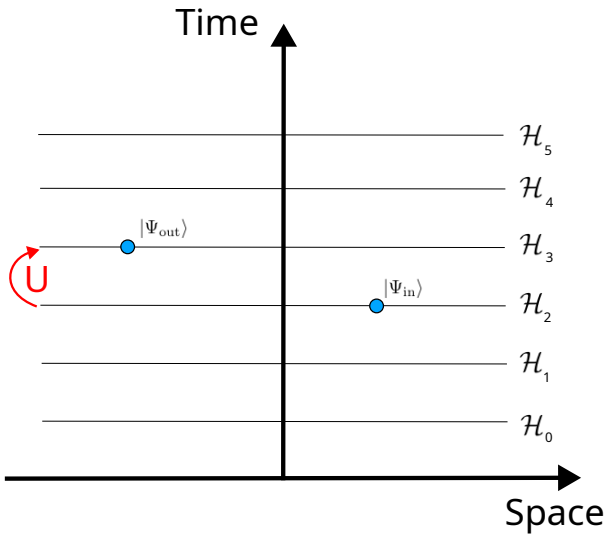

Figure 2.3.1: Foliation of a spacetime using equal time surfaces.

As a rule of thumb, one wants the surfaces to be related by a symmetry in the theory, for example, in Fig. 2.3.1, the surfaces are related by time translation symmetry. For a CFT, a particularly useful one, for reason that will become clear shortly, is to foliate spacetime using $D-1$ spheres of different radii. In other words, we associate a Hilbert space, $\mathcal{H}_r$, to each radius, r. This choice of foliation is called **radial quantization**. In this case, the foliation was made having the dilation symmetry in mind, such that the Hilbert space at r and the Hilbert space at $r+\Delta r$ are connected via the following unitary operator

$$U=e^{iD\Delta r},\text{ where } D=\frac{1}{i}\frac{\partial}{\partial r}. \tag{2.3.1}$$

In radial quantization, the dilation operator plays the same role as the Hamiltonian, P_t, in the equal time foliation, see Fig. 2.3.2 a). Furthermore, a useful transformation is to write the radius, $r\in(0,\infty)$, as a function of a new variable $\tau\in(-\infty,\infty)$. This map is from radial coordinates, (r,n_i)[7], to cylinder coordinates $(\tau\equiv\log r,n_i)$, which means that the dilations, $r\to e^\lambda r$, are mapped to time translations, $\tau\to\tau+\lambda$.

[7] $r=\sqrt{x_0^2+x_ix^i}$ and $n_i=\frac{x_i}{r}$.

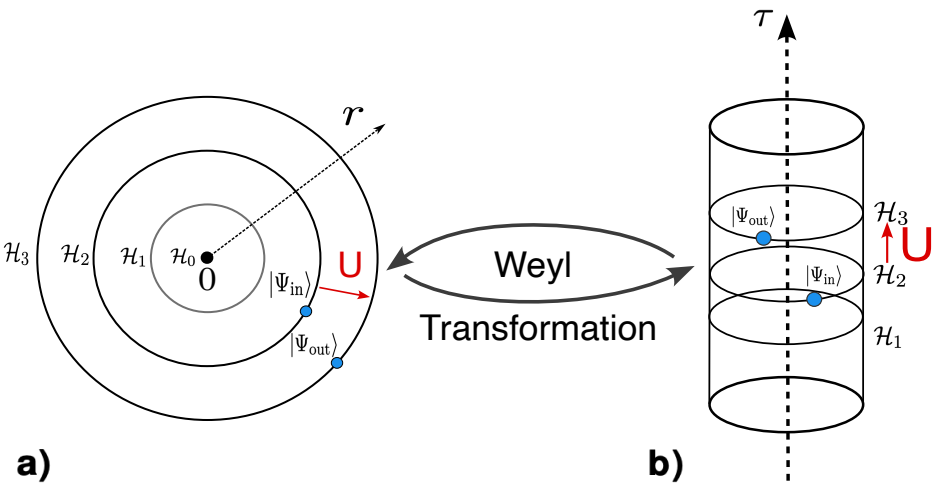

Figure 2.3.2: Map between CFT on the plane and CFT on the cylinder

As displayed in Fig. 2.3.2 b), the circles on the cylinder are the time slides on the equal time foliation. And now the spectrum of the Hamiltonian on the cylinder will be equivalent to the spectrum of the dilation operator on the plane. A consequence of this relation is that we can use some techniques from QFT on the cylinder to study CFT in flat space and vice-versa. Even without computing anything we can argue that because the spectrum of the Hamiltonian in a compact space, such as the cylinder, is discrete and therefore the spectrum on the plane should also be discrete. Radial quantization is relevant because the irreducible representation are classified in terms of the scaling dimension, eigenvalue of D, and angular momentum, eigenvalues of $M_{\mu\nu}$[8]. So, in general, the Hilbert space at each fold, $\mathcal{H}_i$, will be the set of states $\{|\Delta, l, m\rangle\}$.

2.4 Operator-State Correspondence and Spectrum Labeling

In the previous section, we were able to define a Hilbert space at each radius and relate them by an unitary operator. We are now interested in computing observables which is done using the path integral formulation. For example, the overlap, $\langle\phi_f| e^{iD} |0\rangle$, can be written as

$$\langle\phi_f| e^{iD} |0\rangle = \int_{\phi(1,\boldsymbol{n})=\phi_f} D\phi\,(r,\boldsymbol{n})\, e^{iS[\phi]}, \tag{2.4.1}$$

where r is the radius of the sphere and $\boldsymbol{n}$ is a vector of coordinates in S_{D-1}[9].If a local operator, $\mathcal{O}(x)$, is inserted inside the region $r < 1$, then it will change the state at $r = 1$, from the vacuum to something else. The overlap gets modified and is now given by

$$\langle\phi_f| \mathcal{O}(x) |0\rangle = \int_{\phi(1,\boldsymbol{n})=\phi_f} D\phi\,(r,\boldsymbol{n})\, \mathcal{O}(x)\, e^{iS[\phi]}. \tag{2.4.2}$$

[8]This is a direct consequence of the commutator $[M_{\mu\nu}, D] = 0$.

[9]The operator e^{iD} is used to evolve the state $|0\rangle$ from $\mathcal{H}_0$ to $\mathcal{H}_1$ and therefore does not appear in the left side of Eq. 2.4.1.

If we consider the Hilbert space at $r = 1$ to be spawned by $\{|\phi_b\rangle\}$, then the state spawn by $\mathcal{O}(x)$ at $r = 1$ is some linear combination of these states,

$$|\mathcal{O}\rangle \equiv \mathcal{O}(x)|0\rangle = \sum_b \left(\int_{\phi(1,\boldsymbol{n})=\phi_b} D\phi\,(r,\boldsymbol{n})\,\mathcal{O}(x)\,e^{iS[\phi]} \right) |\phi_b\rangle\,. \tag{2.4.3}$$

In this way, we can identify a local operator living inside a region with some state at the boundary, this also happens in a QFT. However, in a CFT, to each state at the boundary we can associate a local operator living inside that region. This two way identification is known as operator-state correspondence.

Through the operator-state correspondence, the definition of local operators is clear and precise. Suppose $\mathcal{O}_\Delta(0)$ generates a state. Because the state and corresponding operators have the same quantum numbers, the operator-state correspondence states the following equivalence

$$\mathcal{O}_\Delta(0) \leftrightarrow |\mathcal{O}_\Delta\rangle \equiv \mathcal{O}_\Delta(0)|0\rangle\,, \tag{2.4.4}$$

where the state $|0\rangle$ is the vacuum. It is also convenient to understand how the conformal group acts on the operators as well as their corresponding states[10]

$$\begin{aligned}
[K_\mu, \mathcal{O}_\Delta(0)] = 0 &\leftrightarrow K_\mu|\mathcal{O}_\Delta\rangle = 0,\\
[D, \mathcal{O}_\Delta(0)] = \Delta\mathcal{O}_\Delta(0) &\leftrightarrow D|\mathcal{O}_\Delta\rangle = \Delta\mathcal{O}_\Delta,\\
[M_{\mu\nu}, \mathcal{O}_\Delta(0)] = S_{\mu\nu}\mathcal{O}_\Delta(0) &\leftrightarrow M_{\mu\nu}|\mathcal{O}_\Delta\rangle = S_{\mu\nu}|\mathcal{O}_\Delta\rangle\,.
\end{aligned} \tag{2.4.5}$$

Operators that are annihilated by the action of K_μ, are called **primary operators**. The multiplet of the state $|\mathcal{O}_\Delta\rangle$, obtained by acting with the generator of translation P_μ, is:

$$\text{Multiplet of } |\mathcal{O}_\Delta\rangle : |\mathcal{O}_\Delta\rangle\,, P_\mu|\mathcal{O}_\Delta\rangle\,, P_\mu P_\nu|\mathcal{O}_\Delta\rangle\,, \ldots\,, \tag{2.4.6}$$

The operators with P_μ, such as $P_\mu\mathcal{O}_\Delta(0)$, are called **descendent operators**. They are obtained from the primary operators by taking derivatives

$$P_\mu\mathcal{O}_\Delta(0) = \partial_\mu\mathcal{O}_\Delta(x)\Big|_{x=0}\,. \tag{2.4.7}$$

If we try to measure the conformal dimension of this operator, then we would get $\Delta + 1$. Thus we can think of P_μ as a creation operator for the conformal dimension. On the other hand, if we act with K_μ on $P_\mu\mathcal{O}_\Delta(0)$ and measure its conformal dimension we would get Δ, meaning that K_μ acts as a annihilation operator for the conformal dimension.

So far, every operator has been inserted at the origin. If we insert an operator at a position x then it will create the state $\mathcal{O}_\Delta(x)|0\rangle$. The operator $\mathcal{O}_\Delta$ at x is related to the operator $\mathcal{O}_\Delta$ at 0 by

$$\mathcal{O}_\Delta(x) = e^{-iPx}\mathcal{O}_\Delta(0)\,e^{iPx} \tag{2.4.8}$$

and after some manipulations[11], we conclude that

$$\mathcal{O}_\Delta(x)|0\rangle = \sum_n \frac{(-ix\cdot P)^n}{n!}\mathcal{O}_\Delta(0)|0\rangle\,, \tag{2.4.9}$$

[10] This can be obtain by using Eq. 2.4.4 and using the fact that the state $|0\rangle$ is killed by K, D and M.

[11] Using Hausdorff formula, $e^A B e^{-A} = B + \frac{1}{1!}[A,B] + \frac{1}{2!}[A,[A,B]] + \ldots$, and the commutation relations.

meaning that the state $\mathcal{O}_\Delta(x)|0\rangle$ will be a linear combination of states belonging to the multiplet of $|\mathcal{O}_\Delta\rangle$.

2.5 Correlators and CFT Data

Before going to the calculation of correlation functions using the path integral formalism, let us try to understand the restrictions coming from symmetries. Consider the 2-point correlator, $\langle\mathcal{O}_{\Delta_1}(x_1)\mathcal{O}_{\Delta_2}(x_2)\rangle$. Translation and rotation invariance imply that the correlator can only be a function of distance between x_1 and x_2. According to the definition of local operator, when applying a dilation of strength λ the operators must transform as

$$\mathcal{O}_{\Delta_1}(x_1)\to\mathcal{O}_{\Delta_1}(\lambda x_1)=\lambda^{-\Delta_1}\mathcal{O}_{\Delta_1}(x_1), \tag{2.5.1}$$

meaning that, if the 2-point function is to stay invariant under scaling, then the two point correlator must be given by

$$\langle\mathcal{O}_{\Delta_1}(x_1)\mathcal{O}_{\Delta_2}(x_2)\rangle=\frac{C}{|x_1-x_2|^{2(\Delta_1+\Delta_2)}}. \tag{2.5.2}$$

Lastly, we can apply the invariance under SCT to prove that Δ_1 must be equal to Δ_2. Symmetries in a CFT fully fix the form of the 2-point correlator, up to Δ_1 [12], to be

$$\langle\mathcal{O}_{\Delta_1}(x_1)\mathcal{O}_{\Delta_2}(x_2)\rangle=\frac{\delta_{\Delta_1,\Delta_2}}{|x_1-x_2|^{2\Delta_1}}. \tag{2.5.3}$$

By similar arguments, one can prove that the 3-point function is given by

$$\langle\mathcal{O}_{\Delta_1}(x_1)\mathcal{O}_{\Delta_2}(x_2)\mathcal{O}_{\Delta_3}(x_3)\rangle=\frac{\lambda_{123}}{|x_1-x_2|^{\Delta_1+\Delta_2-\Delta_3}|x_2-x_3|^{\Delta_2+\Delta_3-\Delta_1}|x_1-x_3|^{\Delta_1+\Delta_3-\Delta_2}}, \tag{2.5.4}$$

where λ_{123} is a constant that cannot be fixed by symmetry or normalization.

As we will show in Section 2.6, other n-point correlators can be written in terms of 2-point correlator and OPE coefficients, meaning that, up to Δ and λ, every correlator is fixed by the symmetries of the CFT. The λ_{123} are called OPE (Operator product expansion) coefficients and describe how products of operators decompose into sums of operators[13]. The set of all OPE coefficients and conformal dimensions is called **CFT Data** and understanding a CFT is synonymous with knowing all the conformal dimensions and OPE coefficients.

[12] In a CFT we choose C to be 1 and as a consequence a new constant in the 3-point function

[13] This is a consequence of the operator product expansion which we will explore in Section 2.6.

2.6 OPE - Operator Product Expansion

Suppose we insert an operator, $\mathcal{O}_2$, at the origin and an operator, $\mathcal{O}_1$, at x. This will generate a state $\mathcal{O}_1(x)\mathcal{O}_2(0)|0\rangle$ at the boundary. Because the Hilbert spaces at each radius are related by dilations, the state $\mathcal{O}_1(x)\mathcal{O}_2(0)|0\rangle$ can be written in the basis of the Hilbert space at the origin. Thus any n-point function can be generated by a linear combination of single operator insertions,

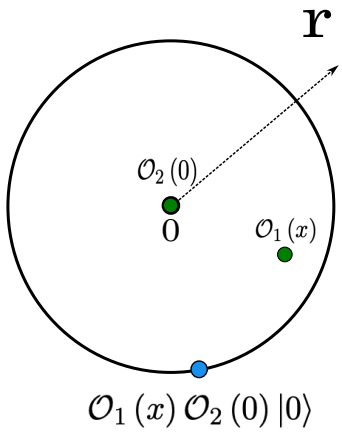

$$\mathcal{O}_1(x)\mathcal{O}_2(0)|0\rangle = \sum_{|\Psi_n\rangle\in\mathcal{H}_0} c_n|\Psi_n\rangle\,. \tag{2.6.1}$$

At $r=0$, the Hilbert space can be composed into states associated with the primary operators and their descendents, thus by organizing Eq. 2.6.1 into conformal multiplets

$$\overbrace{\mathcal{O}_1(x)\mathcal{O}_2(0)|0\rangle} = \sum_{\text{Primaries }\mathcal{O}} c(x,\partial_y)\mathcal{O}(y)\Big|_{y=0}|0\rangle\,. \tag{2.6.2}$$

The OPE is not unique to CFTs. In a QFT it is also possible to write the product of two operators as a linear combination of single operators. However, in QFT that expansion does not converge, whereas in a CFT this expansion remains convergent for a finite distance. OPEs are useful to turn n-point correlators into $(n-1)$-point correlators.

As an exercise, suppose we apply the OPE twice to the 4-point correlators of four similar operators,

$$\langle\mathcal{O}(x_1)\mathcal{O}(x_2)\mathcal{O}(x_3)\mathcal{O}(x_4)\rangle\,. \tag{2.6.3}$$

After applying the OPE twice we are left with a sum of 2-point correlators. Regardless of the pairs of operators we choose to perform the OPE, the result must be the same,[14]

$$\langle\overbrace{\mathcal{O}(x_1)\mathcal{O}(x_2)}\,\overbrace{\mathcal{O}(x_3)\mathcal{O}(x_4)}\rangle = \langle\overbrace{\mathcal{O}(x_1)\overbrace{\mathcal{O}(x_2)\mathcal{O}(x_3)}\mathcal{O}(x_4)}\rangle\,. \tag{2.6.4}$$

From symmetry arguments, the 4-point function can be written as

$$\langle\mathcal{O}(x_1)\mathcal{O}(x_2)\mathcal{O}(x_3)\mathcal{O}(x_4)\rangle = \frac{1}{x_{12}^{2\Delta_\mathcal{O}}x_{34}^{2\Delta_\mathcal{O}}}\sum_\phi \lambda^2_{\mathcal{O}\mathcal{O}\phi}g_{\Delta_\phi,l_\phi}(u,v)\,, \tag{2.6.5}$$

where g_{Δ_ϕ,l_ϕ}, called conformal blocks, are known, operator dependent functions of the cross-ratios u and v, which are defined as

$$u=\frac{x_{12}^2x_{34}^2}{x_{13}^2x_{24}^2} \text{ and } v=\frac{x_{23}^2x_{14}^2}{x_{13}^2x_{24}^2}. \tag{2.6.6}$$

Expanding the OPE, imposing crossing symmetry (Eq. 2.6.4) and labeling the primary operators by their conformal dimension, Δ, one arrives at the bootstrap equation,

$$\sum_\Delta \lambda^2_{\mathcal{O}\mathcal{O}\phi}\left(v^{\Delta_\mathcal{O}}g_{\Delta,l}(u,v)-u^{\Delta_\mathcal{O}}g_{\Delta,l}(v,u)\right)=0. \tag{2.6.7}$$

[14] One can only perform the OPE of $\mathcal{O}_1\mathcal{O}_2$, if it is possible to draw a circle that contains only those operators.

The equation above is used to obtain bounds on the CFT Data. In general, the method is extremely efficient [18, 19] to determine the conformal dimension of the lightest operator [15], usually surpassing state-of-the-art Monte Carlo methods. In the numerical portion of this thesis, we will be interest in operators beyond the lightest ones and, in that regime, the precision of bootstrap methods is worse than Monte Carlo. However, we will use its results to cross examine ours.

2.7 Some Comments about CFTs on a Torus

Throughout this chapter we have talked about CFTs either in the Euclidean or Minkowski space. However, Monte-Carlo (the method we will be using) is more efficient in a system with periodic boundary conditions, also known as the torus. As shown in Fig. 2.7.1, one can build a 2D torus[16] from a sheet of size $L \times L$ by "glueing" certain borders together. During this procedure, the system acquires an extra symmetry called modular invariance, and consequently the correlation function changes. In particular, the 2-point function becomes

$$\langle \mathcal{O}_1(x_1)\,\mathcal{O}_1(x_2)\rangle = \frac{1}{|x_1-x_2|^{2\Delta_1}} f\left(\frac{|x_1-x_2|}{L}\right), \tag{2.7.1}$$

where f is a function with the following property, $f(0) = 1$ and

$$f\left(\frac{x}{L}\right) = \frac{1}{\left(\frac{L}{x}-1\right)^{2\Delta_1}} f\left(1-\frac{x}{L}\right). \tag{2.7.2}$$

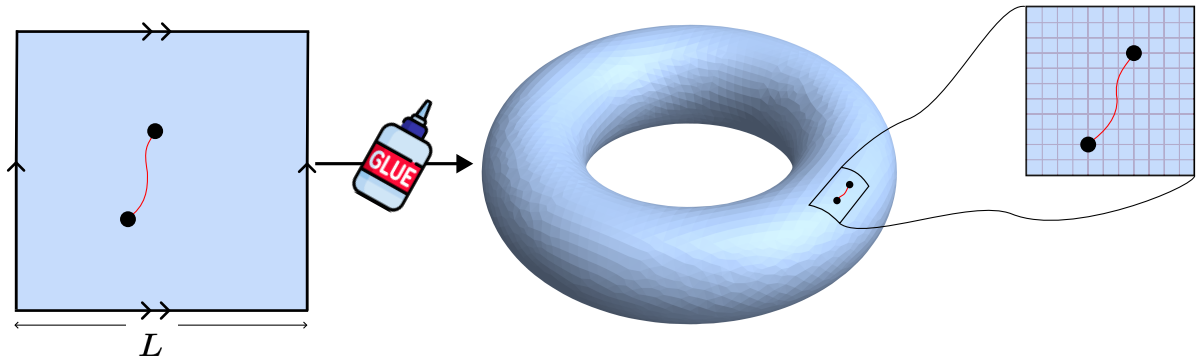

Figure 2.7.1: Torus Geometry

To recover the euclidean results, $\frac{|x_1-x_2|}{L}$ must approach zero, as shown on the right of Fig. 2.7.1. Meaning that in our simulations, we either consider small distances or large systems. In chapter 3, we will see how the idea that some geometrical objects are locally similar to flat space leads to a new set of mathematical tools, called differential geometry.

[15] Operator with the lowest conformal dimension

[16] For more information on 2 dimensional CFTs on the Torus see [16]

Chapter 3

The Art of Building Lagrangians

In a weakly coupled theory, the spectrum can usually be organized as a function of momentum. In the case of strongly coupled CFT, this is often not the case and therefore most analytical method are limited to the lower end of the spectrum. To solve this problem, in the case of a CFT with $U(1)$ symmetry, Hellerman *et al.* [9] proposed that in the large $U(1)$ charge sector the CFT could be described by a superfluid phase. In this chapter we use geometrical arguments, first proposed by Monin *et al.* [10], to describe a CFT with $U(1)$ symmetry in terms of the so called Goldstone modes.

3.1 Review of Differential Geometry

On the following sections we review relevant concept in differential geometry. Because the field of differential geometry is vast, in this exposé, we will focus on the mathematical tools that play a direct role on the construction of the Lagrangian that can describe a system where a symmetry is spontaneously broken. For a more detailed guide see [20].

3.1.1 Basic Definitions

Differential geometry is about extending the familiar notions of vectors and derivatives from $\mathbb{R}^n$ to general spaces. A **manifold**, $\mathcal{M}$, is an n-dimensional space that locally looks like an open disk in $\mathbb{R}^n$[1].

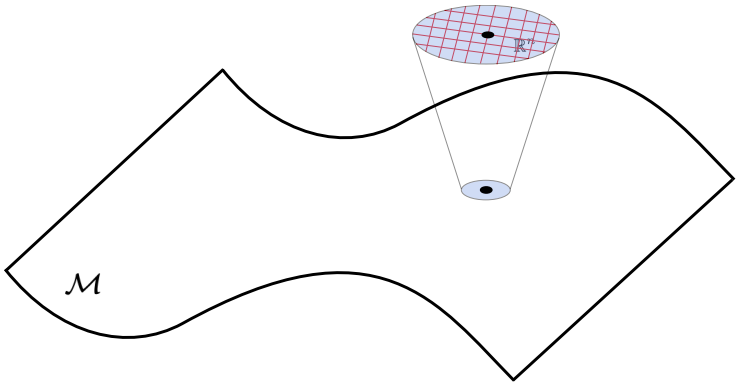

Figure 3.1.1: Mental picture of a Manifold

[1]Mathematician would say: For every $p \in \mathcal{M}$, there exist a neighborhood containing p homeomorphic to an open disk in $\mathbb{R}^n$.

A curve on a manifold, which may represent the trajectory of a particle, can be defined as a map $U_p(t) : t \in [0,1] \to \mathcal{M}$. A vector field, X, is defined by its action on a generic function $f : \mathcal{M} \to \mathbb{R}^1$,

$$(X \cdot f)(p) \equiv \frac{d}{dt} f(U_p(t))\Big|_{t=0} \text{ if } \frac{dU_p(t)}{dt} = X \text{ and } U_p(0) = p. \tag{3.1.1}$$

Next, we consider all the curves that pass through p at $t = 0$ and compute the tangent vector at p for each of them. The set of all those generates a vector space, dubbed the tangent space at the point p, $T_p\mathcal{M}$. Because the manifold is, by definition, locally similar to $\mathbb{R}^n$ we can write Eq. 3.1.1 as

$$(X \cdot f)(p) \equiv \frac{d}{dt} f\left(x_p^i + t\Delta x^i + ...\right)\Big|_{t=0} = \Delta x^i \frac{\partial}{\partial x^i} f. \tag{3.1.2}$$

And, therefore, in coordinates a **vector field** can be expressed as $X = X^i \frac{\partial}{\partial x^i}$[2]. In Section 2.2, we showed that the generators of the conformal group are in general written as $X^i \partial_i$ which we can now identify as vector fields.

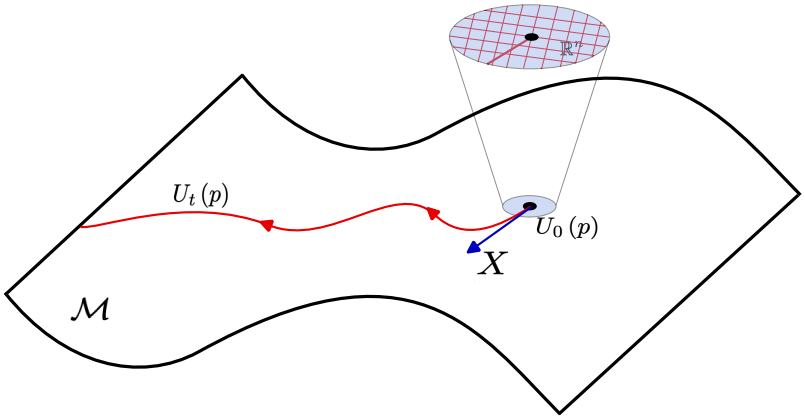

Figure 3.1.2: Mental picture of a vector field

The dual space to $T_p\mathcal{M}$, called cotagent space, $T_p^*\mathcal{M}$, is defined as the space of maps that receive a vector and output a number

$$\omega \in T_p^*\mathcal{M} : T_p\mathcal{M} \to \mathbb{R}$$
$$v \to \langle \omega, v \rangle = \omega_i v^i.$$

A particularly convenient choice of $\langle , \rangle$ is such that the basis of the cotangent space, dx^j, and the basis of the tangent space, $\frac{\partial}{\partial x^i}$, are orthogonal

$$\left\langle \frac{\partial}{\partial x^i}, dx^j \right\rangle = \delta_i^{\ j}. \tag{3.1.3}$$

A **1-form**, ω, is a covector that lives in the cotangent space, $\omega = \omega_i dx^i$. Vector and dual vectors can be combined into tensors by taking their tensor product. In fact, the tensor product of p 1-forms is called a p-form. Furthermore, it is convenient to define the wedge product, $\wedge$, as the antisymetrized tensor product

$$dx^i \wedge dx^j = \frac{1}{2!} dx^i dx^j - dx^j dx^i. \tag{3.1.4}$$

The wedge product is crucial in many calculations, but for our purposes it will appear in the definition of the exterior

[2] In the usual vector notation $\frac{\partial}{\partial x^i}$ are the vector basis and X^i are vector components.

derivative of a 1-form, $\omega = \omega_i dx^i$, and 2-form, $F = F_{ij} dx^i \wedge dx^j$,

$$d\omega = \frac{1}{2!}\frac{\partial \omega_i}{\partial x^j} dx^j \wedge dx^i \text{ and } dF = \frac{1}{3!}\left(\frac{\partial F_{ij}}{\partial x^k} dx^k \wedge dx^i \wedge dx^j\right). \tag{3.1.5}$$

Later in this chapter, we will define a quantity called coset representative Ω. After taking exterior derivatives of that representative, $d\Omega$, and wedge product of those derivatives, will provide the building blocks for constructing a description of a system where symmetries are spontaneously broken.

3.1.2 Metric Tensor, Vielbeins and Covariant Derivatives

The **metric**, g, is a symmetric tensor[3]. For a particular basis it can be written as $g_{\mu\nu} dx^\mu dx^v$. The metric is used to define a notion of distance on the curved manifold, it defines a geometry and consequently a volume form on the manifold,

$$\omega_{\text{Vol}} \equiv \sqrt{|\det g|} dx^1 \wedge dx^2 \wedge ... \wedge dx^n, \tag{3.1.6}$$

where n is the dimension of the manifold [4]. So far, we defined quantities in the basis induced by the choice of coordinates $\{\partial_\mu\}$. Under a change of basis the metric changes as

$$g_{\mu\nu} \to g_{ab} = e^\mu_a e^\nu_b g_{\mu\nu}. \tag{3.1.7}$$

Usually, we want to work in a locally flat manifold and therefore e^μ_a is chosen such that the new metric is either the Lorentzian metric, $e^\mu_a e^\nu_b g_{\mu\nu} = \eta_{ab}$, or the Euclidean metric, $e^\mu_a e^\nu_b g_{\mu\nu} = \delta_{ab}$. This choice of e^μ_a is known as **vielbeins**.

Building a dynamical Lagrangian requires derivatives. A naive approach for computing the derivative of a vector field, whose components are A^μ at a point x, would be to use the $\mathbb{R}^n$ definition,

$$\partial_\nu A^\mu = \lim_{a_\nu \to 0} \frac{A^\mu(x_\nu + a_\nu) - A^\mu(x_\nu)}{a_\nu}. \tag{3.1.8}$$

However, because the basis of the tangent space, $\boldsymbol{e}_\mu$, in which the vector field is defined, changes from point to point in the manifold, our definition of derivative must take that change into account. Having that in mind, the proper definition, called **covariant derivative**, ∇_ν, is given by

$$\nabla_\nu A^\mu e_\mu \equiv \lim_{a_\nu \to 0} \frac{A^\mu(x_\nu + a_\nu)\,\boldsymbol{e}_\mu(x_\nu + a_\nu) - A^\mu(x_\nu)\,\boldsymbol{e}_\mu(x_\nu)}{a_\nu} \tag{3.1.9}$$

$$= \left(\partial_\rho A^\mu + \boldsymbol{e}^\mu \cdot \partial_\rho \boldsymbol{e}_\nu A^\rho\right)\boldsymbol{e}_\mu = \left(\partial_\rho A^\mu + \Gamma^\mu_{\rho\nu} A^\rho\right)\boldsymbol{e}_\mu, \tag{3.1.10}$$

where Γ is called a connection, because it establishes a map between tangent spaces at different points on the manifold[5].

[3] $g_{\mu\nu} : T_p\mathcal{M} \times T_p\mathcal{M}$, $g^{\mu\nu} : T^*_p\mathcal{M} \times T^*_p\mathcal{M}$ and $g^\mu_\nu : T_p\mathcal{M} \times T^*_p\mathcal{M}$

[4] This volume form is invariant under change of coordinates

[5] For a function, f, $\nabla_\mu f = \partial_\mu f$. Furthermore we can generalize this covariant derivative for 1-form and higher order tensors, see [20] .

Using the covariant derivative, we can define two tensors, torsion T and curvature R whose component are

$$\begin{aligned} T^{\rho}_{\mu\nu} &= \Gamma^{\rho}_{\mu\nu} - \Gamma^{\rho}_{\nu\mu} \text{ and} \\ R^{\sigma}_{\rho\mu\nu} &= \partial_{\mu}\Gamma^{\sigma}_{\nu\rho} - \partial_{\nu}\Gamma^{\sigma}_{\mu\rho} + \Gamma^{\lambda}_{\nu\rho}\Gamma^{\sigma}_{\mu\lambda} - \Gamma^{\lambda}_{\mu\rho}\Gamma^{\sigma}_{\nu\lambda}, \text{ respectively.} \end{aligned} \tag{3.1.11}$$

Without going into the detailed calculation, one can prove that the connection is not uniquely defined. As a matter of fact, it transforms as a gauge field, implying the existence of some freedom in the choice of connection. In the presence of a metric tensor, g, the convenient choice of connection is such that $\nabla_{\mu} g_{\sigma\rho} = 0$ for all directions μ, this will ensure that $\Gamma^{\rho}_{\mu\nu} = \Gamma^{\rho}_{\nu\mu}$, implying that the torsion tensor vanishes and the connection can be written as

$$\Gamma^{\rho}_{\mu\nu} = \frac{1}{2} g^{\rho\lambda} \left(\partial_{\mu} g_{\nu\lambda} + \partial_{\nu} g_{\mu\lambda} - \partial_{\lambda} g_{\mu\nu} \right). \tag{3.1.12}$$

This choice is known as the Levi Civita connection.

3.1.3 Gauge Symmetry and Fiber Bundles

Electrodynamics is able to describe the dynamics between the movement of charged particles and changes in electromagnetic field. The vector potential A_{μ}, allows us to construct the 1-form $A \equiv A_{\mu} dx^{\mu}$. Applying the exterior derivative to A yields

$$dA = \frac{1}{2} \left(\partial_{\mu} A_{\nu} - \partial_{\nu} A_{\mu} \right) dx^{\mu} \wedge dx^{\nu}, \tag{3.1.13}$$

where $(\partial_{\mu} A_{\nu} - \partial_{\nu} A_{\mu})$ is the well known field strength tensor, $F_{\mu\nu}$. So, in the language of differential geometry, the field strength tensor is the components of a 2-form, F, defined as $F \equiv dA$. As an exercise, suppose we perform a transformation that shifts A_{μ} by $\partial_{\mu}\Lambda$, in the language of differential geometry, such transformation can be written as $A \to A + d\Lambda$, because, by definition of the exterior derivative, $d^2 = 0$, F remains invariant under $A \to A + d\Lambda$. The invariance of F for different A's is called gauge invariance.

Turns out that there is a more fundamental description of this gauge symmetry and to explain it one needs to introduce the concept of fiber bundles. The ingredients needed to construct a fiber bundle are a manifold and some fields, ϕ^i, whose values correspond to elements of a space $\mathcal{F}$, i.e. a scalar field takes values in $\mathcal{F} = \mathbb{R}$. Using the definition of a manifold, we can define a region, U, around a point, x, where the manifold is homeomorphic to $\mathbb{R}^n$. Inside that region, it is possible to express the fields as a function of those local coordinates, $\phi^i(x)$. That procedure of defining a region where the fields can be express as functions of local coordinates is called product between U and $\mathcal{F}$, a **fiber bundle** is a collection of these products. Once again, it is better to understand this concept by drawing a picture.

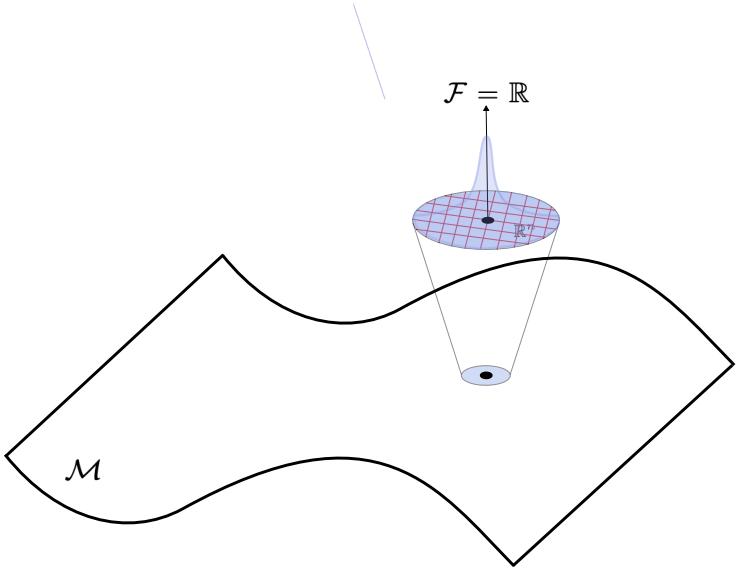

Figure 3.1.3: Mental Picture of a fiber bundle. Where the Fiber is the Real axis associated with the real scalar field

In physics, gauge symmetry is the redundancy we see in Maxwell equations. In math it is the freedom to choose a basis for the fiber. Consider a fiber bundle whose fiber is some N-dimensional vector space. At each point x we can express the field in terms of its local components, $\phi^i(x)$, and a basis, e_i, called frames of the fiber. With that in mind, the field can be written as

$$\phi = \phi^i(x)\, e_i. \tag{3.1.14}$$

Naturally, the frames of the fiber can change as we move from point to point in the manifold. The difference in frames, δe_i, as we move from a point with coordinates x^μ to an infinitesimally close point with coordinates $x^\mu + \delta x^\mu$ must be proportional to δx^μ and, because we can always write the new basis as a linear combination of the old basis, δe_i can be written as

$$\delta e_i = e_j A^j_{i\mu} \delta x^\mu. \tag{3.1.15}$$

The quantity $A^j_{i\mu} dx^\mu$ is defined as the connection of the bundle and it establishes a relation between the frame vector space in a point and the frame vector space in another point. Similarly to section 3.1.2, the connection allows us to define the derivative of ϕ, see [21], as

$$\begin{aligned} D\phi &= e_i \left(\partial_\mu \phi^i + A^i_{j\mu} \phi^j\right) dx^\mu \\ &= e_i \left(D_\mu \phi\right)^i dx^\mu, \end{aligned} \tag{3.1.16}$$

which coincides with the covariant derivative for the gauge potential given by $A^i_{j\mu}$. The gauge symmetry reflects the ambiguity of the choice of the basis, e_i. For example, if we rotate the basis by a matrix, g, such that $e_i \to e_k \left(g^{-1}\right)_{ki}$, then the components of the field transform as $\phi^i \to g^{ij}\phi^j$, leaving the covariant derivative invariant.

From this section one can take two lessons. The first is that gauge symmetry is a purely geometric phenomena. The second is that including internal symmetries requires defining a covariant derivative. With this section we end the mathematical introduction to differential geometry. In the following section, we will formalize the concept of spontaneously broken symmetries in the language of non-linearly realized symmetries and Goldstone/Higgs modes.

3.2 Symmetry Modes and Non-Linearly Realized Symmetries

Consider the theory of a complex field, $\phi(x)$, whose Lagrangian is

$$\mathcal{L} = \partial_\mu \phi^* \partial^\mu \phi + V(\phi), \tag{3.2.1}$$

with $V(\phi) \equiv M^2 \phi^* \phi + \lambda (\phi^* \phi)^2$, $M^2 < 0$ and $\lambda > 0$. Obviously, this theory has $U(1)$ symmetry meaning that $\mathcal{L}$ is invariant under $\phi(x) \to e^{i\alpha}\phi(x)$. The ground-state (configuration of ϕ that minimizes the energy) is a family $\phi_\theta(x) = v e^{i\theta}$, where $v = \sqrt{-\frac{M^2}{2\lambda}}$, and different configurations can be related by a $U(1)$ transformation. Therefore, despite having a Lagrangian that is invariant under $U(1)$, the ground-state spontaneously breaks that symmetry.

In general, we can decompose a complex field into a radial and angular components

$$\phi(x) = (v + \sigma(x)) e^{i\theta(x)}. \tag{3.2.2}$$

Plugging Eq. 3.2.2 into the Lagrangian, we arrive at

$$\mathcal{L} = (\partial_\mu \sigma)^2 + (v+\sigma)^2 (\partial_\mu \theta)^2 + M^2 (v+\sigma)^2 + \lambda (v+\sigma)^4. \tag{3.2.3}$$

At low energies when θ and σ are small, the theory of a complex field can be described by a massive mode σ, called **Higgs mode**, and a massless mode π, called **Goldstone mode**.

Non-linearly realized symmetries are characterized by the Goldstone modes, associated with the spontaneously broken symmetries. These do not transform homogeneously. In other words, the configuration where θ is zero is not mapped to itself after a transformation. In the sections that follow, we will develop a method, named **coset construction**, first proposed in [22, 23]. The coset construction will allow us to start from the broken symmetries and builds a low energy action for the Goldstone bosons associated with those broken symmetries.

3.3 Coset Construction for Global Symmetries

Assume that a theory is invariant under a group, G. When a set of symmetries is spontaneously broken the vacuum of the theory is only invariant under a subgroup, $H \subset G$[6]. For simplicity sake, we will call the set of generators of H by V^a and the remaining generators of G by A^i. Furthermore, we also assume the following commutation relations $\left[V^a, V^b\right] = i f^{abc} V^c$, $\left[A^i, A^j\right] = i f^{ijk} A^k + i f^{ija} V^a$ and $\left[V^a, A^i\right] = i f^{aij} A^j$ [7].

As discussed in Section 3.2, at low enough energy, a theory with spontaneously broken symmetries can be described by a set of massless fields, π^i, called Goldstone bosons. The coset construction [10, 24–26] starts by stating that those fields parametrize the coset, G/H. Thus, we can write $\Omega \in G/H$ as

$$\Omega(\pi) = e^{i\pi A}. \tag{3.3.1}$$

The left action of an element g of G on an element of the coset $\Omega(\pi)$, will not, in general, be an element of the coset. Therefore, in order to maintain consistency, the transformation of Ω needs to be connected

$$\Omega(\tilde{\pi}) \equiv g\Omega(\pi) \to g \cdot \Omega(\pi) U^\dagger(g, \pi), \tag{3.3.2}$$

where $U^\dagger(g,\pi) \in H$ will in general depend on the Goldstone field and the element g. Its job is to project $g\Omega$ onto the same representation of the coset G/H.

[6] The terminology would be that the symmetries in G are non-linearly realized and the symmetries in H are linearly realized. In the case of a complex scalar field the non-linear modes correspond to the π in Eq. 3.2.3 whereas the linear modes correspond to σ.

[7] This is just the statement that H is a subgroup of G. The constants f^{abc} are such that $\text{Tr}\left(V^a V^b\right) = \delta^{ab}$ and $\text{Tr}\left(A^i A^j\right) = \delta^{ij}$.

From Eq. 3.3.2, we conclude that the Goldstone fields will transform in a non-linear fashion. Using the associative property of the group, we can prove that

$$U\left(g_1 g_2, \pi\right) = U\left(g_2, \tilde{\pi}\left(g_1, \pi\right)\right) U\left(g_1, \pi\right) \text{ and } U\left(1, \pi\right) = 1. \tag{3.3.3}$$

Moreover, we require that the compensating term, $U\left(h, \pi\right)$, is h when $h \in H$. Or in other words, we want $\Omega\left(\tilde{\pi}\right) = h\Omega\left(\pi\right)h^{-1}$, since it implies that the Goldstone boson transform linearly under the unbroken symmetries[8]

$$\pi^i A^i \to \pi^i h A^i h^\dagger = \pi^i D^{ij}\left(h\right) A^j. \tag{3.3.4}$$

On the other hand, the action of the unbroken symmetries on the fields is very complicated. Therefore, we want to use $\Omega\left(\pi\right)$ to build quantities that transform covariantly, according to Eq. 3.3.2. The trivial choice would be $\Omega^\dagger\Omega$, but that does not generate any interesting dynamics. In fact, the dynamics come from introducing terms with derivatives, but this raises a problem as $d\Omega$ is not covariant,

$$d\Omega \to d\left(g\Omega\left(\pi\right)U^\dagger\right) = gd\Omega U^\dagger + g\Omega dU^\dagger. \tag{3.3.5}$$

As explained in Section 3.1.3, to solve this problem we need to define a covariant derivative, $D\Omega$, by introducing a gauge connection, ω, $D\Omega \equiv d\Omega - i\Omega\omega$. A possible and very convenient choice of ω is the Maurer-Cartan 1-form, given by $\omega = -i\Omega^\dagger d\Omega$. With a simple calculation, we can show that the connection ω transforms as follows

$$\omega \to -i\left(g\Omega U^\dagger\right)^\dagger d\left(g\Omega U^\dagger\right) = -i\left(g\Omega U^\dagger\right)^\dagger\left(gd\Omega U^\dagger + g\Omega dU^\dagger\right) = U\omega U^\dagger - iUdU^\dagger, \tag{3.3.6}$$

which kills the extra term[9] in Eq. 3.3.5.

Although not mandatory, it is convenient to divide ω into the projection onto to the basis generated by V, ω_V, and the projection onto the basis generated by A, ω_A,

$$\omega \equiv \omega_V + \omega_A = \omega_V^a V^a + \omega_A^i A^i. \tag{3.3.7}$$

The ω_V is called longitudinal component and ω_A is called transverse component. From Eq. 3.3.6, it is straightforward to show that, under G, ω_V transforms like $\omega_V \to U\omega_V U^\dagger - iUdU^\dagger$ whereas ω_A transforms like $\omega_A \to U\omega_A U^\dagger$. Therefore, ω_A will be used to build the low energy action of the Goldstone modes whereas ω_V is used to couple the Goldstone modes to other existing fields.

3.4 Coset Construction for Spacetime Symmetries

Spontaneous breaking of internal symmetries is an extremely rich topic, but in some circumstances[10] we may be interested in spacetime symmetries being broken. In that case, the coset construction methodology has two subtleties [10, 25, 26]. The first appears because the coordinates, x^μ, always transforms non-linearly under translation. Meaning that the coset representative will always have a contribution, $e^{ix^\mu P_\mu}$, from translations[11].

[8] Can be seen by expanding the exponential $\Omega\left(\pi\right) = 1 + \frac{i\pi^i A_i}{1!} + \frac{\left(i\pi^i A_i\right)^2}{2!} + ...$

[9] $D\Omega \to gd\Omega h^\dagger + g\Omega dh^\dagger - ig\Omega h^\dagger\left(hAh^\dagger - ihdh^\dagger\right) = gd\Omega h^\dagger + g\Omega dh^\dagger - ig\Omega Ah^\dagger - g\Omega dh^\dagger = g\left(d\Omega - i\Omega A\right)h^\dagger = gD\Omega h^\dagger$.

[10] Most condensed matter systems, see [27]

[11] In Section 3.2, we showed that when the Goldstone mode, θ, associated with the broken $U\left(1\right)$ symmetry transformed like $\theta \to \theta + \alpha$. Similarly, when we perform a translation the coordinates, x^μ, transform in the same fashion, $x^\mu \to x^\mu + \alpha^\mu$ and that is the reason why we need to include them in the coset representative. However, that does not mean that translation symmetry is broken it means that the coordinates always transform non-linearly with translation.

The second, which we are going to discuss in detail later, is the mismatch between the number of Goldstone modes and the number of broken generators. For example, when the conformal symmetry spontaneously breaks to Poincaré, see Appendix A.1, the system only acquires one Goldstone mode despite five generators being broken[12].

In order to gain some intuition about the coset construction when spacetime symmetries are broken, consider a group G with both spacetime and internal symmetries. Assume further that the Poincaré group remains an unbroken subgroup of G. Following the notation in Section 3.3, we will call the internal broken generators of G by A^i, translations by P^μ, Lorentz transformation by $L^{\mu\nu}$, and the rest of unbroken generators by V^a. All that information allows us to write the coset space representative as

$$\Omega\left(\pi, x\right) = e^{ix_\mu P^\mu} e^{i\pi^i(x) A_i}. \tag{3.4.1}$$

The left action of g will, in general, also change the coordinates x and therefore the coset representative must transform like

$$\Omega\left(\pi\left(x\right), x\right) \to \Omega\left(\pi'\left(x'\right), x'\right) = g\Omega\left(\pi\left(x\right), x\right) U^{-1}\left(g, \pi\left(x\right)\right), \tag{3.4.2}$$

where U is an element of the unbroken group. Similarly to the internal symmetry we will compute the Maurer-Cartan 1-form and divide it into the transverse components, ω_P and ω_A, associated with the broken generators, and the longitudinal components ω_L and ω_V, associated with the unbroken generators[13],

$$\begin{aligned}\omega &= -i\Omega^\dagger d\Omega = \omega_P + \omega_L + \omega_V + \omega_A \\ &= \omega_P^\mu P_\mu + \frac{1}{2}\omega_L^{\mu\nu} L_{\mu\nu} + \omega_V^a V_a + \omega_A^i A_i.\end{aligned} \tag{3.4.3}$$

where ω_P^μ, $\omega_L^{\mu\nu}$, ω_V^a, ω_A^i are function of $\pi\left(x\right)$ and x^μ (See Appendix A.1)

The components of the Maurer-Cartan 1-form which transform in covariant fashion, ω_P and ω_A, will be used to build the Lagrangian. In particular, the volume form from Eq. 3.1.6 is no longer covariant and a new one must be built from covariant quantities such as ω_P^μ (*e.g.* $d\mu = \sqrt{\left|\det g\right|}\,\omega_P^1 \wedge \omega_P^2 \wedge ... \wedge \omega_P^n$). The coupling of the Goldstone fields to other fields is made via the covariant derivative

$$D\psi = \left(d + \omega_J + \omega_V\right)\psi. \tag{3.4.4}$$

As mentioned in the beginning of this section, when a spacetime symmetry is broken the number of Goldstone fields does not have to equal the number of broken generators. By definition the unbroken generators annihilate the vacuum, $V^a\left\langle\phi\right\rangle = 0$. The fluctuations of the vacuum are parametrized by the Goldstone modes $\pi_a\left(x\right)$ and therefore we can write any field configuration as

$$\phi = e^{i\pi^a(x) A_a}\left\langle\phi\right\rangle. \tag{3.4.5}$$

After expanding the exponential, we conclude that the small fluctuations, $\delta\phi$, are given by $i\pi^a\left(x\right) A_a\left\langle\phi\right\rangle$. Now, if there exist a choice of π^a's such that

$$\pi^a\left(x\right) A_a\left\langle\phi\right\rangle = 0, \tag{3.4.6}$$

then we can eliminate a one of the modes for each non-trivial solution of Eq. 3.4.6. An intuitive example, is to

[12] For internal symmetries, there is always one Goldstone mode per broken generator.

[13] This will be true if $[J, A] \sim \sum A$, $[V, A] \sim \sum A$ and $[P, A] \sim \sum P$, which for us will always be the case.

consider the x, y plane with a line at $x = 0$ [28]. In this setup both translation and rotation symmetry are broken. Now, suppose one performs a small local rotation around the origin,

$$\begin{pmatrix} \cos\theta & -\sin\theta \\ \sin\theta & \cos\theta \end{pmatrix} \begin{pmatrix} 0 \\ y \end{pmatrix} = \begin{pmatrix} -y\sin\theta \\ y\cos\theta \end{pmatrix} \approx \begin{pmatrix} 0 \\ y \end{pmatrix} - y\theta \begin{pmatrix} 1 \\ 0 \end{pmatrix}, \tag{3.4.7}$$

meaning that a local rotation can be undone by the appropriate local translation. The previous situation occurs whenever two unbroken generators are related by

$$[P^\mu, A^a] = if^{\mu ab}A_b + if^{\mu ab}V_b \tag{3.4.8}$$

where $f^{\mu ab}$ are the structure constants[14]. If we act with P_μ on Eq. 3.4.6, we get that

$$0 = iP_\mu \pi^a A_a \langle\phi\rangle = i\left[P_\mu, \pi^a A_a\right]\langle\phi\rangle = \left(\partial_\mu \pi^a - f_{\mu ba}\pi^b\right) A_a \langle\phi\rangle . \tag{3.4.9}$$

For example, when there is only nonzero, $f_{\mu 12}$. Then, π_2 can be written in terms of a derivative of π_1. The way to implement this procedure in the coset construction is to require that certain components of the Maurer-Cartan 1-form vanish. Consider the representative of the coset space to be parametrized by

$$\Omega(\pi, x) = e^{ix^\mu P_\mu} e^{i\pi^a A_a}. \tag{3.4.10}$$

The Maurer-Cartan 1-form read

$$\omega = \omega_P^\mu P_\mu + \omega_A^a A_a + \omega_V^a V_a, \tag{3.4.11}$$

where ω_P^μ, $\omega_A^a$and ω_V^a are function of the coordinates and Goldstone modes. In particular,

$$\omega_A^a = \left(\partial_\mu \pi^a - f_{\mu ba}\pi^b\right) dx^\mu, \tag{3.4.12}$$

meaning that $\pi^a(x) A_a \langle\phi\rangle = 0$ and $\omega_A^a = 0$ are equivalent conditions. These conditions are called **inverse Higgs constraints**. In general, if two broken generators are related by a commutator involving P^μ, one is able remove the redundant Goldstone fields by requiring that the respective components of the Maurer-Cartan vanish[15]. In Appendix A.1, we exemplify the use of this formalism to construct a theory with Conformal to Poincaré symmetry breaking.

3.5 Gauging Spacetime Symmetries

In principle, one could use a naive application of Section 3.4 to describe a CFT with spontaneous broken $U(1)$ symmetry as a dynamical Goldstone mode. Unfortunately, computing the Maurer-Cartan 1-form using that approach is very difficult. Instead, we will tackle the problem by gauging the spacetime symmetries, this eliminates the need to include the SCT generators which makes computing the Maurer-Cartan 1-form feasible. From an operational point of view, we move from a theory which is invariant under G to a theory invariant under G plus gauge symmetry. After performing the necessary calculation in the theory with more symmetry, we return to the theory invariant under G by applying a set of constraints. In Section 3.4, we considered the following coset representative

[14] $f^{\mu ab} = -f^{\mu ba}$

[15] In the example of the x, y plane with a string line at $x = 0$ we can verify that $[P, L] \sim \sum P$

$$\Omega\left(\pi,x\right)=e^{ix_{\mu}P^{\mu}}e^{i\pi^{i}(x)A^{i}}, \tag{3.5.1}$$

where x_μ are the local cartesian coordinates, π^i are the fields associated to the Goldstone bosons and A^i are the generators of broken symmetries. The local coordinates x_μ are not unique, such that we can choose the coordinates to be any function, $y^A\left(x\right)$, of x. Therefore, the coset representative can also be expressed as

$$\Omega\left(y,\pi,x\right)=e^{iy^{A}(x)P_{A}}e^{i\pi^{i}(x)A^{i}}. \tag{3.5.2}$$

The action of an element g of G on the new representative of the coset, given by Eq. 3.5.2, is

$$ge^{iy^{A}(x)P_{A}}=e^{iy^{A}(x')P_{A}}U^{-1}\left(x,g\right), \tag{3.5.3}$$

where U is an element of the subgroup of unbroken symmetries. However, according to [29–31], another way of looking at this transformations is to say that the x coordinates remains unchanged but the functions y^A get transformed into y'^A. This is the statement that y^A is a gauge field. More concretely, under a spacetime symmetry transformation g a gauge field $A_\mu\left(x\right)$ transforms as

$$gA_{\mu}\rightarrow gA_{\mu}g^{-1}+g\partial_{\mu}g^{-1} \tag{3.5.4}$$

and under a diffeomorphism , $x\rightarrow x'$, the gauge field transforms as

$$A_{\mu}\left(x\right)\rightarrow A'_{\mu}\left(x'\right)=A_{\nu}\left(x\right)\frac{\partial x^{\nu}}{\partial x'^{\mu}}. \tag{3.5.5}$$

As an example, consider the local gauged Poincaré group, whose commutation relations are

$$\begin{aligned}\left[L^{AB},L^{CD}\right]&=-i\left(\eta^{AD}L^{BC}-\eta^{AC}L^{BD}-\eta^{BD}L^{AC}+\eta^{BC}L^{AD}\right),\\ \left[L^{AB},P^{C}\right]&=-i\left(\eta^{AC}P^{B}-\eta^{BC}P^{A}\right),\\ \left[P^{A},P^{B}\right]&=0.\end{aligned} \tag{3.5.6}$$

The latin indices stand for the coordinates y^A. Following [32, 33] and the discussion in Section 3.1.3, introducing a gauge fields implies that the derivative is promoted to a covariant derivative with the connection $\tilde{e}_\mu^A$ and $\tilde{\omega}_\mu^{AB}$,

$$D_{\mu}=\partial_{\mu}+i\tilde{e}_{\mu}^{A}P_{A}+\frac{i}{2}\tilde{\omega}_{\mu}^{AB}L_{AB}. \tag{3.5.7}$$

The coset representative for a theory with Poincaré invariance and no broken symmetries is $\Omega=e^{iy^{A}(x)P_{A}}$ and the Maurer-Cartan 1-form yields

$$-i\Omega^{-1}D_{\mu}\Omega=e_{\mu}^{A}P_{A}+\frac{1}{2}\omega_{\mu}^{AB}L_{AB}, \tag{3.5.8}$$

where $e_\mu^A=\tilde{e}_\mu^A+\partial_\mu y^A-\tilde{\omega}_\mu^{AB}y_B$ and $\omega_\mu^{AB}=\tilde{\omega}_\mu^{AB}$. The longitudinal component $\frac{1}{2}\omega_\mu^{AB}L_{AB}$ must transform like a gauge connection under the Lorentz group (non-linearly), whereas the transverse component $e_\mu^AP_A$ must transform covariantly. Calling Λ an element of the Lorentz group, the previous statement reads [16]

$$e_{\mu}^{A}\rightarrow\Lambda_{B}^{A}e_{\mu}^{B}\text{ and }\omega_{\mu}^{AB}\rightarrow\Lambda_{C}^{A}\omega_{\mu}^{CD}\left(\Lambda_{D}^{B}\right)^{-1}-i\left(\Lambda\partial_{\mu}\Lambda^{-1}\right)^{AB}. \tag{3.5.9}$$

[16] To prove the following use $e_\mu^AP_A\rightarrow Ue_\mu^AP_AU^\dagger$, $\frac{1}{2}\omega_\mu^{AB}L_{AB}\rightarrow U\frac{1}{2}\omega_\mu^{AB}L_{AB}U^\dagger-iU\partial_\mu U^\dagger$ and $UU^\dagger=U^\dagger U=1$, where U is a element of the Lorentz group.

Therefore, the field e_μ^A transforms like a veilbein from Section 3.1.2 and it can be used to build a metric, $g_{\mu\nu} = e_\mu^A e_\mu^B \eta_{AB}$. The quantity ω_μ^{AB} transform like a connection, so it will be used to couple the theory to other fields.

In most theories with Poincaré invariance, such as general relativity (GR), the degrees of freedom e_μ^A and ω_μ^{AB} are not independent fields. In fact, the connection ω_μ^{AB} is expressed in terms of the veilbeins, e_μ^A. To remove this inconsistency, we need to consider the 2-form field strength tensor, whose components can be computed from $\Omega^{-1}\left[D_\mu, D_\nu\right]\Omega$. Carrying out the calculation we conclude that

$$F_{\mu\nu} = \Omega^{-1}\left[D_\mu, D_\nu\right]\Omega = iT_{\mu\nu}^A P_A + iR_{\mu\nu}^{AB} J_{AB}, \tag{3.5.10}$$

where $T_{\mu\nu}^A$, $R_{\mu\nu}^{AB}$ are the torsion and curvature tensors from GR, respectively. The simplest way to relate the connection to the veilbeins, is to require that the projection, $T_{\mu\nu}^A$, of the field-strength tensor onto P_A vanishes. This will allow us to express the connection as a function of the veilbeins and recover GR. As mentioned in Section 3.1.2, one can always choose the connection, Γ, such that the torsion is zero and Γ is expressed in terms of the metric. As expected, gauging the Poincaré symmetries leads to a theory of GR.

The system at hand will have scale invariance, so we must add a local gauged scale transformations, D, into the mix. Adding that symmetry introduces a new non-trivial commutation relation,

$$\left[D, P^A\right] = iP^A. \tag{3.5.11}$$

Moreover, another local gauged symmetry implies adding another connection, $\tilde{W}_\mu$, meaning that the covariant derivative becomes

$$D_\mu = \partial_\mu + i\tilde{e}_\mu^A P_A + \frac{i}{2}\tilde{\omega}_\mu^{AB} L_{AB} + i\tilde{W}_\mu D. \tag{3.5.12}$$

By choice, the Lorentz group will remain unbroken, meaning that the coset representative is $\Omega = e^{iy^A(x)P_A} e^{i\sigma D}$ and the Maurer-Cartan 1-form reads

$$\Omega^{-1} D_\mu \Omega = iE_\mu^A \left(P_A + \nabla_A \sigma D + \frac{1}{2} e^\sigma \omega_A^{BC} J_{BC}\right), \tag{3.5.13}$$

where $E_\mu^A = e^{-\sigma} e_\mu^A$, $\nabla_A \sigma = e^\sigma e_a^\mu \left(\partial_\mu \sigma + W_\mu\right)$. Computing the 2-form field-strength tensor yields

$$\Omega^{-1}\left[D_\mu, D_\nu\right]\Omega = iT_{\mu\nu}^A P_A + iR_{\mu\nu}^{AB} J_{AB} + iW_{\mu\nu} D. \tag{3.5.14}$$

Again, the only independent degrees of freedom are the veilbeins and the independent Goldstone modes. This is achieved by imposing the inverse Higgs constraints, $\nabla_A \sigma = 0$, and the geometric constraints $T_{\mu\nu}^A = 0$. Turns out, see [34], that this procedure leads to the action that is conformally invariant, which is a massive advantage of gauging the spacetime symmetries, since we did not have to include the SCT generators in our calculations.

In conclusion, by gauging the local spacetime symmetries we are able to obtain a conformally invariant theory without the inclusion of the generator for SCT, K^A, in the calculations[17]. From a operational point of view, the differences between gauging space time symmetries and the method described in Section 3.4 are the use of a covariant derivative and the need to impose additional constraints to ensure that the only independent fields are the veilbeins and Goldstone modes.

This ends the theoretical discussing about the coset construction, in the following section, we will apply this method to the case of a CFT with broken $U\left(1\right)$ symmetry.

[17] This will massively simplify the calculation in Section 3.6

3.6 Coset Construction for a CFT with Broken $U(1)$ Symmetry

After gaining some insight into the coset construction, we are ready to tackle the problem of constructing a 3 dimensional CFT with broken $U(1)$ symmetry [18]. The symmetry breaking pattern is

$$SO(4,1) \times U(1) \to SO(3) \times (D + \mu Q), \tag{3.6.1}$$

where conformal group, $SO(4,1)$, and $U(1)$, whose generator is Q, breaks into the Poincaré group, $SO(3)$, plus a modified dilation given by the mix $D + \mu Q$.

We will be interested in computing the correlators such as

$$\left\langle \mathcal{O}_Q^\dagger(+\infty)\, \mathcal{O}(x_1)\, \mathcal{O}(x_2)\, \mathcal{O}_Q(0) \right\rangle. \tag{3.6.2}$$

When inserted at the origin and infinity, the operators with charge under $U(1)$ can be recasted as boundary conditions on the path integral, see Fig. 3.6.1. The operator at the origin breaks translation invariance, P^μ, whereas the operator at infinity breaks SCT invariance, K^μ. Because all operators in question are scalar in nature, the system will remain invariant under rotations, $L_{\mu\nu}$. Under dilations, the operators at the origin and at infinity are stable, consequently the generator D may or may not be broken, our assumption is that D will break, but the linear combination $D + \mu Q$ will not. With this in mind, the generators are indentified as

$$\begin{cases} D + \mu Q,\ J_{\mu\nu} & \text{unbroken,} \\ D,\ K_\mu,\ Q,\ P_\mu & \text{broken.} \end{cases} \tag{3.6.3}$$

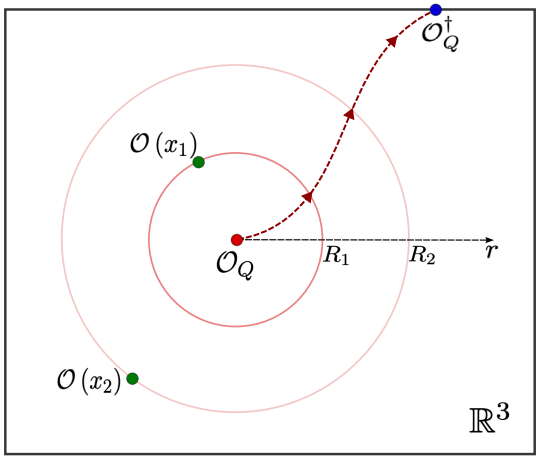

Figure 3.6.1: Visual interpretation for $\left\langle \mathcal{O}_Q^\dagger(+\infty)\, \mathcal{O}(x_1)\, \mathcal{O}(x_2)\, \mathcal{O}_Q(0) \right\rangle$ from the radial quantization perspective .

Performing a change of coordinates from planar, (x_0, x_1, x_2), to the cylinder, $\left(\tau \equiv R \log\left(\frac{|x|}{R}\right), \boldsymbol{n}\right)$[19], the correlator, see Fig. 3.6.2, can be interpreted as the following amplitude

$$\lim_{T\to+\infty} \langle Q, -T|\, \mathcal{O}(x_1)\, \mathcal{O}(x_2)\, |Q, T\rangle. \tag{3.6.4}$$

[18] This was first done in [10]

[19] $\boldsymbol{n}$ is a vector whose components are $\left(n_1 \equiv \frac{x_1}{|x|}, n_2 \equiv \frac{x_2}{|x|}\right)$. R is not the radius, we can think of R as a constant ensures that the dimensions of τ are consistent.

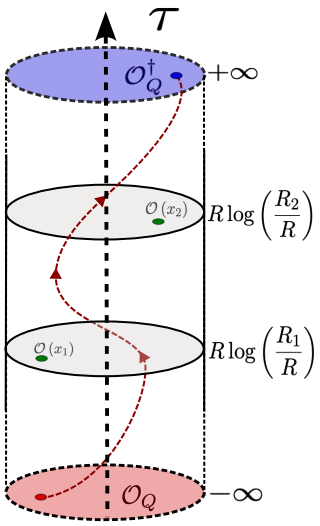

Figure 3.6.2: Visual interpretation for $\left\langle \mathcal{O}_Q^\dagger(+\infty)\,\mathcal{O}(x_1)\,\mathcal{O}(x_2)\,\mathcal{O}_Q(0)\right\rangle$ from the cylinder perspective.

It is possible to relate the generators on the plane, $\{P_\mu, L_{\mu\nu}, D, K_\mu, Q\}$, with the generators on the cylinder, $\left\{\hat{P}_\mu, \hat{L}_{\mu\nu}, \hat{D}, \hat{K}_\mu, \hat{Q}\right\}$. This is achieved by performing a change of variable in the differential representation of the operators, Eq. 2.2.3, and taking the limit $R \to +\infty$ (see [10] for more details)

$$\begin{aligned} D &= -R\hat{P}_0, & J_{0i} &= -R\hat{P}_i, \\ P_0 &= \hat{P}_0 + \frac{\hat{D}}{R} + \frac{\hat{K}_0}{2R^2}, & K_0 &= \frac{1}{2}\hat{K}_0 - R\hat{D} + R^2\hat{P}_0, \\ P_i &= \hat{P}_i + \frac{\hat{J}_{0i}}{R} - \frac{\hat{K}_i}{2R^2}, & K_i &= \frac{1}{2}\hat{K}_i + R\hat{J}_{0i} - R^2\hat{P}_i. \end{aligned} \tag{3.6.5}$$

Using the relations above, we can translate the plane symmetry breaking pattern, Eq. 2.2.3, to the following cylinder symmetry breaking pattern,

$$\begin{cases} \bar{P}_\nu = \hat{P}_\nu + \mu\delta^0_\nu\hat{Q},\ \hat{L}_{ij} & \text{unbroken} \\ \hat{L}_{0i},\ \hat{D},\ \hat{K}_\mu,\ \hat{Q} & \text{broken} \end{cases}. \tag{3.6.6}$$

Having identified the symmetry breaking pattern, we are in the position to write the representative for the coset as[20]

$$\Omega \equiv e^{iy^A(x)\bar{P}_A} e^{i\pi_1(x)D} e^{i\eta^B(x)L_{0B}} e^{i\pi(x)Q} = e^{iy^A P_A} e^{i\pi_1 D} e^{i\eta^B L_{0B}} e^{i\chi Q}, \tag{3.6.7}$$

where $\chi = \mu y^0 + \pi(x)$, π_1 and η^B are the Goldstone bosons[21]. Gauging spacetime symmetries implies introducing several gauge connection $\tilde{e}^A_\mu$, $\tilde{\omega}^{AB}_\mu$ and $\tilde{W}_\mu$, as well as the associated covariant derivative

$$D_\mu = \partial_\mu + i\tilde{e}^A_\mu P_A + \frac{i}{2}\tilde{\omega}^{AB}_\mu L_{AB} + i\tilde{W}_\mu D. \tag{3.6.8}$$

[20] From now on we will be dropping the hats

[21] Because we are using the gauged coset construction we do not need to include the SCT generators in the coset representative

The Maurer-Cartan 1-form (see Appendix A.2 for the explicit calculation) yields

$$-idx^{\mu}\Omega D_{\mu}\Omega = dx^{\mu}E_{\mu}^{A}\left(\bar{P}_{A}+\nabla_{A}\pi_{1}D+\nabla_{A}\chi Q+\nabla_{A}\eta^{a}L_{0a}+\frac{1}{2}\Omega_{A}^{ij}L_{ij}\right), \tag{3.6.9}$$

where

$$\begin{aligned}
E_{\mu}^{A} &= e^{-\pi_{1}}e_{\mu}^{B}\Lambda_{B}^{A}, \quad \nabla_{A}\chi = e^{\pi_{1}}e_{C}^{\nu}\Lambda_{A}^{C}\partial_{\nu}\chi-\mu\delta_{A}^{0}, \quad \nabla_{A}\pi_{1} = e^{\pi_{1}}e_{C}^{\nu}\Lambda_{A}^{C}\left(\partial_{\nu}\pi_{1}+\tilde{W}_{\nu}\right),\\
\nabla_{A}\eta^{a} &= e^{\pi_{1}}e_{C}^{\nu}\Lambda_{A}^{C}\left(\Lambda_{c}^{0}\Lambda_{d}^{a}\omega_{\nu}^{cd}+\left(\Lambda^{-1}\partial_{\nu}\Lambda\right)^{0a}\right),\\
\Omega_{A}^{ab} &= e^{\pi_{1}}e_{C}^{\nu}\Lambda_{A}^{C}\left(\Lambda_{a}^{c}\Lambda_{b}^{d}\omega_{\nu}^{ab}+\left(\Lambda^{-1}\partial_{\mu}\Lambda\right)^{ab}\right).
\end{aligned}$$

Although we will not compute it (see [10, 35] for the explicit calculation) the field strength tensor 2-form is of the form

$$F_{\mu\nu} \equiv \Omega^{-1}\left[D_{\mu},D_{\nu}\right]\Omega = iE_{\mu}^{A}E_{\nu}^{B}\left(T_{AB}^{C}P_{C}+R_{AB}^{CD}J_{CD}+W_{AB}D\right). \tag{3.6.10}$$

With every quantity of interest computed, we need to apply the geometrical constraints, $T_{AB}^{C}=0$ [22]. Because the commutation relations

$$\begin{aligned}
\left[\bar{P}_{A},L_{0B}\right] &= i\delta_{AB}\left(\mu Q-\bar{P}_{0}\right)\\
\left[\bar{P}_{0},D\right] &= -i\left(\bar{P}_{0}+\mu Q\right),
\end{aligned} \tag{3.6.11}$$

relate L_{0B} to Q and D to Q, we need to impose two inverse Higgs Constraints $\nabla_{A}\chi=0$ and $\nabla_{A}\pi_{1}=0$ resulting in the set of equations

$$\begin{cases}
\mu e^{-\pi_{1}} = \left(\delta^{ab}e_{b}^{\mu}e_{a}^{\nu}\partial_{\mu}\chi\partial_{\nu}\chi\right)^{\frac{1}{2}},\\
\beta_{i} = \frac{e_{i}^{\mu}\partial_{\mu}\chi}{e_{0}^{\nu}\partial_{\nu}\chi},\\
\tilde{W}_{\nu} = -\partial_{\nu}\pi_{1}.
\end{cases} \tag{3.6.12}$$

Having applied the necessary constraints we are left with two independent fields, e_{μ}^{A} and χ. The invariant rank 2 tensor at lowest order in $\partial\chi$ is

$$E_{\mu}^{A}E_{A}^{\nu} = \mu^{-2}\left(g^{\rho\sigma}\partial_{\rho}\chi\partial_{\sigma}\chi\right)g_{\mu}^{\nu}, \tag{3.6.13}$$

where g is the metric of $\mathbb{R}\times S^{2}$. Therefore, an invariant volume measure would be $\mu^{3}\sqrt{\det\left(E_{\mu}^{A}E_{A}^{\nu}\right)}=\sqrt{\det g}\left(\partial^{\mu}\chi\partial_{\mu}\chi\right)^{\frac{3}{2}}$, meaning that at lowest order action is

$$S = \frac{c_{1}}{6}\int d^{3}x\sqrt{\det g}\left(\partial^{\mu}\chi\partial_{\mu}\chi\right)^{\frac{3}{2}}, \tag{3.6.14}$$

where c_{1} is a model dependent coefficient. The most effective way of building the sub-leading terms is to notice that this is an effective theory of gravity whose metric, $\hat{g}$, given by $\hat{g}=\left(\partial^{\mu}\chi\partial_{\mu}\chi\right)g$ and the lowest order action can be written

[22] $T_{AB}^{C}=0$ allows us to write $\tilde{\omega}_{\mu}^{AB}$ as a function of $\tilde{W}_{\mu}$ and e_{μ}^{A}.

$$S = \frac{c_1}{6}\int d^3x\sqrt{\det \hat{g}}. \tag{3.6.15}$$

As discussed at the end of Appendix A.1, the next order correction will be given in terms of the modified curvature tensor $\hat{R}^{\rho}_{\mu\nu\sigma}$ and its contraction , $\hat{R}_{\mu\nu}$ and $\hat{R}$,

$$S = \int d^3x\sqrt{\det \hat{g}}\left(\frac{c_1}{6} - c_2\hat{R} + c_3\hat{R}^{\mu\nu}\partial_\mu\chi\partial_\nu\chi + O\left(R^2\right)\right), \tag{3.6.16}$$

where c_2 and c_3 are other model dependent coefficients. For metrics that are related by a Weyl transformations, $\hat{g} \to gf\left(\phi\left(x\right)\right)$, one can express the transformed Ricci scalar, $\hat{R}_{\mathsf{s}}$, and Ricci tensor, $\hat{R}_{\mu\nu}$, as a function of the original quantities and the covariant derivative ∇^μ on $\mathbb{R}\times S^2$. The relation is as follows

$$\begin{aligned}\hat{R}_{\mu\nu} = R_{\mu\nu} + \frac{f^{''}f - \left(f'\right)^2}{2f^2}\left(\left(2-d\right)\partial_\mu\phi\partial_\nu\phi - g_{\mu\nu}\partial^\rho\phi\partial_\rho\phi\right) + \frac{f'}{2f}\left(\left(2-d\right)\nabla_\mu\partial_\nu\phi - g_{\mu\nu}\nabla^\rho\nabla_\rho\phi\right) + \\ + \frac{1}{4}\frac{\left(f'\right)^2}{f^2}\left(d-2\right)\left(\partial_\mu\phi\partial_\nu\phi - g_{\mu\nu}\partial_\rho\phi\partial^\rho\phi\right)\end{aligned} \tag{3.6.17}$$

and

$$\hat{R}_s = \frac{1}{f}R_{\mathsf{s}} + \frac{1-d}{f}\left(\frac{f^{''}f-\left(f'\right)^2}{f^2}\partial^\mu\phi\partial_\mu\phi + \frac{f'}{f}\nabla^\mu\nabla_\nu\phi\right) + \frac{1}{4f}\frac{\left(f'\right)^2}{f^2}\left(d-2\right)\left(1-d\right)\partial_\mu\phi\partial^\mu\phi. \tag{3.6.18}$$

In the limit $R\to\infty$, the effective metric reduces to

$$\hat{g} = \begin{pmatrix} 1 & 0 & 0 \\ 0 & -R^2 & 0 \\ 0 & 0 & -R^2\sin^2\theta \end{pmatrix}\left(\partial\chi\right)^2, \tag{3.6.19}$$

where $\partial\chi = \left(g^{\mu\nu}\partial_\mu\chi\partial_\nu\chi\right)^{1/2}$. By identifying, $\phi = \partial\chi$, $f = \left(\partial\chi\right)^2$, $d=3$ and g as the metric of $\mathbb{R}\times S^2$, we obtain

$$\begin{aligned} R_{\mathsf{s}} &= \frac{R_{\mathsf{s}}}{\left(\partial\chi\right)^2} + \frac{2\partial^\mu\left(\partial\chi\right)\partial_\mu\left(\partial\chi\right)}{\left(\partial\chi\right)^4} - 2\frac{\nabla^\mu\nabla_\mu\left(\partial\chi\right)}{\left(\partial\chi\right)^2}, \\ \hat{R}_{\mu\nu} &= R_{\mu\nu} + \frac{2}{\left(\partial\chi\right)^2}g_{\mu\nu}\partial^\rho\left(\partial\chi\right)\partial_\rho\left(\partial\chi\right) - \frac{1}{\left(\partial\chi\right)}\left(\nabla_\mu\partial_\nu\left(\partial\chi\right) + g_{\mu\nu}\nabla^\rho\nabla_\rho\left(\partial\chi\right)\right). \end{aligned} \tag{3.6.20}$$

In our calculations we neglect the terms that contain $\nabla\partial\chi$ since they vanish at lowest order using the equation of motion[23]. With all the previous considerations, the action, in euclidean space and for the $U(1)$ broken symmetry, become

Action for a CFT with broken $U(1)$ - Superfluid Action

$$
\begin{aligned}
S &= \int d^3x\sqrt{\det g}\,(\partial\chi)^3\left(\frac{c_1}{6} - c_2\hat{R} + c_3\hat{R}^{\mu\nu}\partial_\mu\chi\partial_\nu\chi + O\left(R^2\right)\right) = \\
&= -\frac{c_1}{6}\int d^3x\sqrt{\det g}\,(\partial\chi)^3 + \\
&+c_2\int d^3x\sqrt{\det g}\,(\partial\chi)^3\left(\frac{R_{\mathsf{s}}}{(\partial\chi)^2} + \frac{2\partial^\mu(\partial\chi)\,\partial_\mu(\partial\chi)}{(\partial\chi)^4}\right) + \\
&-c_3\int d^3x\sqrt{\det g}\,(\partial\chi)^3\frac{1}{(\partial\chi)^4}\left[R^{\mu\nu}\partial_\mu\chi\partial_\nu\chi + \frac{2}{(\partial\chi)^2}g^{\mu\nu}\partial_\mu\chi\partial_\nu\chi\partial^\rho(\partial\chi)\,\partial_\rho(\partial\chi) - \right. \\
&\left. -\frac{1}{(\partial\chi)}\left(\nabla^\mu\partial^\nu(\partial\chi)\right)\partial_\mu\chi\partial_\nu\chi\right],
\end{aligned}
\tag{3.6.21}
$$

where $\partial\chi \equiv \left(-\partial_\mu\chi\partial^\mu\chi\right)^2$, $g = \begin{pmatrix} 1 & 0 & 0 \\ 0 & R^2 & 0 \\ 0 & 0 & R^2\sin^2\theta \end{pmatrix}$, $R_{\mu\nu} = \begin{pmatrix} 0 & 0 & 0 \\ 0 & 1 & 0 \\ 0 & 0 & \sin^2\theta \end{pmatrix}$ and $R_{\mathsf{s}} = \frac{2}{R^2}$.

The superfluid action is an universal one, in the sense that, the information about the model is encoded only in the coefficients c_1, c_2 and c_3. Together with a technique called large charge expansion, this action provides a systematic way of calculating the conformal dimension and OPE coefficients of charged operators . In Chapter 4, we will dive into detailed calculations and the interesting properties associated with the expansion around large quantum numbers.

[23] Those can be obtain by minimizing action on Eq. 3.6.15, resulting in the equation of motion $\nabla^\mu\partial_\mu\chi = 0$

Chapter 4

Expansion in Large Quantum Numbers

Perturbative techniques around small quantities have been around since the dawn of QFT, successfully matched experiments, such as the magnetic moment of the electron, with remarkable precision [36]. Unfortunately perturbative methods require weakly coupled theories. One example of its shortcomings is quantum chromodynamics. Aiming to find non-perturbative methods, Hooft [37, 38] pioneered what is now known as the large N expansion, which consist of solving a theory with $SU(N)$ symmetry when N is infinite and expanding its predictions in powers of $\frac{1}{N}$. Years later, the idea of the large N expansion was crucial in the development of the AdS/CFT conjecture by Maldacena [1]. More recently, Alday *et al.* [5, 6, 8] used the large spin expansion to compute the large spin spectrum of a CFT. Recently and relevant to this thesis, Cuomo and others (in [9, 10, 35, 39]) developed a novel approach based on saddle point computation around the large $U(1)$ charge sector.

4.1 Invitation to Large Quantum Number Expansion

In this section we will motivate the use of perturbative techniques in the large quantum number limit. Before tackling the full problem, it is pedagogical to consider a toy model in which the fundamental ideas can be easily discussed, the simple rigid rotor model [10] whose Lagrangian is

$$\mathcal{L}\left[\theta,\dot{\theta},\dot{\phi}\right]=\frac{1}{2}\left(\dot{\theta}^2+\dot{\phi}^2\sin^2\theta\right). \tag{4.1.1}$$

The eigenfunctions of this Hamiltonian are the spherical harmonics, $Y_{lm}(\theta,\phi)$, with corresponding eigenvalues, $E_{lm}=\frac{m(m+1)}{2}$. Our goal is to derive, in a semiclassical context, the spectrum. Throughout that process, we will develop some techniques and insight that will prove useful in the large charge limit of a CFT.

The equation of motion for ϕ [1] tells us that the corresponding conjugate momentum, $p_\phi=\dot{\phi}\sin^2\theta$, is conserved. Canonical quantization of ϕ and p_ϕ implies that p_ϕ can only take integer values, m. For reasons that will become apparent later, the energy of a state with momentum m is connected to the probability amplitude of the system going from a configuration $|\theta_i,m\rangle$, at $-\frac{T}{2}$, to a configuration $|\theta_f,m\rangle$, at $\frac{T}{2}$. In the path integral formulation, this amplitude is written as

$$\langle\theta_f,m|\,e^{-iHT}\,|\theta_i,m\rangle=\int_{\theta,\phi(-T/2)=\theta_i,\phi_i}^{\theta,\phi(T/2)=\theta_f,\phi_f}D\theta D\phi\,e^{-im(\phi_f-\phi_i)}e^{i\int dt\mathcal{L}}. \tag{4.1.2}$$

[1] $\frac{d}{dt}\left(\dot{\phi}\sin^2\theta\right)=0$

For the upcoming analysis and simulations it is convenient to work in imaginary time, which can be achieved via the Wick rotation $t \to -it$. In imaginary time, the amplitude in Eq. 4.1.2 becomes

$$\langle \theta_f, m | \, e^{-HT} \, | \theta_i, m \rangle = \int_{\theta,\phi(-\tau/2)=\theta_i,\phi_i}^{\theta,\phi(\tau/2)=\theta_f,\phi_f} D\theta D\phi \, e^{-(\int dt \mathcal{L} + im(\phi_f - \phi_i))}. \tag{4.1.3}$$

Organizing the different field configurations by their energy E_i, with n-th excited state having energy E_n, we can express the amplitude as

$$\langle \theta_f, m | \, e^{-HT} \, | \theta_i, m \rangle = \sum_n c_n e^{-E_n T}, \tag{4.1.4}$$

implying that for a long enough time the path integral is dominated by lowest energy configuration,

$$\lim_{\tau \to +\infty} \langle \theta_f, m | \, e^{-HT} \, | \theta_i, m \rangle = c_0 e^{-E_0 T} \left(1 + O\left(e^{-(E_1 - E_0)T} \right) \right). \tag{4.1.5}$$

In particular, we can try to expand the path integral around the field configuration, $\{\theta_s, \phi_s\}$, that extremizes the action

$$\theta_s = \theta_0 \quad \text{and } \phi_s(t) = -imt + \phi_0, \tag{4.1.6}$$

such that the action is

$$\int d\tau \mathcal{L} + im(\phi_f - \phi_i) = \frac{1}{2} T m^2 \sin^2 \theta_0 - m^2 T. \tag{4.1.7}$$

Eq. 4.1.5 implies that the amplitude will not depend on the fields at the boundary. A convenient choice would be $\theta_i = \theta_f = \frac{\pi}{2}$, $\phi_i = \phi_s\left(-\frac{T}{2}\right)$ and $\phi_f = \phi_s\left(\frac{T}{2}\right)$. After perturbing the classical solutions with small excitations, ξ and η, around θ_s and ϕ_s, we are able to write the amplitude in Eq. 4.1.2 as

$$\langle \frac{\pi}{2}, m | \, e^{-iHT} \, | \frac{\pi}{2}, m \rangle = e^{\frac{m^2}{2} T} \int D\xi D\eta \exp\left\{ \int dt \left[\mathcal{L}^{\text{free}} + \mathcal{L}^{\text{int}} \right] \right\}, \tag{4.1.8}$$

where $\mathcal{L}^{\text{free}} = \frac{1}{2}\left(\dot{\xi}^2 + \dot{\eta}^2 + m^2 \xi^2 \right)$ is the kinetic term and $\mathcal{L}^{\text{int}} = \frac{m^2}{2}\left(\sin^2 \xi - \xi^2 \right) - \left(\frac{\dot{\eta}^2}{2} - im\dot{\eta} \right) \sin \xi^2$ is the interactive term. The lowest energy state can be computed from the equation

$$\begin{aligned} E_0(m) &= -\frac{1}{T} \log \langle \frac{\pi}{2}, m | \, e^{-iHT} \, | \frac{\pi}{2}, m \rangle \\ &= \frac{m^2}{2} + \frac{m}{2} + \Lambda_{\text{UV}} + \sum_n a_n \left(\frac{1}{m} \right)^n, \end{aligned} \tag{4.1.9}$$

where $\frac{m^2}{2}$ comes from the classical solution, $\frac{m}{2} + \Lambda_{\text{UV}}$ are due to the kinetic term and a_n are the numeric coefficient that appear after summing over all possible diagrams of order n. The interactions are responsible for $\sum_n a_n \left(\frac{1}{m} \right)^n$, since terms such as $\dot{\eta}\dot{\eta}\xi\xi$ will contribute with

$$m \int_{-\infty}^{+\infty} dt \, \langle \dot{\eta}\dot{\eta}\xi\xi \rangle \propto \int_{-\infty}^{+\infty} d\omega \, \omega^2 \frac{1}{\omega^2} \frac{m}{\omega^2 + m^2} = \frac{1}{m} \int_{-\infty}^{+\infty} d\omega \left(\sum_{n=0}^{+\infty} \left(\frac{\omega}{m} \right)^{2n} \right). \tag{4.1.10}$$

Because $\dot{\eta}\dot{\eta}$ terms cancel and terms coming from the interactions contribute with a sum in positive powers of $\frac{1}{m}$, the ground state energy for large m becomes

$$E_0(m) = \frac{m(m+1)}{2} + \Lambda_{\text{UV}} + \sum_{n=1}^{+\infty} a_n \left(\frac{1}{m}\right)^n . \tag{4.1.11}$$

Surprisingly, our perturbative approach yields the exact results for the first order correction.

4.2 Large Charge Expansion

Inspired by the surprising result in Section 4.1 and [9, 10, 40], we will try to compute the ground-state energy on the cylinder, equivalent to the conformal dimension on the plane, for a state with large $U(1)$ charge. In Section 3.6, we proved that a CFT with a broken $U(1)$ symmetry can be described by a Goldstone boson χ whose dynamics, at leading order, is fully determined by the Euclidean action, Eq. 3.6.21,

$$S[\chi] = -\frac{c_1}{6} \int_{-T/2}^{+T/2} dt \int_{S^2} d^2x \sqrt{\det g} \left(-\partial^\mu \chi \partial_\mu \chi\right)^{\frac{3}{2}} + \dots \tag{4.2.1}$$

The ground-state energy can be computed from the probability amplitude for the transition of a state with charge Q, at a time $-\frac{T}{2}$, to a state with charge Q, at a time $\frac{T}{2}$. As explained in Section 4.1, in the limit of $T \to \infty$, the integral does not depend on the specific configuration of fields at the boundary and therefore we may choose the initial and final states as we please. Similarly to the rigid rotor example, we can write the transition amplitude as

$$\langle Q| e^{-HT} |Q\rangle = \int D\chi \exp\left\{-S[\chi] - iQ(\chi_f - \chi_i)\right\}. \tag{4.2.2}$$

Because $\chi_f - \chi_i$ can be written as $\int_{-T/2}^{+T/2} dt\, \dot{\chi}$, the amplitude becomes

$$\langle Q| e^{-H\tau} |Q\rangle = \int D\chi \exp\left\{ - \int_{-T/2}^{+T/2} dt \int_{S^2} d^2x \sqrt{\det g} \left(\mathcal{L} + \frac{iQ}{4\pi R^2}\dot{\chi}\right)\right\}. \tag{4.2.3}$$

Recall that χ is defined as field $\pi(x,t)$ plus some contribution from a linear field $-i\mu t$, such that $\chi = -i\mu t + \pi$ [2]. The first term in χ is the saddle point solution and π are the fluctuations. According to that interpretation, it is possible to extract μ by requiring that the δS cancels the current $\frac{iQ}{4\pi R^2}$ when $\chi \to \chi + \delta\chi$,

$$\begin{aligned} \frac{Q}{4\pi R^2} &= \left.\frac{\partial \mathcal{L}}{\partial \dot{\chi}}\right|_{\chi = -i\mu t} \\ \frac{Q}{4\pi R^2} &= \frac{c_1}{2}\mu^2 - c_2 \frac{2}{R^2} + \mathcal{O}\left(\mu^{-2}\right) \end{aligned} \tag{4.2.4}$$

where c_2 comes from the sub-leading terms in Eq. 3.6.21.

[2] The it appear because we are working in imaginary time and $\dot{\chi} = -i\mu$

This equation can be solved perturbatively and the leading terms are

$$\mu R = \sqrt{\frac{2}{c_1}\left(\frac{Q}{4\pi} + 2c_2\right)} = \sqrt{\frac{Q}{2\pi c_1}}\left(1 + \frac{4\pi c_2}{Q} + O\left(Q^{-1}\right)\right), \tag{4.2.5}$$

consequently, when Q is large, $\mu R \backsim \sqrt{\frac{Q}{2\pi c_1}}$. Substituting Eq. 4.2.5 into Eq. 3.6.21, we are able to evaluate the action at the saddle point,

$$\begin{aligned} S_{\text{saddle}} &= \int_{-T/2}^{+T/2} dt \int_{S^2} d^2x \frac{\sqrt{\det g}}{R^3}\left(-\frac{c_1}{6}(\mu R)^3 + \frac{Q}{4\pi}\mu R + 2c_2 \mu R\right) \\ &= -\frac{T}{R}\left\{\frac{2}{3}\frac{1}{\sqrt{2\pi c_1}}Q^{\frac{3}{2}} + 8\pi c_2\left(\frac{Q}{2\pi c_1}\right)^{\frac{1}{2}} + O\left(Q^{-\frac{1}{2}}\right)\right\} \end{aligned} \tag{4.2.6}$$

The goal is to compute the conformal dimension on the plane, which, according to Eq. 3.6.5, is related to the energy by $\Delta_Q = RE_Q$, such that

$$\Delta_Q = -\frac{R}{T}\log\left\langle Q\right| e^{-H\tau}\left|Q\right\rangle, \tag{4.2.7}$$

After taking quantum fluctuations into account, the conformal dimension is

$$\Delta_Q = -\frac{R}{T}S_{\text{saddle}} - \frac{R}{T}\frac{1}{2}\log\left(-\partial_\tau^2 - \triangle_{S^2}\right), \tag{4.2.8}$$

where $\triangle_{S^2} = \frac{1}{R^2\sin\theta}\partial_\theta\left(\sin\theta\partial_\theta\right) + \frac{1}{R^2\sin^2\theta}\partial_\phi^2$. After the necessary calculation[3], we conclude that the conformal dimension for an operator with charge Q is

Conformal Dimensions of Charged Operator

$$\Delta_Q = \frac{2}{3}\frac{1}{\sqrt{2\pi c_1}}Q^{\frac{3}{2}} + 8\pi c_2\left(\frac{Q}{2\pi c_1}\right)^{\frac{1}{2}} - 0.0937254 + O\left(Q^{-\frac{1}{2}}\right). \tag{4.2.9}$$

Once again, this result is universal for a CFT with $U(1)$ broken symmetry. The only model dependent quantities are the coefficients c_1, c_2[4]. In order to test this prediction, we must specify a model, and we chose the three dimensional $O(2)$ model for reasons that will be explained in chapter 5.

[3] For a detailed calculation of $-\frac{1}{2}\log\left(-\partial_\tau^2 - \Delta_{S^2}\right)$ see Appendix A.3.

[4] The conformal dimension of charged operator in an arbitrary dimension was computed by Cuomo and can be found in [35].

Chapter 5

The $O(2)$ Model

The superfluid description of a CFT with spontaneously broken $U(1)$ symmetry predicts the conformal dimension, Eq. 4.2.9, of operators with large $U(1)$ charge. Our goal is to provide numerical evidence that supports this description, for which we require a testing ground. The simplest model that fulfills that role is the $O(2)$ model. Interestingly, in the 70s/80s, Kosterlitz and Thouless independently discovered that the $O(2)$ model exhibited a new kind of phase transition a topological phase transition, for which, they, together with Haldane, won the 2016's Nobel prize in Physics. We will mostly focus on the two dimensional $O(2)$ model, but the upcoming analysis can be easily generalized for three dimensions.

5.1 Lattice Formulation and Phase Transition

The $O(2)$ model is a lattice model[1] where the degrees of freedom, at every site, are two dimensional unit vectors, $\mathbf{S}_i$, usually parametrized by an angle

$$\boldsymbol{S}_i = (\cos\theta_i, \sin\theta_i)\,. \tag{5.1.1}$$

Those unit vectors are called spins. As described by the red arrows in the figure on the right, the spins only interact with their nearest neighbors and the strength of that interaction is given by $-\boldsymbol{S}_i \cdot \boldsymbol{S}_j$. This is translated into the Hamiltonian

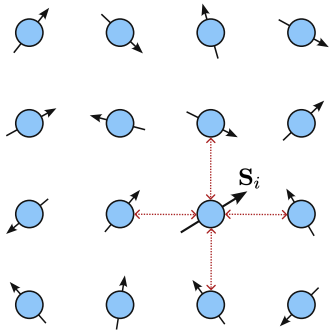

$$H_{\text{O2}}(\{\theta_i\}) = -\sum_{\langle i,j\rangle} \boldsymbol{S}_i \cdot \boldsymbol{S}_j = -\sum_{\langle i,j\rangle} \cos(\theta_i - \theta_j)\,, \tag{5.1.2}$$

where $\langle i,j\rangle$ is notation for summing when the site i and j are nearest neighbors[2]. The $U(1)$ symmetry is directly present in the Hamiltonian. Suppose one rotates all the spins by the same angle, α, because the difference between angles, $\theta_i - \theta_j$, remains unchanged and thus we conclude that the Hamiltonian is invariant under $\theta_i \to \theta_i + \alpha$.

[1] See Altland's book [41] for a very nice review on the $O(2)$ model, just be aware that he calls it XY model.

[2] $\langle i,j\rangle$ is defined such that interaction are only counted once. For example, in two dimension it only accounts for the neighbors in the up and right of each site.

In the continuum limit, the $O(2)$ model can be described by the Hamiltonian [42]

$$H_{\text{O2}} = \frac{1}{2}\int d^2\boldsymbol{r}\,(\nabla\theta(\boldsymbol{r}))^2\,, \tag{5.1.3}$$

where $\theta(\boldsymbol{r})$ is a continuous periodic field and $\boldsymbol{r} \equiv (x, y)$ is the position on the 2D plane. The equation of motion for $\theta(r)$ can be found using the Euler-Lagrange equations. It turns out that $\theta(\boldsymbol{r})$ is either a constant or a vortex like solution around a point, $\boldsymbol{r}_0$,

$$\oint_{\text{Closed path } C} d\boldsymbol{l}\cdot\nabla\theta(\boldsymbol{r}) = \begin{cases} 2\pi n & \text{if } \boldsymbol{r}_0 \text{ is inside } C \\ 0 & \text{otherwise} \end{cases}, \tag{5.1.4}$$

where n is an integer known as winding number. Solutions with $n = 1$ are called vortex, whereas $n = -1$ are called anti-vortex, Fig.5.1.1 a) and Fig.5.1.1 b) respectively.

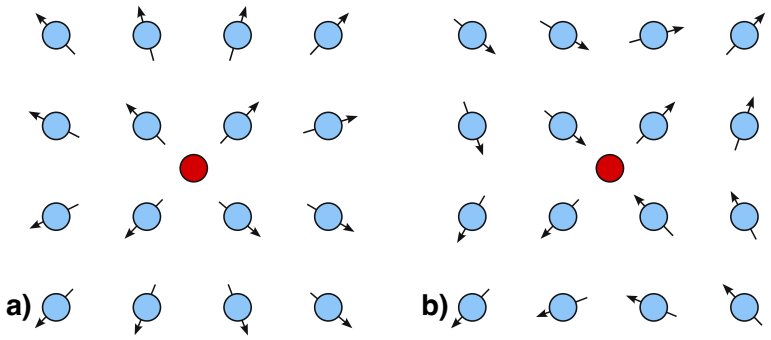

Figure 5.1.1: a) Lattice Vortex, b) Lattice Anti-Vortex

In the continuum limit, a vortex centered at the origin with winding number n corresponds to the configuration

$$\nabla\theta(x, y) = \frac{n}{(x^2 + y^2)^2}(y, -x)\,. \tag{5.1.5}$$

At the center of the vortex $\theta(x, y)$ is not defined. This gives us an excuse to introduces a natural UV cutoff, a, that corresponds to a small radius around the center of the vortex. The free energy of such configuration is given by

$$F_{\text{Free}} = \frac{\beta}{2}\int_0^L dr d\theta\, r\frac{n^2}{r^2} = \pi\beta n^2 \log\left(\frac{L}{a}\right) + F_{\text{center}}, \tag{5.1.6}$$

where L is a cutoff introduced to avoid long-distance IR divergences and F_{center} is the contribution from the center of the vortex, $r < a$. From the free energy, we conclude that the formation of vortices with a high winding number is not energetically favorable, hence we focus on $n = \pm 1$. Obviously, the vacuum state corresponds to the configuration of $\theta(\boldsymbol{r})$ that minimizes the energy, $\theta(\boldsymbol{r})$ is 0, but, due to thermal fluctuations, vortex can momentarily appear and disappear, the probability of that happening is given by

$$p_{\text{vortex}} = \left(\frac{L}{a}\right)^2 \frac{e^{-F_{\text{Free}}}}{\mathcal{Z}} = \frac{e^{-F_{\text{center}}}}{\mathcal{Z}}\left(\frac{L}{a}\right)^{2-\pi\beta}, \tag{5.1.7}$$

where $\mathcal{Z}$ is the partition function[3]. The term $\frac{e^{-F_{\text{center}}}}{\mathcal{Z}}$ only depends on the temperature, meaning we can think of them as normalization constants.

[3]The free energy F is a direct measure of the "score" for the competition between energy and entropy. The entropy of a system with one vortex is $\log\left(\frac{L}{a}\right)^2$ and the energy of a vortex is $E_{\text{vortex}} = \pi n^2 \log\left(\frac{L}{a}\right)$. The free energy, F, is given by $F = E - TS$ therefore when $TS > E$ collective behavior wins whereas when $E > TS$ the single particle behavior wins.

Surprisingly, the probability can either grow or decrease with L depending on whether $2-\pi\beta$ is greater or smaller than zero. Therefore, above a certain temperature vortices *proliferate*. Transitions that occur due to a proliferation of topological defects, such as vortices, are often called topological phase transitions.

The two dimensional $O(2)$ model was the first system to exhibit such transitions and therefore was named after the physicists Berezinskii, Michael Kosterlitz and David Thouless, as Kosterlitz-Thouless transition or BKT transition. Experiments with thin films of He-4 have shown a transition in the superfluid density of that material, which , according to Pollock *et al.* [43], is directly related to the winding number. Naturally, the simple arguments presented above do not tell the entire story. In fact, below the critical temperature the system is only composed of bounded vortex/anti-vortex pairs, whereas above the critical temperature the vortex and anti-vortex are unbounded, see Fig.5.1.2.

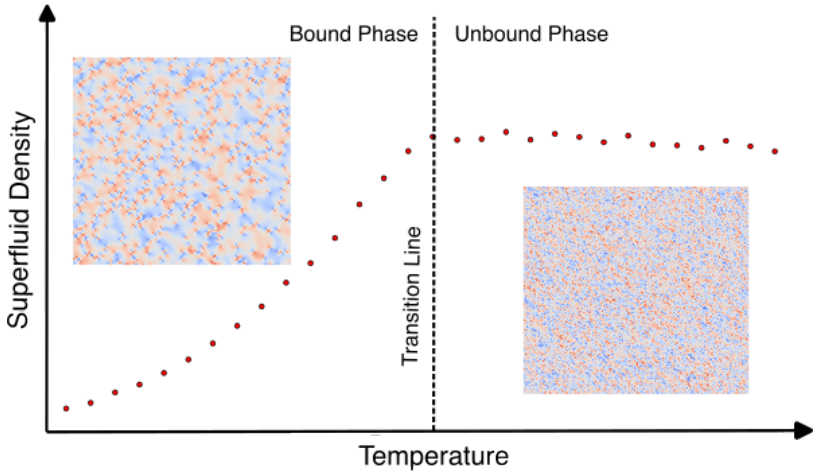

Figure 5.1.2: Phase diagram of the $O(2)$ model in two dimension.

Recall that the prime goal is to verify the validity of Eq. 4.2.9, which would require measuring the correlation function of charged operators, $\mathcal{O}_Q(x)$. Having chosen the three dimensional $O(2)$ model as the testing ground, we need to find a representation of an operator with charge Q, or in other words, a function $f(\theta_x)$ that transforms according to

$$f(\theta_x) \to e^{iQ\alpha} f(\theta_x), \text{ when } \theta_x \to \theta_x + \alpha. \tag{5.1.8}$$

The simplest possibility is $e^{iQ\theta(x)}$. In the continuum limit, the correlation function of charged operators is by

$$\left\langle \mathcal{O}_Q(x)\, \mathcal{O}_Q^\dagger(y) \right\rangle \equiv \left\langle e^{iQ\theta(x)} e^{-iQ\theta(y)} \right\rangle \underset{\text{CFT}}{=} \frac{1}{|x-y|^{2\Delta_Q}}. \tag{5.1.9}$$

In the language of path integrals, the lattice correlation function can be expressed as[4]

$$C_Q(\beta, x, y) \equiv \left\langle e^{iQ\theta_x} e^{-iQ\theta_y} \right\rangle = \frac{1}{\mathcal{Z}} \int D\theta e^{iQ\theta_x} e^{-iQ\theta_y} \exp\left[-\beta H_{\text{O2}}(\{\theta_i\})\right], \tag{5.1.10}$$

where $D\theta \equiv d\theta_1 ... d\theta_N$, N is the number of sites and $\mathcal{Z}$ is the partition function defined as $\mathcal{Z} \equiv \int D\theta \exp\left[-\beta H_{\text{O2}}(\{\theta_i\})\right]$.

[4] $\theta_x \equiv \theta(x)$ at the site whose position is x

Although Eq. 5.1.10 is a perfectly good representation of the correlation function, as an integral over the degrees of freedom θ_i, it is not the most computationally (numerical) friendly. Turns out that a more convenient way of representing the correlation function is by redefining the degrees of freedom as integer variables on the dual lattice[5].

5.2 Dual-Lattice Formulation

The map between the lattice formulation and the dual-lattice [44–47] formulation is quite an elegant one. Let us start by showing how it would work on the partition function, $\mathcal{Z}$, defined as

$$\mathcal{Z}(\beta) = \int \left(\prod_{i \in \text{Sites}} d\theta_i \right) \prod_{\langle i,j \rangle} \left[e^{\beta \cos(\theta_i - \theta_j)} \right]. \tag{5.2.1}$$

The first step, requires writing $e^{\beta \cos(\theta_i - \theta_j)}$ in terms of its Fourier components and momentum, k_{ij},

$$e^{\beta \cos(\theta_i - \theta_j)} = \sum_{k_{ij}=-\infty}^{+\infty} I_{k_{ij}}(\beta)\, e^{i k_{ij}(\theta_i - \theta_j)}, \tag{5.2.2}$$

where the modified Bessel functions of the first kind, $I_{k_{ij}}(\beta)$, obey $I_{k_{ij}}(\beta) = I_{-k_{ij}}(\beta)$ and

$$I_{k_{ij}}(\beta) = \sum_{m=0}^{+\infty} \frac{1}{\Gamma(m+1)\,\Gamma(m+|k_{ij}|+1)} \left(\frac{\beta}{2} \right)^{2m+|k_{ij}|}. \tag{5.2.3}$$

Plugging Eq. 5.2.2 into the partition function, Eq. 5.2.1, we get

$$\mathcal{Z}(\beta) = \sum_{\{k_{ij}\}} \left\{ \left(\prod_{\langle i,j \rangle} I_{k_{ij}}(\beta) \right) \prod_{i \in \text{Sites}} \left[\int d\theta_i \prod_{\substack{j \text{ Neighbor} \\ \text{of } i}} e^{i k_{ij}(\theta_i - \theta_j)} \right] \right\}. \tag{5.2.4}$$

Grouping the terms that have the same θ_k for all k, we are able to write the partition function as

$$\mathcal{Z}(\beta) = \sum_{\{k_{ij}\}} \left\{ \left(\prod_{\langle i,j \rangle} I_{k_{ij}}(\beta) \right) \prod_{i \in \text{Sites}} \left(\int d\theta_i \exp \left[i \sum_{\substack{j \text{ Neighbor} \\ \text{of } i}} k_{ij}\, \theta_i \mu_{ij} \right] \right) \right\}, \tag{5.2.5}$$

where μ_{ij} is the sign of the direction that connects the sites i with j [6]. Because the integral $\int_0^{2\pi} d\theta\, e^{iA\theta}$ is only different from zero when A is zero, the partition function becomes[7]

$$\mathcal{Z}(\beta) = (2\pi)^N \sum_{\{k_{ij}\}} \left\{ \left(\prod_{\langle i,j \rangle} I_{k_{ij}}(\beta) \right) \prod_{i \in \text{Sites}} \delta \left[\sum_{\substack{j \text{ Neighbor} \\ \text{of } i}} k_{ij} \mu_{ij} \right] \right\}. \tag{5.2.6}$$

[5] Set of all the directed line segments that connect the nearest neighboring sites

[6] In two dimensions, positive is defined as pointing right or up.

[7] $\delta(x) \equiv \begin{cases} 1 & x = 0 \\ 0 & \text{otherwise} \end{cases}$.

After some manipulations we have arrived at an expression for the partition function that does not depend on lattice variables, θ_i. However not all configurations from the space of k_{ij}'s contribute for the partition function. For a configuration to contribute for the partition it must obey the condition

$$\sum_{\substack{j \text{ Neighbor} \\ \text{of } i}} k_{ij}\mu_{ij} = 0, \text{ for every site } i. \tag{5.2.7}$$

An interpretation for Eq. 5.2.6 is to think of k_{ij} as set of arrows, where the number of arrows represents the modulus of k_{ij} and the direction in which the arrows are pointing is the sign of k_{ij}. In that framework, the condition in Eq. 5.2.7 is equivalent to the statement that at each site the number of arrows that point inwards has to be the same as the number of arrows that point outwards. An example of a configuration that would contribute to the partition function is displayed in Fig. 5.2.1 a), we will often refer to configurations that contribute for the partition function as **closed configurations**.

Computing the correlator, $C_Q(\beta, x, y)$, in Eq.5.1.10 can be divided into two tasks. The first requires computing the denominator, which corresponds to evaluating the partition function. In the dual lattice, this is synonymous with computing the weighted sum over all possible closed configurations,

$\mathcal{Z}(\beta) =$ 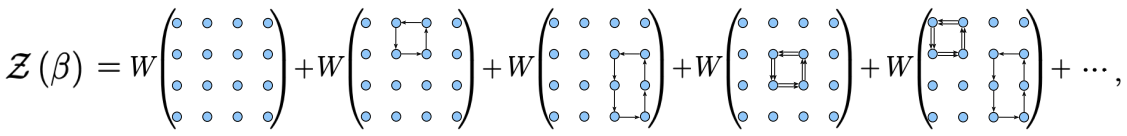 $+ \cdots,$

where the weight of each configuration is defined by the function

$$W(\{k_{ij}\}, \beta) = \prod_{\langle i,j \rangle} I_{k_{ij}}(\beta). \tag{5.2.8}$$

The second task, would be evaluating the numerator, N_Q, in Eq. 5.1.10. The explicit formula is

$$N_Q(\beta, x, y) = \int \left(\prod_{i \in \text{Sites}} d\theta_i \right) \prod_{\langle i,j \rangle} \left[e^{\beta \cos(\theta_i - \theta_j)} \right] e^{iQ\theta_x} e^{-iQ\theta_y}, \tag{5.2.9}$$

and, after substituting Eq. 5.2.9 in Eq. 5.2.2, we arrive at

$$N_Q(\beta, x, y) = \sum_{\{k_{ij}\}} \left\{ \left(\prod_{\langle i,j \rangle} I_{k_{ij}}(\beta) \right) \left[\int \left(\prod_{i \in \text{Sites}} d\theta_i \right) \left(\prod_{i \in \text{Sites}} \prod_{\substack{j \text{ Neighbor} \\ \text{of } i}} e^{ik_{ij}(\theta_i - \theta_j)} \right) e^{iQ\theta_x} e^{-iQ\theta_y} \right] \right\}. \tag{5.2.10}$$

Grouping the terms with the same θ_k, we have additional contributions from $e^{iQ\theta_x}$ and $e^{-iQ\theta_y}$, on θ_x and θ_y, respectively. Consequently the $N_Q(\beta, x, y)$ is given by

$$N_Q(\beta, x, y) = (2\pi)^N \sum_{\{k_{ij}\}} \left\{ \left(\prod_{\langle i,j \rangle} I_{k_{ij}}(\beta) \right) \prod_{i \in \text{Sites}} \delta \left[\sum_{\substack{j \text{ Neighbor} \\ \text{of } i}} k_{ij}\mu_{ij} + Q\delta_{ix} - Q\delta_{iy} \right] \right\}. \tag{5.2.11}$$

In the case of denominator, all the contributing configurations had an equal number of arrows going in and out of a site, for that reason we called them closed configurations. For the numerator, the two special points x and y have, respectively, Q arrows going in and Q arrows coming out. For example, a configuration that would contribute for the numerator $N_2(\beta, x, y)$ is displayed in Fig. 5.2.1 b). We refer to configurations that contribute for the numerator, $N_Q(\beta, x, y)$, as Q**-open configurations** at x and y.

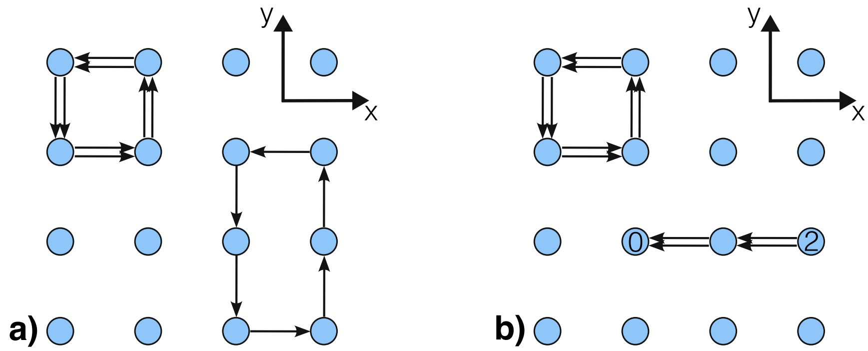

Figure 5.2.1: a) Example of a configuration that contributes for the partition function, b) Example of a configuration that contributes for the numerator of $N_2\left(\beta, 0, 2\right)$.

Looking at Eq. 5.2.11, we see that the numerator is weighed sum over all Q-open configurations at x and y,

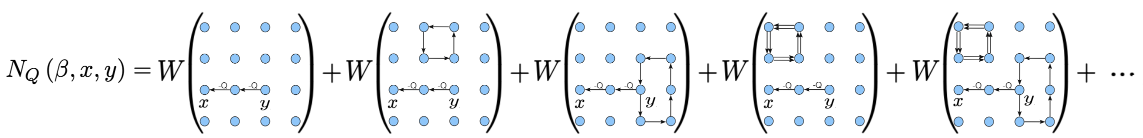

where the weight, W, is still computed by Eq. 5.2.8. In conclusion, the correlation function of Q is the ratio between the weighted sums of Q-open configurations and closed configurations, $C_Q = \frac{N_Q}{\mathcal{Z}}$. Moreover, the dual lattice formulation allows us to express the ratio of correlation functions, $\frac{C_Q}{C_{Q-1}}$, as a ratio between the weighted sum of Q-open configurations and the weighted sum of $\left(Q-1\right)$-open configuration,

$$\frac{C_Q}{C_{Q-1}} = \frac{N_Q/\mathcal{Z}}{N_{Q-1}/\mathcal{Z}},$$

the partitions function cancels giving $\frac{N_Q}{N_{Q-1}}$. As we explain in Section 6.3.2, this will be the main reason why we are able to measure the correlation function for large Q.

In the dual lattice representation of the $O\left(2\right)$ model, all the observables, such as N_Q, require evaluating a sum over an infinitely large space of configurations. Problems that require summing over a large dimensional space [8] can be tackled using a stochastic approach, such as Monte-Carlo.

[8]For the problem in hand, the space in question would be a subset of $\mathbb{Z}^{3N}$, where N is the number of sites in the lattice.

Chapter 6

Monte-Carlo Methods

Having decided on the model to study and what observables to compute, we need a method that is able to compute Eq. 5.2.6 and Eq. 5.2.11. As we will discuss, the traditional methods of integration are unfeasible. Instead, we will use a class of stochastic methods called Monte-Carlo. Historically, the earliest versions of Monte-Carlo were used to estimate π in the famous Buffon's needle problem. Applications to physics, although unpublished, were first made by Fermi to tackle a problem related to neutron diffusion. The modern version of Monte-Carlo, known as Markov chain Monte-Carlo, was developed by Neumann and Ulam while they were working in the nuclear weapons project at Los Alamos. Just out of curiosity, the name Monte-Carlo was the code name suggested by Metropolis, who was inspired by the famous Monte-Carlo casino in Monaco. Nowadays, Monte-Carlo is used in many fields from data science and medicine to condensed matter and high energy. Part of what makes it so widely used is that at its core, Monte-Carlo is all about a simple idea called importance sampling. The review portion of this chapter is based on the following books and lectures notes [48–53].

6.1 Importance Sampling

Importance sampling is technique which allows one to perform a sum/integral stochastically. Suppose the problem at hand requires computing the following integral

$$I = \int dx\, f(x)\,, \tag{6.1.1}$$

where $f(x)$ is some well-behaved function. Notice that we are allowed to multiply the integrand by one, $\frac{p(x)}{p(x)}$ where $p(x)$ is an arbitrary well-behaved function, such that the integral becomes

$$I = \int dx\, p(x)\, \frac{f(x)}{p(x)} \equiv \int dx\, p(x)\, M(x)\,. \tag{6.1.2}$$

Apparently we have done nothing, but if we think of $p(x)$ as a probability distribution for the variable x, then the integral becomes the average of $M(x)$ when probability distribution of x is $p(x)$. Methods that use this idea of evaluating a sum/integral stochastically are called Monte-Carlo methods.

The steps for Monte-Carlo method are

Monte-Carlo Algorithm

1. Identify the random variable or set of random variables X;
2. Identify the probability distribution p for X;
3. Generate N independent values of X following the distribution p;
4. Compute the average, $\langle \bar{M} \rangle = \frac{1}{N}\sum_i M(X_i)$, using the N independent samples.

The variance of the average goes with $\frac{1}{N}$. Meaning that, as we increase the number of points in our sample, the estimate of $\langle M \rangle$ converges to the exact average with $\frac{1}{\sqrt{N}}$. For spaces with low dimensionality[1], Monte-Carlo is worse than the quadrature methods or other more advanced techniques. However, when the space has large dimensionality, Monte-Carlo makes the otherwise untractable problem feasible.

The problem of computing the partition function, Eq. 5.2.6, and numerator, Eq. 5.2.11, can be reduced to performing a sum over the space of closed configuration and the space of Q-open configuration, respectively. To formulate the problem in a way one can directly apply the Monte-Carlo techniques we introduce two functions, $O_c(\boldsymbol{k})$ and $O_o(\boldsymbol{k}, x, y, Q)$[2], defined as

$$O_c(\boldsymbol{k}) = \prod_{i \in \text{Sites}} \delta\left(\sum_{\substack{j \text{ Neighbor} \\ \text{of } i}} k_{ij}\mu_{ij} \right) \quad \text{and} \quad O_o(\boldsymbol{k}, x, y, Q) = \prod_{i \in \text{Sites}} \delta\left(\sum_{\substack{j \text{ Neighbor} \\ \text{of } i}} k_{ij}\mu_{ij} + Q\delta_{ix} - Q\delta_{iy} \right). \tag{6.1.3}$$

Using the functions above we can write the partition function and numerator as a sum over $\mathbb{Z}^{3N}$

$$\mathcal{Z}(\beta) = \sum_{\boldsymbol{k} \in \mathbb{Z}^{3N}} O_c(\boldsymbol{k}) W(\boldsymbol{k}, \beta) \quad \text{and} \quad N_Q(\beta, x, y) = \sum_{\boldsymbol{k} \in \mathbb{Z}^{3N}} O_o(\boldsymbol{k}, x, y, Q) W(\boldsymbol{k}, \beta), \tag{6.1.4}$$

where $W(\boldsymbol{k}, \beta) = \prod_{\langle i,j \rangle} I_{k_{ij}}(\beta)$. In the stochastic approach, this sum is equivalent to the average of $O_c(\boldsymbol{k})$ or $O_o(\boldsymbol{k}, x, y, Q)$ when the $\boldsymbol{k}$ is a random variable that follows the distribution $W(\boldsymbol{k}, \beta)$.

One of the steps in the Monte-Carlo recipe, number 3, requires generating a sample of $\boldsymbol{k}$ following $W(\boldsymbol{k}, \beta)$. This is in general not trivial. Fortunately, we can use a technique, called Markov process, to generate those samples.

6.2 Markov Process

Consider a space of events, $\mathbb{E}$, composed of a possibly infinite number of events E_j. In the problem at hand, the space of events corresponds to $\mathbb{Z}^{3N}$ and each event correspond to a configuration $\mathbf{k}_j$. A Markov process requires defining a Markov time, τ, and a transition probability between event, T_{ij}[3]. The Markov process also assumes that, T_{ij}, does not depend on the Markov time.

Using the quantities defined above and assuming that at $\tau = 0$ the system was in E_1, we can write the probability of the system being in E_n, at $\tau = 1$, as T_{1n}, $P_1(E_n) = T_{1n}$.

[1] Dimension 4 or lower

[2] $\mathbf{k}$ symbolizes a configurations of k_{ij}'s.

[3] T_{ij} stands for the transition probability between a configuration E_i at $\tau - 1$ and event E_j at τ.

For a general time, t, the probability that the system is in E_n, provided it was in E_1 at $\tau = 0$, is

$$P_t(E_n) = \sum_{\substack{i_1, i_2, \ldots, \\ i_m, \ldots, i_{t-1}}} T_{1i_1} T_{i_1 i_2} T_{i_2 i_3} \ldots T_{i_{m-1} i_m} T_{i_m i_{m+1}} \ldots T_{i_{t-1} n}. \tag{6.2.1}$$

The expression in Eq. 6.2.1 can be interpreted as the weighted sum over all possible sequence of events such that the event at $\tau = 0$ is E_1 and at $\tau = t$ is E_n, where the weight of each sequence is given by $T_{1i_1} T_{i_1 i_2} T_{i_2 i_3} \ldots T_{i_{m-1} i_m} T_{i_m i_{m+1}} \ldots T_{i_{t-1} n}$. Consider a space with 5 events, Fig. 6.2.1, the probability of the system being in event E_3 at time 4 knowing it started in E_3 will be given by the weighted sum of all possible paths, the lines in Fig. 6.2.1. For example, the red line has a weight $T_{34} T_{43} T_{32} T_{23}$.

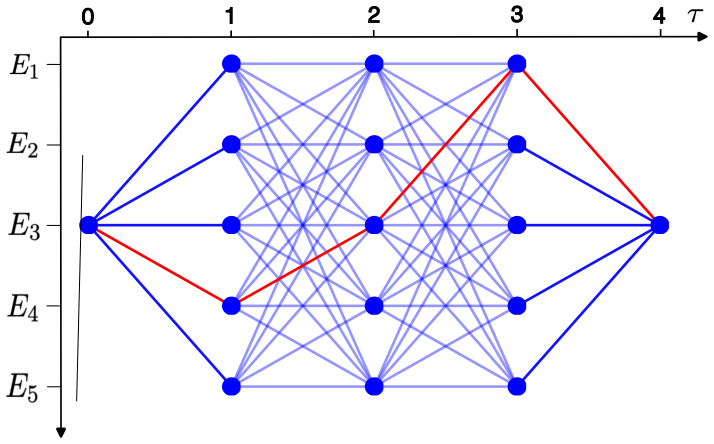

Figure 6.2.1: Example of a Event space with 5 events, the lines represent all the possible sequences of events.

The statement in Eq. 6.2.1 can be rewritten in a more compact manner by defining a probability vector associated with Markov time t,

$$\boldsymbol{P}_t \equiv \begin{bmatrix} P_t(E_1) & P_t(E_2) & \ldots & P_t(E_n) & \ldots \end{bmatrix}^T, \tag{6.2.2}$$

and the Markov matrix,

$$\boldsymbol{\Omega} \equiv \begin{bmatrix} T_{11} & \cdots & T_{1i} & \cdots & T_{nn} & \cdots \\ \vdots & \ddots & \vdots & \ddots & \vdots & \ddots \\ T_{j1} & \cdots & T_{ji} & \cdots & T_{jn} & \cdots \\ \vdots & \ddots & \vdots & \ddots & \vdots & \ddots \\ T_{n1} & \cdots & T_{ni} & \cdots & T_{nn} & \cdots \\ \vdots & \ddots & \vdots & \ddots & \vdots & \ddots \end{bmatrix}. \tag{6.2.3}$$

Therefore, Eq. 6.2.1 becomes

$$\boldsymbol{P}_t = \boldsymbol{\Omega}^t \boldsymbol{P}_0. \tag{6.2.4}$$

A relevant question is whether or not this procedure converges as the Markov time increases, or in other words, if there is an equilibrium distribution $\boldsymbol{P}_e$ defined as

$$\lim_{t \to +\infty} \boldsymbol{\Omega}^t \boldsymbol{P}_0 = \boldsymbol{P}_{\text{eq}}. \tag{6.2.5}$$

Suppose that we are able to diagonalize the matrix $\boldsymbol{\Omega}$ and compute its eigenvectors, v_i, and their respective eigenvalues, λ_i. Then, we could write $\boldsymbol{\Omega}$ as $\boldsymbol{S}^{-1}\boldsymbol{\Omega}_D\boldsymbol{S}$, where $\boldsymbol{\Omega}_D$ is a diagonal matrix containing the eigenvalues of $\boldsymbol{\Omega}$ and $\boldsymbol{S}$ is the matrix responsible for the change of basis, from the original basis to the basis span by the eigenvectors of $\boldsymbol{\Omega}$. Consequently, $\boldsymbol{\Omega}^t$ can be written as $\boldsymbol{S}^{-1}\boldsymbol{\Omega}_D^t\boldsymbol{S}$. Thus as t goes to infinity the only eigenvalues that contribute for the equilibrium distribution must have modulus equal to 1[4]. Depending on the transition amplitudes, different phenomena can occur, namely, oscillatory solutions for complex values of λ and multiple equilibrium distribution when several eigenvector have eigenvalues equal to 1. For our purposes, we will neglect those special cases and work with a Markov matrix that is well behaved in the sense that it converges to a unique equilibrium distribution.

So far we have gone in one direction that is to say, we started with the rules in the form of transition probabilities and arrived at equilibrium distribution. Recall that in order to use the Monte-Carlo method, we must be able to generate samples from a distribution, $W(E)$, or in other words we would like to find the transition probabilities such that the equilibrium distribution is $W(E)$. That requires introducing two classes of Markov matrices.

The first are the so called **ergodic** matrices, they are characterized by obeying the ergodicity condition,

$$\forall_{i,j}, \exists\tau : [\Omega^\tau]_{ij} > 0, \tag{6.2.6}$$

which translates to the statement that if one waits for a long enough Markov time, then the probability of the system transitioning from E_i to E_j will be finite. The ergodicity condition ensures that there is only one eigenstate whose eigenvalue has modulus one. Therefore, the equilibrium distribution is unique and does not depend on the initial event.

The other class of matrices are those which respect the **detailed balance** condition,

$$T_{ij}\tilde{P}_j = T_{ji}\tilde{P}_i, \ \forall_{i,j}. \tag{6.2.7}$$

Matrices that obey this condition always converge to the equilibrium distribution given by $\tilde{\boldsymbol{P}}$.

In conclusion, we can generate a sequence of events that follows a given distribution, $W(E)$, by choosing a Markov matrix that is both ergodic and obeys the detailed balance condition for $\tilde{\boldsymbol{P}} = W(E)$.

6.3 Metropolis–Hastings Algorithm

The Metropolis–Hastings algorithm is a way of implementing a Markov process, thus, generating a sequence of random samples from a given distribution. From now on, we will focus on the problem at hand, meaning that the space of events is $\mathbb{Z}^{3N}$, where N is the number of sites, and the events correspond to the different configurations, $\mathbf{k}_a$. For implementation sake, it is convenient to divide the transition amplitude into two steps the **proposal** and **acceptance** step such that the transition amplitude, T_{ab}, that a configuration $\mathbf{k}_a$ goes to a configuration $\mathbf{k}_b$ is given by

$$T_{ab} = g_{ab}A_{ab}, \tag{6.3.1}$$

where g_{ab} is the probability of proposing a transition to the configuration $\mathbf{k}_b$, provided we are in $\mathbf{k}_a$, and A_{ab} is the probability of accepting that proposal.

[4] Because the $\sum_j T_{ij}$ equals 1 for all i, we can prove that all the eigenvalues must have modulus less or equal to 1.

In order for the equilibrium distribution to be $W(\boldsymbol{k}, \beta)$, the detailed balance equation must be satisfied,

$$g_{ab}A_{ab}W(\boldsymbol{k}_a, \beta) = g_{ba}A_{ba}W(\boldsymbol{k}_b, \beta), \tag{6.3.2}$$

for all the configurations $\boldsymbol{k}_a$ and $\boldsymbol{k}_b$. Because both g_{ab} and A_{ab} are unknown, they cannot be fixed using only one equation. In the Metropolis-Hastings algorithm, we choose to fix A_{ab} and leave the proposal function to be arbitrary. The so called **Metropolis choice** corresponds to the following solution of Eq. 6.3.2

$$A_{ab} = \min\left\{1, \frac{g_{ba}W(\boldsymbol{k}_b, \beta)}{g_{ab}W(\boldsymbol{k}_a, \beta)}\right\}. \tag{6.3.3}$$

Of course, there is a lot of freedom when choosing the proposal function, but the detailed balance condition together with the ergodicity condition fixes the equilibrium distribution to be $W(\boldsymbol{k}, \beta)$. As we will discuss in section 6.3.2, the choice of proposal function impacts the efficiency of the algorithm.

6.3.1 Proposal Function g_{ab} and Extending the Configuration Space

The choice of proposal function plays a crucial role on the efficiency of the Monte-Carlo. Suppose we choose a proposal function that takes a initial configuration $\mathbf{k}_a$ and selects, with uniform probability, a k_{ij} proposing it either goes to $k_{ij}+1$ or $k_{ij}-1$, with probability $\frac{1}{2}$. On average, this would imply that the probability of having closed configuration decreases significantly with N. In fact, in the limit where the number of sites is large, the highest probability of generating a closed loop, such as Fig. 6.3.1 a), is $2N\left(\frac{I_1(\beta)}{I_0(\beta)}\right)^4\left(\frac{1}{3N}\frac{1}{2}\right)^4$ and the highest probability of generating a open loop, such as Fig. 6.3.1 b), is $2N\left(\frac{I_1(\beta)}{I_0(\beta)}\right)^x\left(\frac{1}{3N}\frac{1}{2}\right)^x$.

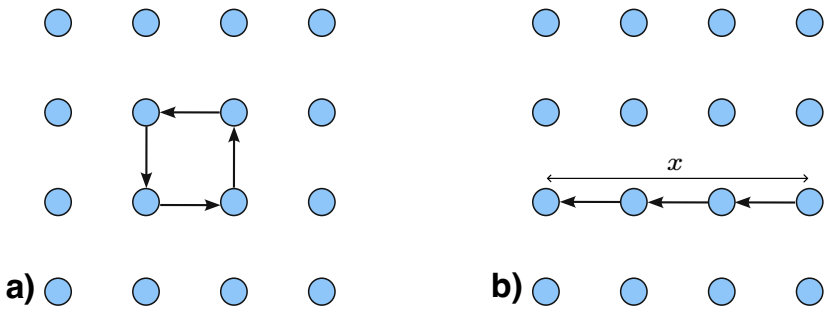

Figure 6.3.1: a) Example of closed configuration; b) Example of Open Configuration

If the configurations where O_o and O_c are non-zero are generated with a small frequency, then we will need a bigger sample to have an accurate estimate for the average[5]. Notice that this does not violate Eq. 6.1.2. If we let the simulation run for a very large Markov time or, in other words, the sample size is huge, the estimate for average will converge to the exact value.

Turns out, according to [44–46], there is a better way of choosing the proposal function which requires extending the configuration space in which the Markov process takes place. The current configuration space is composed of the degree of freedom, k_{ij}, which are defined in the dual lattice. We introduce two degrees of freedom called head, H, and tail, T. In contrast to the k_{ij}'s, H and T correspond to a site's position on the lattice. Since the new degrees of freedom live on the lattice, the weight of each configuration remains unchanged,

$$W(\mathbf{k}, H, T, \beta) = \prod_{\langle i,j\rangle} I_{k_{ij}}(\beta). \tag{6.3.4}$$

[5] In particular, this problem is amplified when we are trying to determine the average of a quantity that is either 0 or 1.

The new choice of proposal function is such that it proposes to change the current configuration, $\{\mathbf{k}_a, H_a, T_a\}$, to a new configuration $\{\mathbf{k}_b, H_b = H_a + \boldsymbol{\delta}, T_b = T_a\}$, where $\boldsymbol{\delta}$ is a direction on the lattice and $\mathbf{k}_b$ is the same as $\mathbf{k}_a$ with the exception of $k_{H\,H+\boldsymbol{\delta}}$ which is substituted by $k_{H\,H+\boldsymbol{\delta}} + \text{sign}\boldsymbol{\delta}$. This means that g_{ab} is zero for all configuration except those where H_b is a neighbor of H_a, $T_a = T_b$ and $\mathbf{k}_b$ is the same as $\mathbf{k}_a$ expect for $k_{H_a\,H_b}$. For example, consider a two dimensional lattice where the current configuration, $\mathbf{k}_a$, is zero everywhere. In that setting the proposal function g_{ab} would be defined as

$$g_{ab} = \begin{cases} \frac{1}{4} & \text{if } b = \\ 0 & \text{otherwise} \end{cases}$$

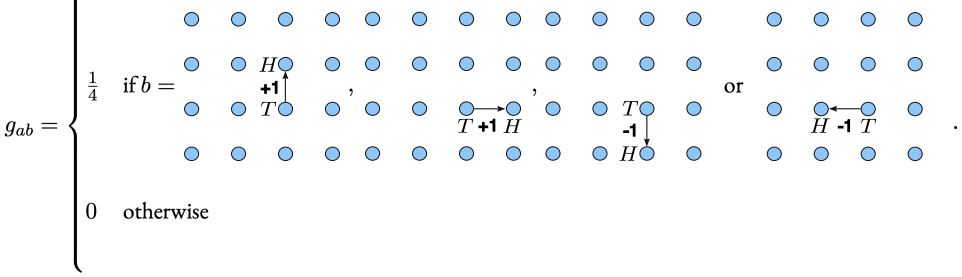

Provided that the ergodicity equation is satisfied, the detailed balance condition, Eq. 6.3.2, fixes the equilibrium distribution to be $W(\boldsymbol{k}, H, T)$.

For the proposal function in the beginning of the section, it is trivial to prove that given enough Markov time any configuration can be generated, in other words, the Markov matrix is ergodic. However, for the proposal function in the extended configuration space, we can prove that only closed configuration and Q-open configuration can be generated, see Fig. 6.3.3. Any configuration that is open in four sites, for example Fig. 6.3.2, cannot be generated from the proposal function in the extended space. This proves that the Markov matrix **is not ergodic in** $\mathbb{Z}^{3N}$, as we will see shortly this is not a problem, but rather an advantage.

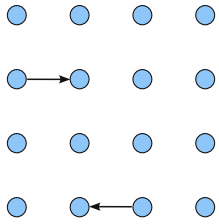

Figure 6.3.2: Example of a configuration that cannot be generated from the proposal function in the extended configuration space.

For simplicity, let us call the set of all closed and Q-open configurations $\mathbb{CO}$. By definition $\mathbb{CO}$ is a subset of $\mathbb{Z}^{3N}$, allowing us to write the partition function, $\mathcal{Z}$, as

$$\mathcal{Z}(\beta) = \sum_{\boldsymbol{k}\in\mathbb{CO}} O_c(\boldsymbol{k})\, W(\boldsymbol{k}, \beta) + \cancelto{0}{\sum_{\boldsymbol{k}\in\mathbb{Z}^{3N}/\mathbb{CO}} O_c(\boldsymbol{k})\, W(\boldsymbol{k}, \beta)}. \tag{6.3.5}$$

Since $O_c(\boldsymbol{k})$ is only non-zero for the closed configuration which are contained in the subset $\mathbb{CO}$, the second term in Eq. 6.3.5 is zero. Meaning that the partition function can be computed in the subset $\mathbb{CO}$, where the proposal function does not break ergodicity[6].

[6] A similar argument can be used to prove that $N_Q(\beta, x, y) = \sum_{\boldsymbol{k}\in\mathbb{CQO}} O_o(\boldsymbol{k}, x, y, Q)\, W(\boldsymbol{k}, \beta)$.

6.3.2 Description of the Metropolis Algorithm

The choice to split the transition probability into a proposal and an acceptance probabilities was not random. It was done with the intention of building an algorithm that could be implemented with relative ease. The Metropolis algorithm for generating a sample of configurations, $\{\mathbf{k}, H, T\}$, following a distribution $W(\mathbf{k}, H, T)$ is:

Metropolis Algorithm

1. Initialize $\mathbf{k}$, H and T;
2. Choose a initial configuration $\mathbf{k}_{\text{initial}}$ and a position, $\mathbf{r}_{\text{initial}}$ on the lattice;
3. Set $\mathbf{k} = \mathbf{k}_{\text{initial}}$ and $H, T = \mathbf{r}_{\text{initial}}$;
4. With uniform probability choose a direction $\boldsymbol{\delta}$;
5. Propose moving H to $H + \delta$ and changing $k_{H\,H+\boldsymbol{\delta}}$ to $k_{H\,H+\boldsymbol{\delta}} + \text{sign}\,\boldsymbol{\delta}$;
6. Accept that proposal with a probability min $\left\{1, \frac{I_{k_{H\,H+\boldsymbol{\delta}}+\text{sign}\,\boldsymbol{\delta}}(\beta)}{I_{k_{H\,H+\boldsymbol{\delta}}}(\beta)}\right\}$;
7. Store the new configuration $(\mathbf{k}, H, T)$;
8. Repeat 4 until satisfied with the number of sampled configurations;

In contrast to other Monte-Carlo methods, the initial condition of the system is extremely important as it will select what quantity is being measured. Suppose one wants to measure $\frac{N_1(\beta,x,y)}{\mathcal{Z}(\beta)}$, then the initial condition should be: $\mathbf{k}_{\text{initial}}$ is a closed configuration, *e.g.* all k's equal to zero, and $\mathbf{r}_{\text{initial}}$ is equal to y. The reason becomes apparent in Fig. 6.3.3. Notice that when the position of the head is equal to the position of the tail, configurations 0 and 3, the configuration is closed. However, when the position of the head is equal to x, configuration 6 and 7, the configuration is 1-open at x and y. In the extended configuration space, measurements are made by counting the number of times $H = y$ and $H = T$. Then, the value of the correlation is $\frac{\langle \delta_{Hy} \rangle}{\langle \delta_{HT} \rangle}$. This algorithm was first proposed in 1998 by Prokof'ev *et al.* [46, 54–56] and is often referred to as **worm algorithm**.

So far, we have discussed a version of the Metropolis algorithm that only works for $Q = 1$. A trivial way of generalizing it is by changing step 5

$$\text{New } 5: \text{ Propose moving H to H+}\delta \text{ and changing } k_{H\,H+\boldsymbol{\delta}} \text{ to } k_{H\,H+\boldsymbol{\delta}} + Q\,\text{sign}\,\boldsymbol{\delta}.$$

Or in other words, instead of changing the k's by ± 1 we change them by $\pm Q$. However, this minor change in the algorithm comes at huge cost. For instances, suppose one wants to compute the correlation function when $Q = 4$, then the probability of changing a k from 0 to 4, at $\beta = 0.4541652$, is about 10^{-4}. Whereas, at the same temperature, the probability of changing a k from 0 to 1 is about 10^{-1}. Meaning that, the algorithm for $Q = 4$ is 10^4 times slower than when $Q = 1$ and this gets worse as Q increases. In 2018, Banerjee *et al.* [44] found a solution to this problem. As mention at the end of Section 5.2, in the dual lattice representation, the ratio between correlation functions, $\frac{C_{Q+1}}{C_Q}$, can be computed from the measurement of $\frac{N_{Q+1}(\beta_c,x,y)}{N_Q(\beta_c,x,y)}$. Banerjee *et al.* modified the Metropolis algorithm in such a way that they are able to directly measure $\frac{N_{Q+1}}{N_Q}$. In the Banerjee's algorithm step 5 remains unchanged, but the $\mathbf{k}_{\text{initial}}$ is a Q-open configuration at x, y and $\mathbf{r}_{\text{intial}}$ is equal to y. Then, the value for $\frac{N_{Q+1}}{N_Q}$ is given by $\frac{\langle \delta_{Hy} \rangle}{\langle \delta_{HT} \rangle}$.

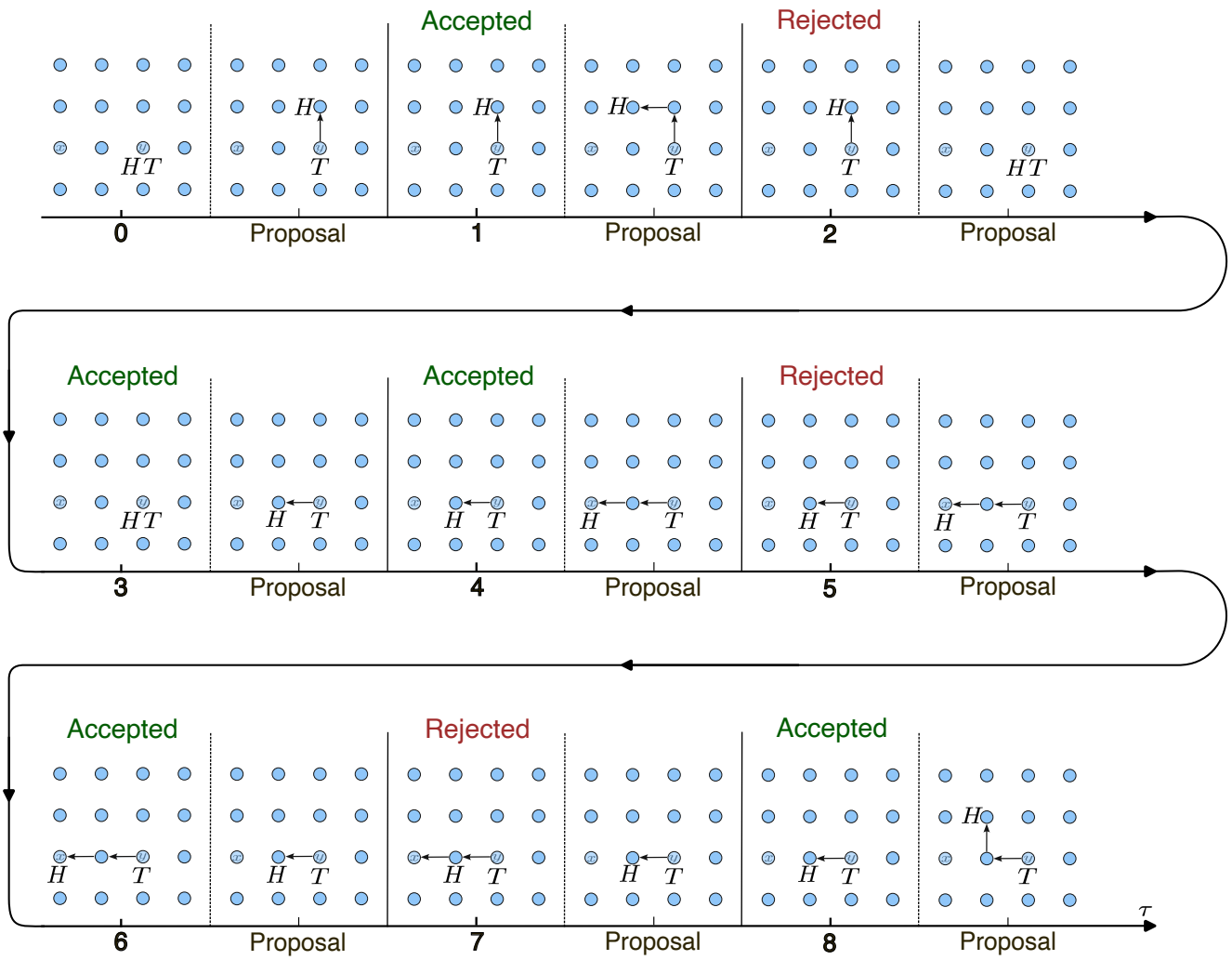

Figure 6.3.3: Example of a Markov Chain generated using the Metropolis-Hasting Algorithm.

Notice that, in the case of $Q = 1$, the Metropolis algorithm only generates configurations that contribute for N_1 and $\mathcal{Z}$, *e.g.* it never generates a 2-open configuration. In the Banerjee's algorithm, the only configurations that are generated are those that contribute for N_{Q+1} and N_Q, *e.g.* it never generates $(Q+2)$-open configurations or closed configurations. Consequently, both the Metropolis and Banerjee's algorithm only generate configurations in the desired sector of the configuration space, thus making both algorithms extremely efficient. As we will see in the section that follows, we can improve on the work of Banerjee by introducing a continuous-time update.

6.4 Continuous-Time Algorithm

In Chapter 2.1, we explained that the CFT description is only valid at the critical temperature, β_c, where the system is believed to acquire conformal symmetry. According to the plot in Fig. 6.4.1, as we increase the k, for example by increasing the $U(1)$ charge, the acceptance ratio becomes very small. Consequently, a significant portion of the computational time would be spent without making the system evolve.

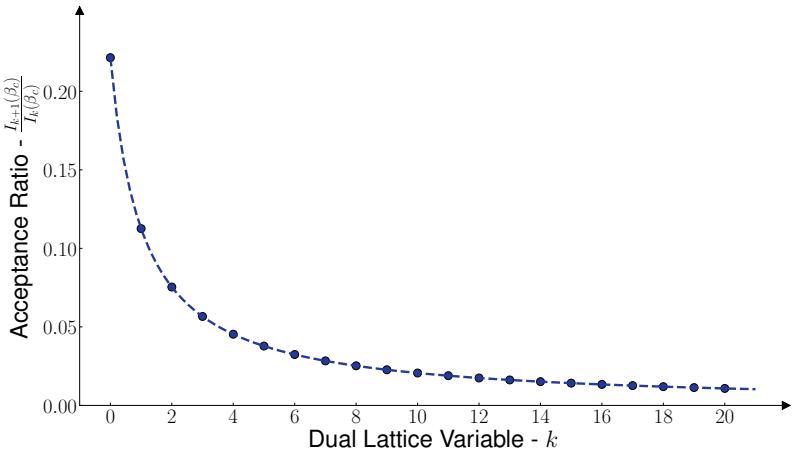

Figure 6.4.1: Acceptance ratio $\frac{I_{k+1}(\beta_c)}{I_k(\beta_c)}$ as a function of dual lattice degree of freedom k, when $\beta_c = 0.4541652$.

A way to circumvent this problem is to use the so called continuous-time algorithm. This algorithm works by listing all the possible configurations that can be achieved based on the system's current configuration. Then it generates a configuration according to a function h_{ab} which makes the acceptance probability 1

$$h_{ab} = \frac{\min\left\{1, \frac{g_{ba}W(\mathbf{k}_b)}{g_{ab}W(\mathbf{k}_a)}\right\}}{\sum\limits_b \min\left\{1, \frac{g_{ba}W(\mathbf{k}_b)}{g_{ab}W(\mathbf{k}_a)}\right\}}. \tag{6.4.1}$$

If the Markov time were to be incremented by 1, as in the Markov algorithm, then the equilibrium distribution would not be $W(\boldsymbol{k}_a, H, T)$. Instead it must take a continuous value, hence the name continuous-time algorithm. The continuous time changes by adding the average of Markov time, Δt_a, that the system would spent in a configuration before moving on, from the perspective of the Metropolis algorithm. For the three dimensional $O(2)$ model, the time increment, Δt_a, is given by

$$\Delta t_a = \frac{1}{\frac{1}{6}\sum\limits_b \min\left\{1, \frac{g_{ba}W(\mathbf{k}_b)}{g_{ab}W(\mathbf{k}_a)}\right\}}. \tag{6.4.2}$$

Furthermore, the average of an observable, $A(\boldsymbol{k}, H, T)$, must account for the continuous time. Suppose that, after running the process of proposing and accepting for N iteration, we are left with a set of

$$\{A_1(\boldsymbol{k}_1, H_1, T_1), ..., A_N(\boldsymbol{k}_N, H_N, T_N)\},$$

the definition of the average of A, $\langle A \rangle$, which takes into account the continuous time is

$$\langle A \rangle = \frac{\sum\limits_n A_n(\boldsymbol{k}_1, H_1, T_1)\,\Delta t_n}{\sum\limits_n \Delta t_n}. \tag{6.4.3}$$

The continuous-time algorithm for generating a sample of configurations, $(\mathbf{k}, H, T)$, following a distribution $W(\mathbf{k}, H, T)$ can be implement using the following footprint:

Continuous-Time Algorithm

1. Initialize $\mathbf{k}$, H and T;
2. Choose a initial configuration $\mathbf{k}_{\text{initial}}$ and a position, $\mathbf{r}_{\text{initial}}$ on the lattice;
3. Set $\mathbf{k} = \mathbf{k}_{\text{initial}}$ and $H, T = \mathbf{r}_{\text{initial}}$;
4. Compute the time increment, $\Delta t_{(\mathbf{k},H,T)}$, and store it;
5. According to the probability h_{ab}, choose a direction $\boldsymbol{\delta}$;
6. Move H to $H + \delta$ and change $k_{H\,H+\boldsymbol{\delta}}$ to $k_{H\,H+\boldsymbol{\delta}} + \text{sign}\,\boldsymbol{\delta}$;
7. Store the new configuration $(\mathbf{k}, H, T)$;
8. Repeat from 4 until satisfied with the number of sampled configurations;
9. Take the average of the observable of interest $A(\boldsymbol{k}_1, H_1, T_1)$ using $\langle A \rangle = \frac{\sum_n A_n(\boldsymbol{k}_1, H_1, T_1)\Delta t_n}{\sum_n \Delta t_n}$.

6.4.1 Comparison Between Metropolis and Continuous-Time Algorithms

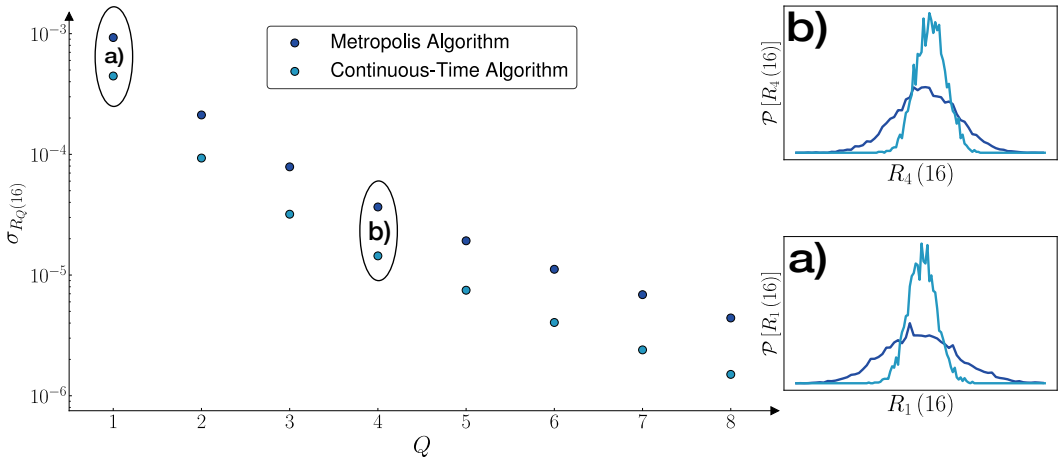

Figure 6.4.2: Standard deviation of $\frac{N_Q}{N_{Q-1}}$, σ, as a function of the $U(1)$ charge, Q, for $x = 0$, $y = 16$ and a lattice size of $32 \times 32 \times 32$ for both the Metropolis and continuous-time algorithms, when $\beta = 0.4541652$.

Although we can have some intuition supporting that the continuous-time should be faster than the Metropolis algorithm, we would like to confirm it and quantify it. In order to benchmark both algorithms we compared the standard deviation, σ, which corresponds to the error in the measurements. The standard deviation was computed in the same computational-time (15 days) for the same cpu, in Fig. 6.4.2. We see that the dark blue dots, corresponding to the metropolis algorithm, are consistently above the light blue dots, hence in the same cpu time we can get better precision by using the continuous-time algorithm.

Chapter 7

Error Control

In this chapter, use data generated using the continuous time algorithm to study how different errors, such as, stochastic fluctuations, finite-size effects and discretization effects, affect the estimates of the correlation functions. Using that information, we will devise a measuring strategy that minimizes those errors. Throughout this chapter and chapter 8, we will use the critical temperature for the 3D $O(2)$, $\beta_c = 0.4541652$, determined by Ballesteros *et al.* [57].

7.1 Variance Scaling with Sample Size

Before jumping into the larger scale simulation it is good practice to check whether the algorithm can actually measure anything in a reasonable time. Because the simulation will end up having a massive amount of continuous time, we opted to use the number of times the head was equal to the tail as the time scale, called hits on the tail. From an implementation point of view, this means that, for a system with a size $L \times L \times L$, we stored the values of the numerator and denominator each L^2 hits on the tail. Although this redefinition clearly changes the probability distribution of N_Q and $\mathcal{Z}$, it does not change the ratios $\frac{N_{Q+1}}{N_Q}$ and $\frac{N_1}{\mathcal{Z}}$. In the new time scale, we will refer to the size of the run as N, such that the total run time is $N \times L^2$ hits on the tail. The statement that a Monte-Carlo algorithm can measure an observable, is equivalent to the statement that the variance of that observable goes to zero as we increase N. For example, consider a lattice of size $32 \times 32 \times 32$ and the observable $\frac{N_1(\beta_c,0,y)}{\mathcal{Z}(\beta_c)}$.

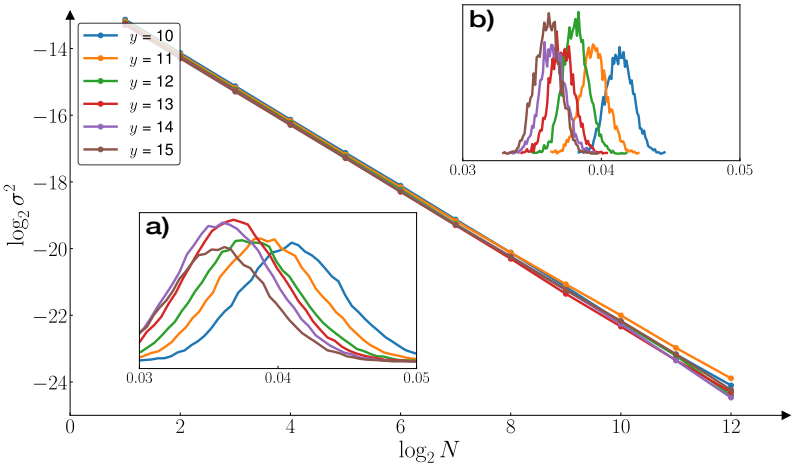

Figure 7.1.1: Variance of $\frac{N_1(\beta_c,0,y)}{\mathcal{Z}(\beta_c)}$, σ^2, as a function of the run's size, N, for different y's and a system size of $32 \times 32 \times 32$; a) Probability distribution of $\frac{N_1(\beta_c,0,y)}{\mathcal{Z}}$ for a run of $2^5 \times 32^2$; b) Probability distribution of $\frac{N_1(\beta_c,0,y)}{\mathcal{Z}(\beta_c)}$ for a run of $2^8 \times 32^2$.

As displayed on the main plot in Fig. 7.1.1, the variance of $\frac{N_1(\beta_c,0,y)}{\mathcal{Z}(\beta_c)}$ decreases with the size of the run, according to $\frac{1}{N}$. This becomes evident when we look at the distributions of $\frac{N_1(\beta_c,0,y)}{\mathcal{Z}(\beta_c)}$ for a run size of 2^5, Fig. 7.1.1 a), and a run of size 2^8, Fig. 7.1.1 b). On the one hand, we notice a decrease in the width of the distribution, on the other hand, the average remains roughly unchanged. Proving that, as long as we have a big enough sample size, we can indeed measure $\frac{N_1(\beta_c,0,y)}{\mathcal{Z}(\beta_c)}$ with increasing precision.

7.2 Finite-Size Effects and Discretization Effects

As described in section 2.5, conformal field theory states that the correlation function between operators with charge Q and $-Q$, under $U(1)$, is

$$\langle \mathcal{O}_Q(x)\,\mathcal{O}_{-Q}(y)\rangle \underset{\text{CFT}}{=} \frac{1}{|x-y|^{2\Delta_Q}}, \tag{7.2.1}$$

where $|x-y|$ is the euclidean distance between x and y. For now let us set the $U(1)$ charge equal to 1 and x to 0. We know that $\langle \mathcal{O}_1(0)\,\mathcal{O}_{-1}(y)\rangle$ can be evaluated stochastically by computing the average of $\frac{N_1(\beta_c,0,y)}{\mathcal{Z}(\beta_c)}$. Unfortunately, when performing the Monte-Carlo simulation we are restricted to a system of finite-size, namely $L\times L\times L$, where L is the number of lattice sites in one direction, also called **linear size**. In Fig. 7.2.1 we plot the correlator, computed from the average of $\frac{N_1(\beta_c,0,y)}{\mathcal{Z}(\beta_c)}$, for different L's and y's, $\langle \mathcal{O}_1(0)\,\mathcal{O}_{-1}(y)\rangle_L$[1] . According to Eq. 7.2.1, the plot of the correlator as a function of the distance, when represented in $\log_2$-$\log_2$ scale, should be a straight line. Instead, what we observe in Fig. 7.2.1 is that, as we increase L, the curve becomes, as it should, closer and closer to the continuum limit.

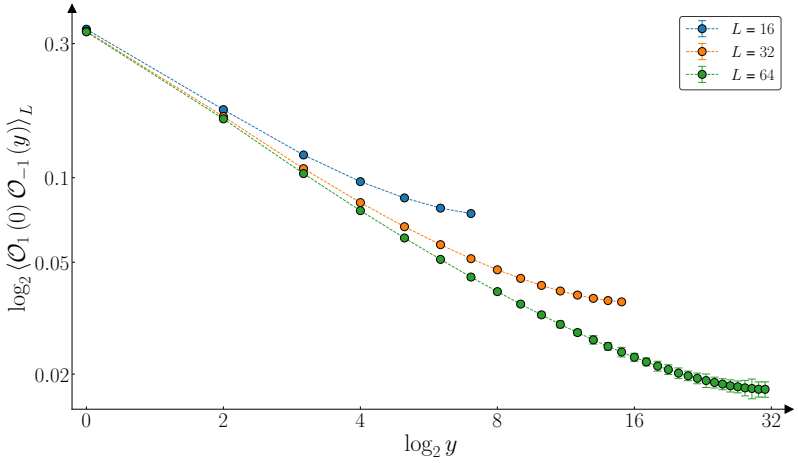

Figure 7.2.1: $\langle \mathcal{O}_1(0)\,\mathcal{O}_{-1}(y)\rangle_L$ as a function of the position, y, for different system sizes, $L\in\{16,32,64\}$.

One could argue that the deviation from the theoretical curve could be caused by the stochastic nature of the computation. However that is not true since, for example, in the curve corresponding to $L=64$, the error bars, which are a direct measure of the stochastic fluctuations, do not include the data points for the other linear sizes.

Achieving precise measurement of the conformal dimensions requires taking into account the finite-size effects. A possibility, would be to use perturbation theory around a CFT. Our argument is much simpler and only requires dimensional analysis. Computing $\langle \mathcal{O}_1(0)\,\mathcal{O}_{-1}(y)\rangle_L$ is a problem that has three typical length scales: the distance y; the linear size L; and the lattice spacing, a. Because the correlation function must maintain its physical dimensions the only possibility is that

[1] $\mathcal{O}_1(0)$ is a short notation for an operator evaluated at $(0,0,0)$ and $\mathcal{O}_{-1}(y)$ is a short notation for an operator at $(ya,0,0)$, where a is the lattice spacing.

$$\langle \mathcal{O}_1(0)\,\mathcal{O}_{-1}(y)\rangle_L = \frac{1}{y^{2\Delta_1}} f\left(\frac{y}{L}, \frac{a}{L}\right). \tag{7.2.2}$$

where $\lim_{L\to\infty} f\left(\frac{y}{L}, \frac{a}{L}\right) = 1$. One way to confirm this statement is to plot $y^{2\Delta_1}\langle \mathcal{O}_1(0)\,\mathcal{O}_{-1}(y)\rangle_L$ as a function of $\frac{y}{L}$, if our prediction is true then

$$y^{2\Delta_1}\langle \mathcal{O}_1(0)\,\mathcal{O}_{-1}(y)\rangle_L = f\left(\frac{y}{L}, \frac{a}{L}\right). \tag{7.2.3}$$

From the bootstrap methods [18], roughly sketched in section 2.6, we know that Δ_1 is approximately 0.519. In Fig. 7.2.2 we represent the same data as in Fig. 7.2.1, multiplied by $y^{2\times 0.519}$, and the curves match the prediction, in Eq. 7.2.3. The fact that they do not precisely collapse into a single curve is evidence that $f\left(\frac{y}{L}, \frac{a}{L}\right)$ becomes independent of $\frac{y}{L}$.

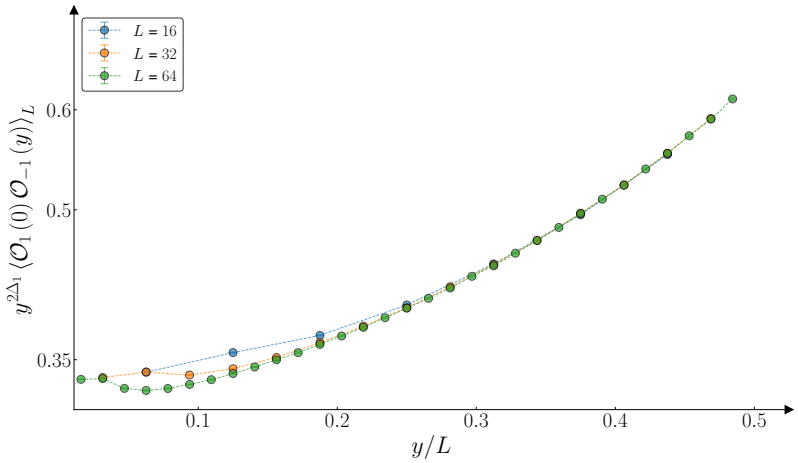

Figure 7.2.2: $y^{2\Delta_1}\langle \mathcal{O}_1(0)\,\mathcal{O}_{-1}(y)\rangle_L$ as a function of the relative position y for different system sizes, $L \in \{16, 32, 64\}$.

From lattice finite-size effect analysis, we concluded that the finite-size is responsible for introducing a factor, $f\left(\frac{y}{L}, \frac{a}{L}\right)$, that becomes independent of $\frac{y}{L}$ for a certain y. Thus, we can define a quantity

$$\begin{aligned} R_1(L,0,y) \equiv & \frac{1}{2}\log_2 \frac{\langle \mathcal{O}_1(0)\,\mathcal{O}_{-1}(y)\rangle_L}{\langle \mathcal{O}_1(0)\,\mathcal{O}_{-1}(2y)\rangle_{2L}} = \\ = & \frac{1}{2}\log_2 \frac{\frac{1}{y^{2\Delta_1}} f\left(\frac{y}{L}, \frac{a}{L}\right)}{\frac{1}{(2y)^{2\Delta_1}} f\left(\frac{y}{L}, \frac{a}{2L}\right)} \\ = & \frac{1}{2}\log_2 \frac{f\left(\frac{y}{L}, \frac{a}{L}\right)}{f\left(\frac{y}{L}, \frac{a}{2L}\right)} + \Delta_1. \end{aligned} \tag{7.2.4}$$

According to Eq. 7.2.4 and the findings in Fig. 7.2.2, for a fixed linear size R_1 should not depend on the position y. Furthermore, because $f\left(\frac{y}{L}, \frac{a}{L}\right)$ goes to 1 when L goes to infinity, R_1 should go to the exact value for the conformal dimension. Using the data represented in Fig. 7.2.2, we computed $R_1(L,0,y)$ and the results are displayed in Fig. 7.2.3.

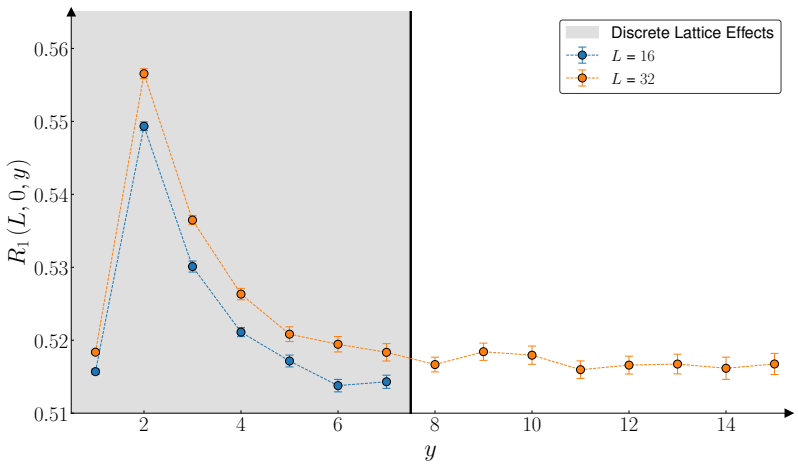

Figure 7.2.3: $R_1(L, 0, y)$ as a function of y for different system sizes, $L \in \{16, 32\}$

Fig. 7.2.3 contains two distinct behaviors. To the right of the black line, R_1 is constant, as predicted in Eq. 7.2.4. To the left of the black line, the behavior of R_1 seems to depend on the position y and therefore contradict Eq. 7.2.4. Since the error bars on the left side do not include the values on the right-side, the discrepancy cannot be justified by the stochastic nature of the calculation. As it turns out, this discrepancy is due to function $f\left(\frac{y}{L}, \frac{a}{L}\right)$ depending on $\frac{y}{a}$ for small values of y. The dependence on $\frac{a}{L}$ appear because the CFT prediction is valid if the system is invariant under the group of continuous transformation, but the lattice is only invariant a discrete subset.

7.3 Measurement Strategy for the Conformal Dimensions

With all the sources of error identified, we layout the strategy used to compute the conformal dimensions. Aiming to mitigate the statistical error, we choose to evaluate the ratio of correlation functions, $K_Q(L, x, y) \equiv \frac{\langle \mathcal{O}_Q(x)\mathcal{O}_{-Q}(y)\rangle_L}{\langle \mathcal{O}_{Q-1}(x)\mathcal{O}_{-Q+1}(y)\rangle_L}$, which can be directly measured from the average of $\frac{N_Q(\beta_c,x,y)}{N_{Q-1}(\beta_c,x,y)}$. Notice that when Q is 1, we recover the correlation function, $\langle \mathcal{O}_1(x)\mathcal{O}_{-1}(y)\rangle_L$. We can reconstruct any correlation function by

$$C_Q(L, x, y) \equiv \langle \mathcal{O}_Q(x)\mathcal{O}_{-Q}(y)\rangle_L = \prod_{q=1}^{Q} K_Q(L, x, y). \tag{7.3.1}$$

A clear advantage to computing the ratio of correlation functions is that they are much bigger than the correlation function itself. For example, consider the correlation function for Q equal to 8, if the operators are separated by 10 lattice spacings, then the correlation function is expected to be around 10^{-16}. Not even the improved algorithm using the continuous-time update can measure observables of this order of magnitude. For reference, measuring something this small would, on average, mean that the function $O_o(\mathbf{k}, x, y, Q)$ is 1 every 10^{16} hits on tail. Even if the hits on tail were to happen every 10^{-9} seconds, maximum processing speed for most cpus, it would take 115 days to get a single hit, and much longer until we could get a reasonable measurement. On the other hand, if we directly sample K_Q, which for the same conditions is around 10^{-3}, it is possible to obtain a bigger sample of $O_o(\mathbf{k}, x, y, Q)$ an therefore a more precise measurement.

Another source of error are the finite-size effects. With that in mind, we define a generalization of R_1, the function R_Q as

$$R_Q(L, 0, y) \equiv \frac{1}{2}\log_2 \frac{K_Q(L, 0, y)}{K_Q(2L, 0, 2y)}, \tag{7.3.2}$$

In the limit $L \to \infty$, R_Q admits the following expansion in powers of $\frac{1}{L}$,

$$R_Q\left(L,0,y\right) \underset{L\to+\infty}{\sim} \Delta_{Q+1} - \Delta_Q + \frac{c}{L}, \tag{7.3.3}$$

where $c \in \mathbb{R}$. According to Fig. 7.2.3, the expansion in powers of $\frac{1}{L}$ is only valid for large distances where the sub-leading contribution from the projection onto spin 4 operators is negligible. In Fig. 7.3.1, we show a detailed study of the discrete effects as a function of the charge. The results indicate that, for a system of linear size equal to 32, the discrete effects are negligible when y greater than 7[2], given our stochastic errors

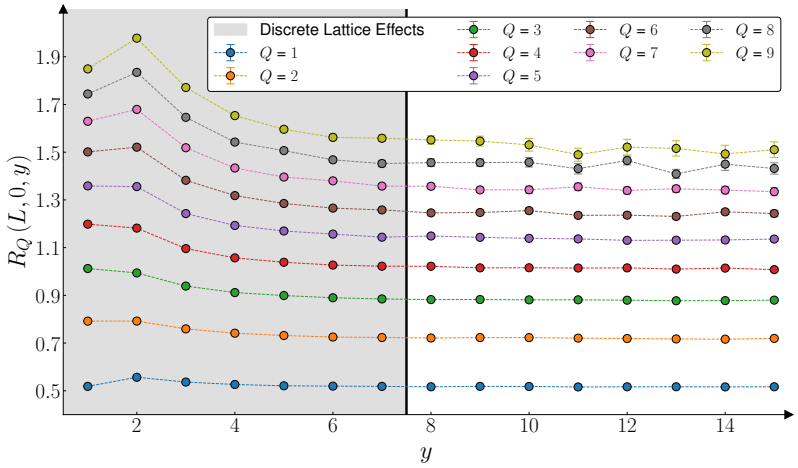

Figure 7.3.1: $R_1\left(L,0,y\right)$ as a function of y for different $U\left(1\right)$ charges, $Q \in \{1,2,3,4,5,6,7,8,9\}$, and a fixed system size of $L = 32$.

According to Eq. 7.3.3, $R_Q\left(L\right)$ is suppose to be constant for a y greater than 7. However, Fig. 7.3.1 shows that when we increase the charge the statistical fluctuations increase. Because the simulations at different y's are independent, $R_Q\left(L\right)$ can be estimated by averaging $R_Q\left(L,0,y\right)$ for different y's. The uncertainty on the final result will be given, according to the central limit theorem, by the variance of $R_Q\left(L,0,y\right)$ divided by the number of different y's.

Our strategy will be to compute $R_Q\left(L,0,y\right)$ for $y \in \{8,9,10,11,12\}$ and use those values to estimate $R_Q\left(L\right)$ using

$$R_Q\left(L\right) = \frac{1}{5}\sum_{y=8}^{12} R_Q\left(L,0,y\right). \tag{7.3.4}$$

The error of that estimate corresponds to the standard deviation of $R_Q\left(L,0,y\right)$ for $y \in \{8,9,10,11,12\}$ divided by $\sqrt{5}$. Since the goal is to extract $\Delta_Q - \Delta_{Q-1}$, we repeated the previous process for $L \in \{32,48,64\}$. According to the expansion in Eq. 7.3.3, for large L, $R_Q\left(L\right)$ will be linear in $\frac{1}{L}$, allowing us to extrapolate the function $R_Q\left(L\right)$ and compute $R_Q\left(\infty\right)$, which corresponds to $\Delta_Q - \Delta_{Q-1}$. In Fig. 7.3.2, we represent the values $R_Q\left(L\right)$ for different L's as well as the respective extrapolation, $R_Q\left(\infty\right)$.

[2]We perform the same study for $L \in \{48,64\}$ and concluded y greater than 7 the discrete lattice effects are negligible. However, the statistical fluctuations increase with increasing L.

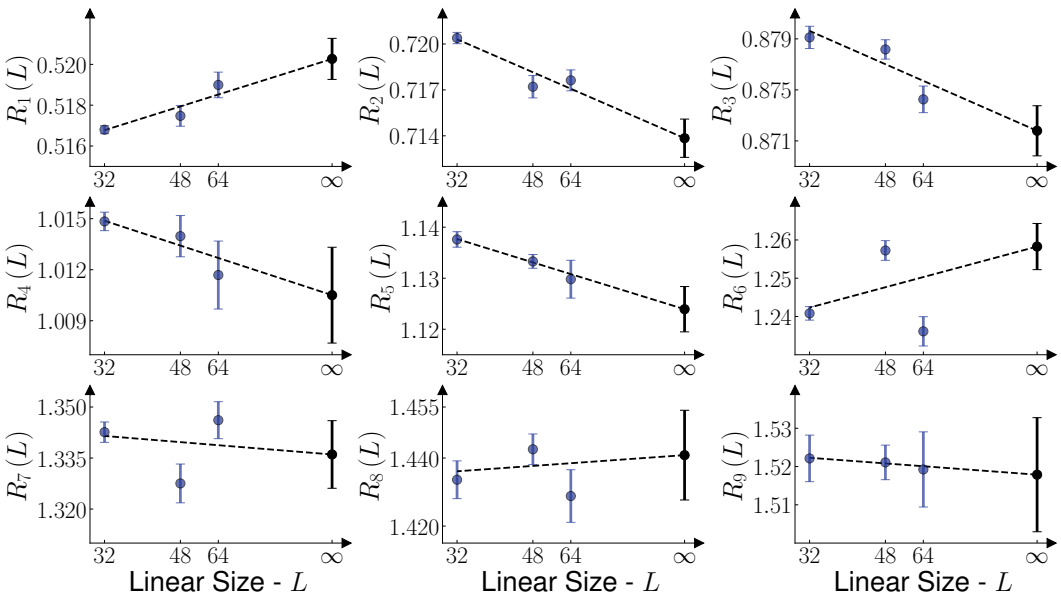

Figure 7.3.2: $R_Q(L)$ as a function of L for different $Q \in \{1,2,3,4,5,6,7,8,9\}$. The points in dark blue correspond to the numerical data and the points in black correspond to the linear extrapolation, $R_Q(\infty)$.

Since $R_1(\infty)$ is Δ_1, we can reconstruct the conformal dimension $\Delta_Q = \sum_{q=1}^{Q} R_q(\infty)$. When the charge is greater than 7, the stochastic fluctuations are greater than the deviations from finite-size effects. Therefore, for a charge greater then 7, we used the value of $R_Q(32)$ as the value of extrapolation to infinity and use double the error of that measurement as the error for the extrapolation to infinity.

With this new strategy and the continuous time update, we were able to surpass the precision from previous results by Banerjee *et al.* [44] and evaluate the conformal dimension for operators with up to charge 20 under $U(1)$. The results are showcased in chapter 8.

Chapter 8

Results

In this chapter we use the data obtained with the continuous-time algorithm and the measuring strategy, outlined in Chapter 7. We determine the conformal dimensions of scalar operators with charge up to 20. Then, we assess the quality of the prediction made by superfluid effective theory, Eq. 4.2.9, by checking the qualitative properties of its analysis.

8.1 Difference Between Conformal Dimensions - $\Delta_Q - \Delta_{Q-1}$

On the previous chapter, we outlined the measuring strategy used to compute $\Delta_Q - \Delta_{Q-1}$ from the extrapolation of $R_Q(L)$ when L is infinite. According to the prediction from Section 4.2, when the charge is large, the conformal dimension admits the expansion

$$\Delta_Q = \frac{2}{3}\frac{1}{\sqrt{2\pi c_1}}Q^{\frac{3}{2}} + 8\pi c_2\left(\frac{Q}{2\pi c_1}\right)^{\frac{1}{2}} - 0.0937254 + O\left(Q^{-\frac{1}{2}}\right). \tag{8.1.1}$$

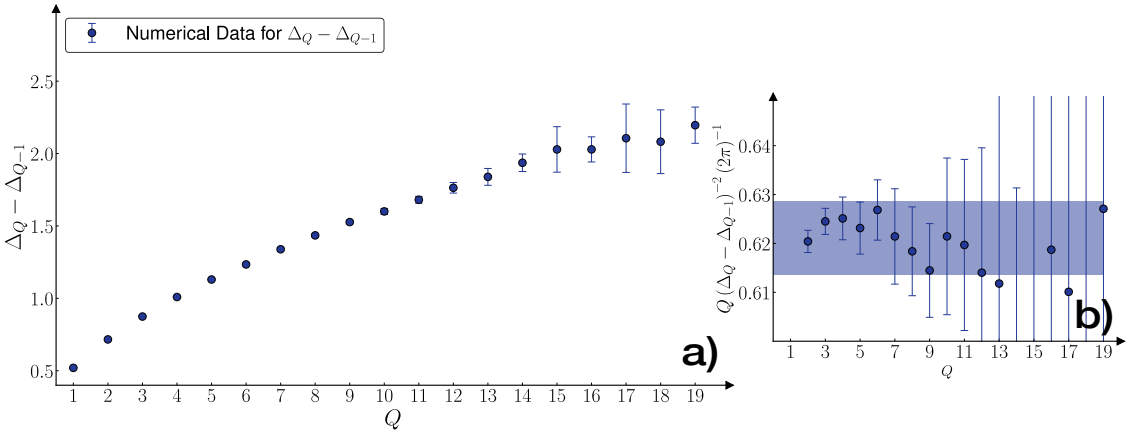

Figure 8.1.1: In the plot a) we are displaying the numerical data for $\Delta_Q - \Delta_{Q-1}$ as a function of the $U(1)$ charge, Q.; Plot b) corresponds to $Q(\Delta_Q - \Delta_{Q-1})^{-2}(2\pi)^{-1}$, computed using the numerical data, as a function Q.

In Fig. 8.1.1 a), we represent the numerical data for $\Delta_Q - \Delta_{Q-1}$, see Table B.1.1, as a function of Q. In Fig. 8.1.1 b), we plot $Q(\Delta_Q - \Delta_{Q-1})^{-2}(2\pi)^{-1}$ as a function of Q. For a large enough charge, Eq. 8.1.1 predicts that

$$Q(\Delta_Q - \Delta_{Q-1})^{-2}(2\pi)^{-1} \underset{Q\gg 1}{\sim} c_1 + O\left(Q^{-1}\right). \tag{8.1.2}$$

This is corroborated by Fig. 8.1.1 b), where we plot , $Q\left(\Delta_Q - \Delta_{Q-1}\right)^{-2}(2\pi)^{-1}$ obtained numerically, and see that is appears to converge to a constant, c_1, $0.621\,(7)$. Furthermore, that value for c_1 is compatible with the one obtained from direct fits to Δ_Q, as shown in Fig. 8.3.2.

8.2 Conformal Dimensions - Δ_Q

From the numerical data in Fig. 8.1.1 a) we can reconstruct the conformal dimensions, Δ_Q, by applying

$$\Delta_Q = \sum_{q=1}^{Q} \left(\Delta_q - \Delta_{q-1}\right). \tag{8.2.1}$$

In Fig. 8.2.1 a), we show the conformal dimension, Δ_Q, see Table B.1.1, as a function of Q. If Eq. 8.1.1 is to be true then the $\Delta_Q/Q^{1/2}$ should be linear in Q. In Fig. 8.2.1 b), we plot the $\Delta_Q/Q^{1/2}$ as a function of Q and conclude that, as predicted, it grows linear with Q. This is a direct proof that the leading behavior of Δ_Q is $Q^{3/2}$.

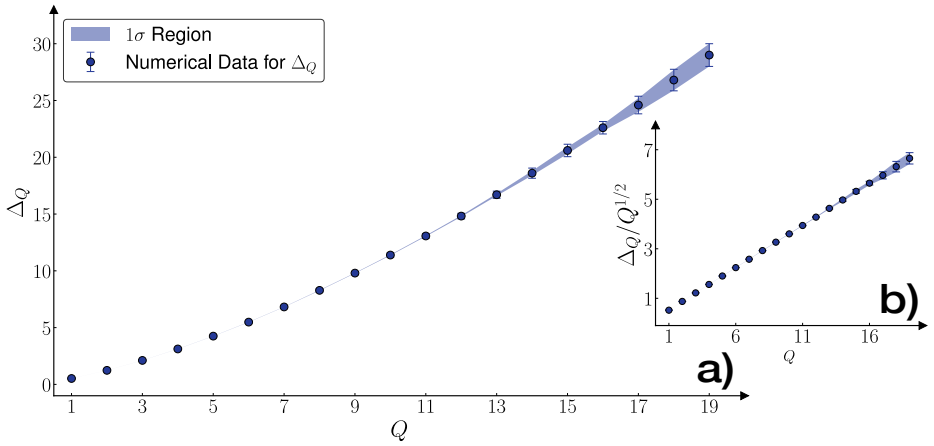

Figure 8.2.1: Plot a) shows to the conformal dimensions Δ_Q, computed from the numerical data in Fig. 8.1.1 using $\Delta_Q = \sum_{q=1}^{Q} (\Delta_q - \Delta_{q-1})$, as a function of the $U\,(1)$ charge, Q; Plot b) corresponds to $\Delta_Q/Q^{1/2}$, computed using the data in the main plot of this figure, as a function Q.

We can assess the quality of our result for low charges, $Q \in [1, 4]$, by comparing them with known result is the literature. In Fig. 8.2.2, we see that for charge equal to 1, 2 the bootstrap results are more precise. However, for Q equal to 3 and 4 the Monte-Carlo results become more precise. Furthermore, all the results are compatible within 2 standard deviations.

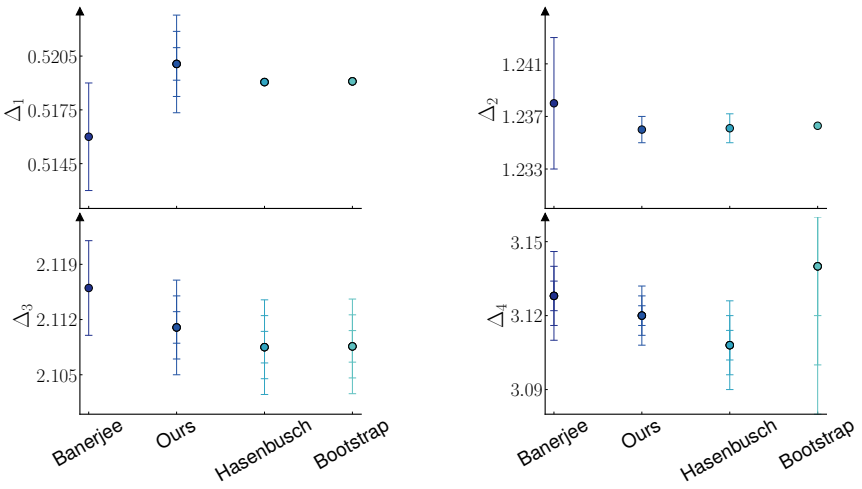

Figure 8.2.2: Comparison between our results [58] and those of Banerjee's *et al.* [44], Hasenbush *et al.* [59, 60] and bootstrap result from Chester *et al.* [18].

8.3 Coefficients c_1 and c_2

In Fig. 8.2.1, we proved that the leading behavior for Δ_Q is $Q^{3/2}$. In this section we will investigate whether or not the sub-leading contributions are given by Eq. 8.1.1. To do so we tried to fit the numerical data for Δ_Q, to the function, $\Delta_Q^{\text{fit}}(c_1, c_2)$,

$$\Delta_Q^{\text{fit}}(c_1, c_2) = \frac{2}{3}\frac{1}{\sqrt{2\pi c_1}}Q^{\frac{3}{2}} + 8\pi c_2\left(\frac{Q}{2\pi c_1}\right)^{\frac{1}{2}} - 0.0937254, \tag{8.3.1}$$

by minimizing the error function given by $E(c_1, c_2) = \sum_{Q=1}^{19} \frac{\left(\Delta_Q - \Delta_Q^{\text{fit}}(c_1,c_2)\right)^2}{\sigma^2(\Delta_Q)}$ with respect to c_1 and c_2. First we started by fitting all the data, meaning we used the conformal dimensions for operators with charge between 1 and 19. As shown by the green line the in Fig. 8.3.1 b), the relative error between the numerical of the fit decreases until charge 6 and then starts to increase again. However, because Eq. 8.1.1 is a asymptotic expansion in Q, the more consistent approach would be to fit the data using values of Δ_Q for a large Q and assess whether they provide a good approximation for lower values of Q. The red line in Fig. 8.3.1 b) shows that, when performing a fit using Δ_Q with $Q \in [8, 19]$, the relative error rapidly decreases and stays constant from $Q \in [6, 19]$. The quality of the new fit is visible, in Fig. 8.3.1 a) the fit from $Q \in [8, 19]$ perfectly matches all charges above 6, whereas the fit using all the charges starts to fail for charges bigger than 8.

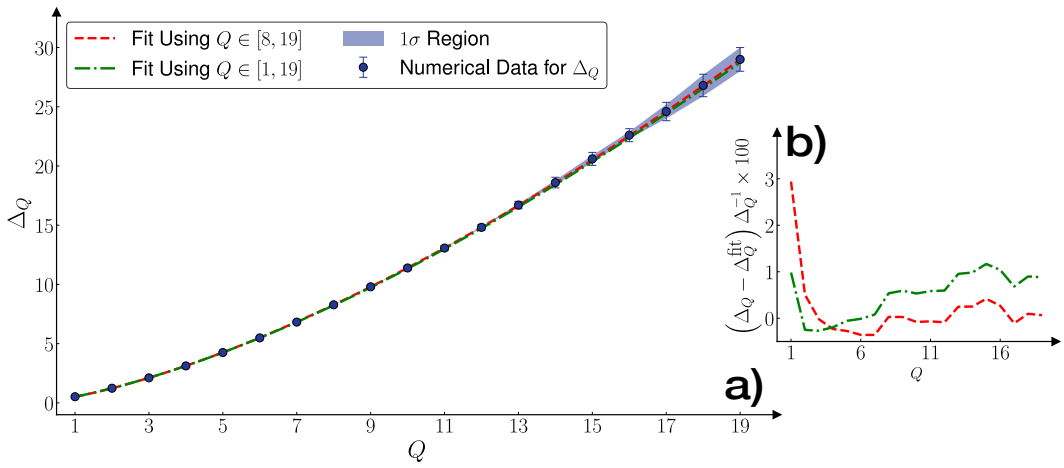

Figure 8.3.1: a) Plot of numerical data for Δ_Q and the fits using the conformal dimensions for $Q \in [1, 19]$ and for $Q \in [8, 19]$; b) Relative error between the fits in a) and the data for different Q's.

Despite being a asymptotic expansion, the large charge expansion appears to work for charges as low as 3. Moreover, for charges 1 and 2, which are the smallest possible, the asymptotic series seems to predict the values with a remarkable 3% relative error. An important question would be to ask what large charge exactly means. With that in mind, we studied how the fit varied as we decrease the number of charges included in the fit, or in other words, we fitted Δ_Q^{fit} to the data for $Q \in [Q_{\text{min}}, 19]$ and varied the lower cutoff, Q_{min}. Turns out that, the fit becomes stable for a charge greater than 4, see Fig. 8.3.2 and Fig. 8.3.3, allowing us to determine c_1 and c_2,

$$c_1 = 0.617\,(5) \quad \text{and } c_2 = 1.93\,(9) \times 10^{-2}. \tag{8.3.2}$$

In particular, this value of c_1 is compatible with the one determined in Fig. 8.1.1 b).

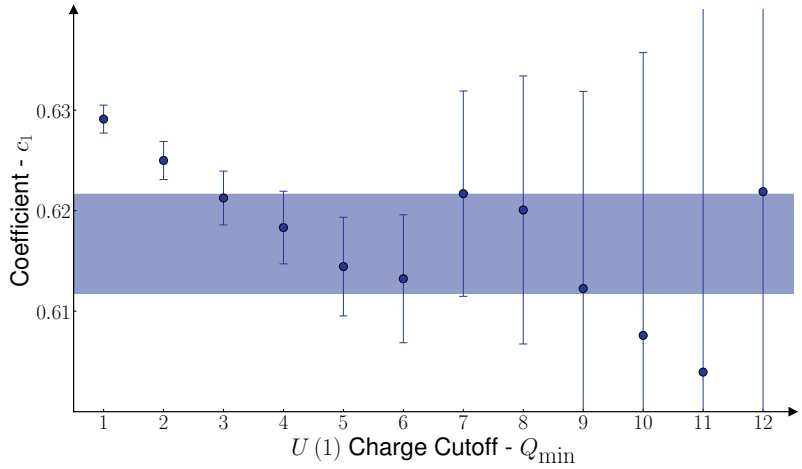

Figure 8.3.2: Coefficient c_1, from Eq. 8.3.1, when we fit the data Δ_Q for $Q \in [Q_{\text{min}}, 19]$ as a function of the lower cutoff Q_{min}.

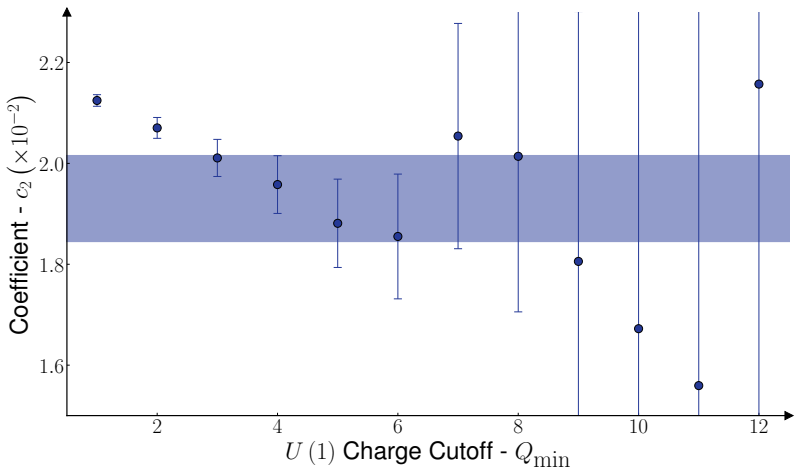

Figure 8.3.3: Coefficient c_2, from Eq. 8.3.1, when we fit the data Δ_Q for $Q \in [Q_{\text{min}}, 19]$ as a function of the lower cutoff Q_{min}.

8.4 Casimir Energy - Coefficient c_0

The large charge expansion predicts that the zeroth order term in Q is -0.0937254. In section 8.3, we assumed it to be true and it yielded accurate result. In this section, we will relax that assumption and let c_0 be a free parameter,

$$\Delta_Q^{\text{fit}}(c_1, c_2, c_0) = \frac{2}{3}\frac{1}{\sqrt{2\pi c_1}}Q^{\frac{3}{2}} + 8\pi c_2 \left(\frac{Q}{2\pi c_1}\right)^{\frac{1}{2}} + c_0. \tag{8.4.1}$$

Similar to 8.3, for Eq. 8.4.1 to be a good fit it must remain stable. As shown in Fig. 8.4.1, the most likely value for the coefficients c_0 is highly dependent on the lower cutoff for the values of the charge, going to the extreme of changing sign from charge 6 to 7 and 9 to 10.

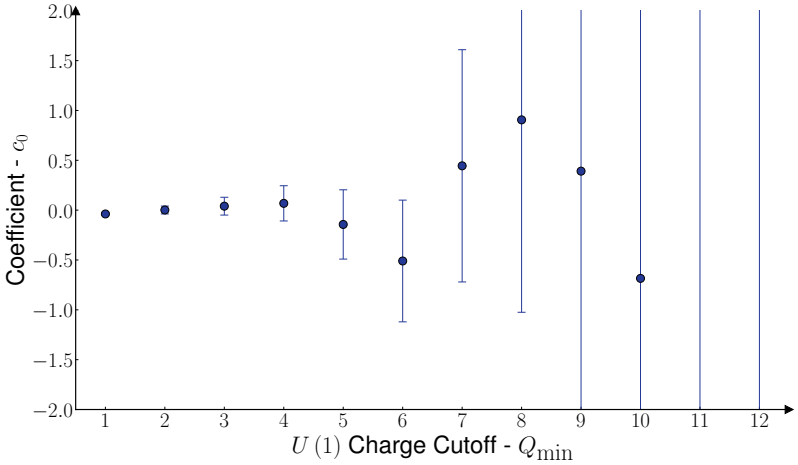

Figure 8.4.1: Coefficient c_0, from Eq. 8.4.1, when we fit the data Δ_Q for $Q \in [Q_{\text{min}}, 19]$ as a function of the lower cutoff Q_{min}.

A better way to estimate c_0 is by defining a quantity, $\mathcal{A}(Q)$, as

$$\mathcal{A}(Q) \equiv \mathcal{N}(Q)^{-1}\left(2\frac{\Delta_{Q+1}}{\sqrt{Q+1}} - \frac{\Delta_{Q+2}}{\sqrt{Q+2}} - \frac{\Delta_Q}{\sqrt{Q}}\right), \tag{8.4.2}$$

where

$$\mathcal{N}(Q) \equiv \frac{2}{\sqrt{Q+1}} - \frac{1}{\sqrt{Q+2}} - \frac{1}{\sqrt{Q}}. \tag{8.4.3}$$

If the prediction that c_0 is -0.0937254, then $\mathcal{A}(Q)$ admits the following asymptotic expansion

$$\mathcal{A}(Q) \underset{Q\gg 1}{\sim} -0.0937254 + O\left(Q^{-1/2}\right). \tag{8.4.4}$$

This means that if we use the numerical data for Δ_Q to compute $\mathcal{A}(Q)$, it should converge to a constant, -0.0937254, as the charge increases. In Fig. 8.4.2 we plotted $\mathcal{A}(Q)$, computed using the numerical data for Δ_Q.

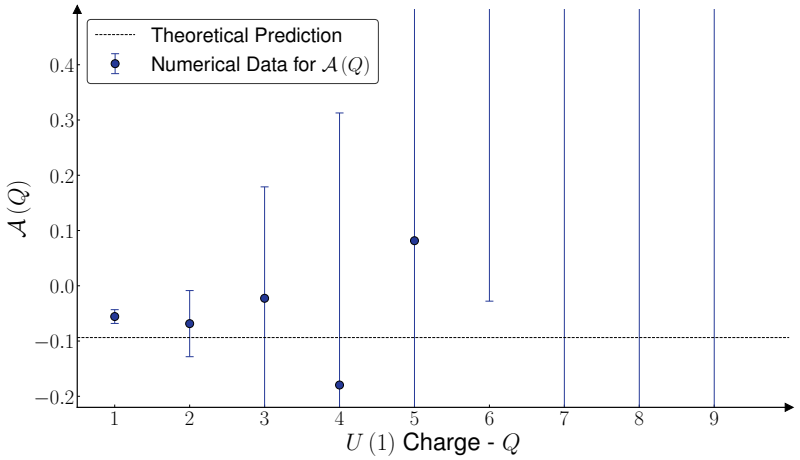

Figure 8.4.2: Estimate for the Casimir energy $\mathcal{A}_Q$ as a function of Q

When Q is 1, the numerical value for $A(Q)$ is clearly different from the expected value. The reason is because for $Q = 1$ the sub-leading terms are of order $O(1)$, and this should only be valid asymptotically. Indeed, as we increase the charge there is some evidence that $\mathcal{A}$ converges to -0.0937254, unfortunately, because the error bars rapidly increase we are unable to draw definite conclusions.

Chapter 9

Conclusions, Other Work and Future Work

In this thesis, namely Chapter 8, we studied whether the superfluid effective field theory is an accurate description of a CFT with $U(1)$ broken symmetry. In practice, that can be checked by verifying if the conformal dimension of scalar operators with large charge under $U(1)$ is given by

$$\Delta_Q = \frac{2}{3}\frac{1}{\sqrt{2\pi c_1}}Q^{\frac{3}{2}} + 8\pi c_2\left(\frac{Q}{2\pi c_1}\right)^{\frac{1}{2}} - 0.0937254 + O\left(Q^{-1/2}\right), \tag{9.0.1}$$

where $c_{3/2} = \frac{2}{3}\frac{1}{\sqrt{2\pi c_1}}$, $c_{1/2} = \frac{8\pi c_2}{\sqrt{2\pi c_1}}$. The evidence we have gathered strongly indicates that the superfluid description is useful. Furthermore, it appear as if the asymptotic expansion is valid for operator with charge as small as 1.

In Section 2.5, we concluded that a CFT can be fully described by the set of all conformal dimensions and the set of all OPE coefficients, formally called CFT data. So far the superfluid action, Eq. 3.6.21, can accurately predict the conformal dimensions of charged scalar operators. Meaning that in order to declare the superfluid action as the accurate effective description, it should also accurately predict the OPE coefficients and the conformal dimensions of operators with spin. The OPE coefficients, λ, first appear in the 3-point correlation function,

$$\left\langle \mathcal{O}_{Q_1}(x_3)\,\mathcal{O}_{Q_2}(x_2)\,\mathcal{O}_{-Q_1-Q_2}(x_1)\right\rangle = \frac{\lambda_{Q_1,Q_2,-Q_1-Q_2}}{x_{23}^{\Delta_{Q_1}+\Delta_{Q_2}-\Delta_{Q_1+Q_2}}\,x_{12}^{\Delta_{Q_1+Q_2}+\Delta_{Q_2}-\Delta_{Q_1}}\,x_{13}^{\Delta_{Q_1}+\Delta_{Q_1+Q_2}-\Delta_{Q_2}}}, \tag{9.0.2}$$

where $x_{ij} \equiv |x_i - x_j|$. I will not go into great detail, but it is fairly easy to rewrite the 3-point function as a product of two 2-point functions, for which we can use the continuous-time algorithm, described in Section 6.4. The superfluid prediction for the OPE coefficients are

$$\lambda_{Q_1,Q_2,-Q_1-Q_2} = \exp\left[\frac{c_{3/2}}{2\sqrt{\pi}}Q_1^{3/2}f(y) + O\left(\min\{Q_1,Q_2\}^{1/2}\right)\right], \tag{9.0.3}$$

where $y = \sqrt{Q_2/Q_1}$, $f(y)$ is known function and both $Q_1,\, Q_2 \gg 1$. Not only would we like to verify that the prediction in Eq. 9.0.3 is valid, we also need to verify that the coefficient $c_{3/2}$, in Eq. 9.0.3, is compatible with the $c_{3/2}$ in Eq. 9.0.1. In [58], we were able to perform the first ever measurements of this quantity when Q_1 is equal to Q_2, concluding that the $c_{3/2}$, $0.4(1)$, is compatible with the value for $c_{3/2}$, $0.339(1)$, computed using the data for the conformal dimensions, see Fig. 9.0.1.

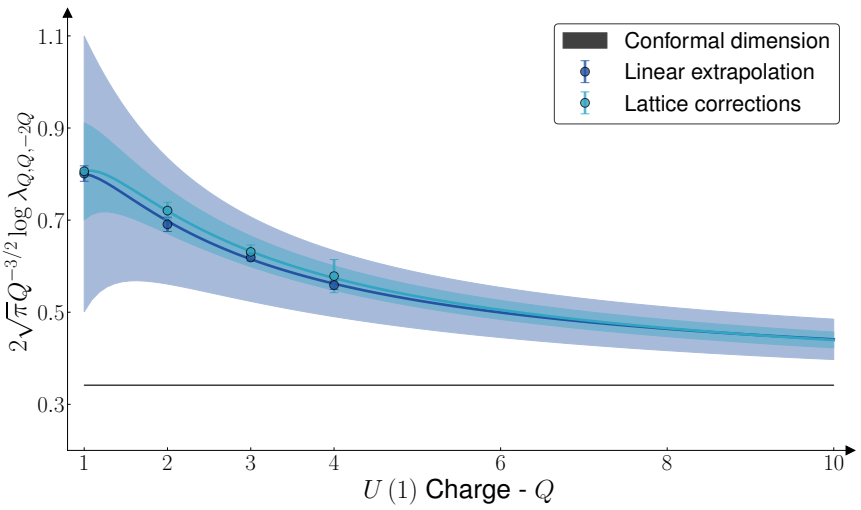

Figure 9.0.1: $2\sqrt{\pi}Q^{-3/2}\log\lambda_{Q,Q,-2Q}$ as a function of Q, adapted from [58]. The black line corresponds to the $c_{3/2} = 0.339\,(1)$ computed using the conformal dimensions. In the dark blue points we assumed that the finite-size effects are linear in $\frac{1}{L}$, whereas in the light blue points correspond to performing perturbation theory around a CFT.

The last piece for the CFT data are the conformal dimensions for operators with spin, J. Currently, we are working on measuring the conformal dimension of the lightest charged operator with spin $J = 2$, where the superfluid EFT prediction for the conformal dimensions is $\Delta\,(Q) + \sqrt{3}$. Besides verifying whether or not that prediction is true, we are interested in finding if, similarly to the scalar operators, the prediction converges for small values of Q. Afterwards, it would be interesting to study the conformal dimension of spin operators as a function of $\frac{J}{Q}$, where the $O\,(2)$ model is expected to have a rich phase diagram, see [61, 62].

Future work must pass through the increase in precision for measurements of the Casimir energy, Fig. 8.4.2. Additionally, when we computed the OPE coefficients, we were able to do it for Q_1 equal to $Q_2 \in [1, 4]$. In order to improve the precision in the measurement of $c_{3/2}$, one needs to go to a bigger charge, ideally 10. Needless to say that, achieving more precise measurements for both the Casimir energy and $c_{3/2}$, requires improved Monte-Carlo methods, which, unfortunately, is a non-trivial problem due to the complex interplay between generating more samples, in the same computational time, and the amount of correlation between those samples. Regarding the spin operators, we are currently working on operator with spin 2. However, one of the possible direction of study could focus on finding a general strategy that would allow the study of the conformal dimension as a function of the spin and the charge in a systematic manner.

As a final remark, the surprising accuracy of the large charge expansion is reminiscent of the success of the complex spin for the QCD and Yang-Mills spectrum and the large spin bootstrap in the $O\,(N)$ models. In both these examples, the CFT data shared analyticity properties with spin. It remains an open question whether or not the CFT data of the $O\,(2)$ model enjoys similar analyticity properties with respect to charge.

Bibliography

[1] Juan M. Maldacena. “The Large N Limit of Superconformal Field Theories and Supergravity.” In: *International Journal of Theoretical Physics* 38 (1999), p. 1113. DOI: 10.1023/A:1026654312961.

[2] Slava Rychkov. “EPFL Lectures on Conformal Field Theory in D>= 3 Dimensions.” In: *Springer* (2017). DOI: 10.1007/978-3-319-43626-5.

[3] David Simmons-Duffin. “TASI Lectures on the Conformal Bootstrap.” In: (2016). arXiv: 1602.07982 [hep-th].

[4] P. Di Francesco, P. Mathieu, and D. Sénéchal. “Conformal Field Theory.” In: *Island Press* (1996).

[5] Zohar Komargodski and Alexander Zhiboedov. “Convexity and Liberation at Large Spin.” In: *J. High Energ. Phys.* 2013 (2013), p. 140. DOI: 10.1007/JHEP11(2013)140.

[6] A. Liam Fitzpatrick et al. “The Analytic Bootstrap and AdS Superhorizon Locality.” In: *J. High Energ. Phys.* 2013 (2013), p. 4. DOI: 10.1007/JHEP12(2013)004.

[7] Luis F. Alday and Juan Maldacena. “Comments on operators with large spin.” In: *J. High Energy Phys.* 2007 (2007), p. 19. DOI: 10.1088/1126-6708/2007/11/019.

[8] Luis F. Alday and Agnese Bissi. “Higher-spin correlators.” In: *J. High Energ. Phys.* 2013 (2013), p. 202. DOI: 10.1007/JHEP10(2013)202.

[9] Simeon Hellerman et al. “On the CFT Operator Spectrum at Large Global Charge.” In: *J. High Energ. Phys.* 2015 (2015), p. 71. DOI: 10.1007/JHEP12(2015)071.

[10] Alexander Monin et al. “Semiclassics, Goldstone Bosons and CFT data.” In: *J. High Energ. Phys.* 2017 (2017), p. 11. DOI: 10.1007/JHEP06(2017)011.

[11] Alexander M. Polyakov. “Conformal symmetry of critical fluctuations.” In: *JETP Lett.* 12 (1970), pp. 538–541.

[12] Sheer El-Showk et al. “Solving the 3D Ising Model with the Conformal Bootstrap.” In: *Phys. Rev. D* 86 (2012), p. 025022. DOI: 10.1103/PhysRevD.86.025022.

[13] Filip Kos et al. “Precision islands in the Ising and O(N) models.” In: *J. High Energ. Phys.* 2016 (2016), p. 36. DOI: 10.1007/JHEP08(2016)036.

[14] Simon Caron-Huot. “Analyticity in Spin in Conformal Theories.” In: *J. High Energ. Phys.* 2017 (2017), p. 78. DOI: 10.1007/JHEP09(2017)078.

[15] David Simmons-Duffin, Douglas Stanford, and Edward Witten. “A spacetime derivation of the Lorentzian OPE inversion formula.” In: *J. High Energ. Phys.* 2018 (2018), p. 85. DOI: 10.1007/JHEP07(2018)085.

[16] Dimitris Manolopoulos and Konstantinos Sfetsos. *Conformal Field Theory Lecture Notes*. 2020.

[17] Ulrich Mosel. *Path integrals in field theory: An introduction*. Vol. 1. Springer, 2004.

[18] Shai M. Chester et al. “Carving out OPE space and precise O(2) model critical exponents.” In: *J. High Energ. Phys.* 2020 (2020), p. 142. DOI: 10.1007/JHEP06(2020)142.

[19] Filip Kos et al. “Bootstrapping the O(N) Archipelago.” In: *J. High Energ. Phys.* 2015 (2015), p. 106. DOI: 10.1007/JHEP11(2015)106.

[20] David Tong. *University of Cambridge Part III Mathematical Tripos*.

[21] Jason Bennett. “A pedagogical review of gravity as a gauge theory.” In: (2021). arXiv: 2104.02627 [gr-qc].

[22] P. Goodard, A. Kent, and D. Olive. “Virasoro algebras and coset space models.” In: *Physics Letters B* 152 (1985), pp. 88–92. DOI: 10.1016/0370-2693(85)91145-1.

[23] K. Gawędzki and A. Kupiainen. “Coset construction from functional integrals.” In: *Nuclear Physics B* 320 (1989), pp. 625–668. DOI: 10.1016/0550-3213(89)90015-1.

[24] Juan Pablo Hoyos Daza. “Composite Higgs models.” In: (2019). arXiv: 1908.10204 [hep-ph].

[25] Daniel Naegels. “An introduction to Goldstone boson physics and to the coset construction.” In: (2021). arXiv: 2110.14504 [hep-th].

[26] Riccardo Penco. “An Introduction to Effective Field Theories.” In: (2020). arXiv: 2006.16285 [hep-th].

[27] Alberto Nicolis et al. “Zoology of condensed matter: Framids, ordinary stuff, extra-ordinary stuff.” In: (2015). arXiv: 1501.03845 [hep-th].

[28] Ian Low and Aneesh V. Manohar. “Spontaneously Broken Spacetime Symmetries and Goldstone’s Theorem.” In: *Phys. Rev. Lett.* 88 (2002), p. 101602. DOI: 10.1103/PhysRevLett.88.101602.

[29] Luca V. Delacretaz et al. “(Re-)Inventing the Relativistic Wheel: Gravity, Cosets, and Spinning Objects.” In: *J. High Energ. Phys.* 2014 (2014), p. 8. DOI: 10.1007/JHEP11(2014)008.

[30] Georgios K. Karananas and Alexander Monin. “Gauging nonrelativistic field theories using the coset construction.” In: *Phys. Rev. D* 93 (2016), p. 064069. DOI: 10.1103/PhysRevD.93.064069.

[31] Georgios Karananas. “Poincaré, Scale and Conformal Symmetries:Gauge Perspective and Cosmological Ramifications.” In: (2016). DOI: 10.5075/epfl-thesis-7173.

[32] E. A. Ivanov and J. Niederle. “Gauge formulation of gravitation theories. I. The Poincaré, de Sitter, and conformal cases.” In: *Phys. Rev. D* 25 (1982), p. 976. DOI: 10.1103/PhysRevD.25.976.

[33] E. A. Ivanov and J. Niederle. “Gauge formulation of gravitation theories. II. The special conformal case.” In: *Phys. Rev. D* 25 (1982), p. 988. DOI: 10.1103/PhysRevD.25.988.

[34] Georgios K. Karananas and Alexander Monin. “Weyl and Ricci gauging from the coset construction.” In: *Phys. Rev. D* 93 (2016), p. 064013. DOI: 10.1103/PhysRevD.93.064013.

[35] Gabriel Francisco Cuomo. “Large charge, semiclassics and superfluids :from broken symmetries to conformal field theories.” 2020. DOI: 10.5075/epfl-thesis-8397.

[36] P. Kusch and H. M. Foley. “The Magnetic Moment of the Electron.” In: *Phys. Rev.* 74 (1948), p. 250. DOI: 10.1103/PhysRev.74.250.

[37] G. ’t Hooft. “A two-dimensional model for mesons.” In: *Nuclear Physics B* 75 (1974), pp. 461–470. DOI: 10.1016/0550-3213(74)90088-1.

[38] G. ’t Hooft. “A planar diagram theory for strong interactions.” In: *Nuclear Physics B* 72 (1974), pp. 461–473. DOI: 10.1016/0550-3213(74)90154-0.

[39] Gabriel Cuomo. “The OPE meets semiclassics.” In: *Phys. Rev. D* 103 (2021), p. 085005. DOI: 10.1103/PhysRevD.103.085005.

[40] Gabriel Cuomo. “A note on the large charge expansion in 4d CFT.” In: *Physics Letters B* 812 (2021), p. 136014. DOI: 10.1016/j.physletb.2020.136014.

[41] Alexander Altland and Ben D. Simons. “Condensed Matter Field Theory.” In: *Cambridge University Press* (2010). DOI: 10.1017/CBO9780511789984.

[42] David Tong. “Statistical field theory.” In: *Lecture Notes* (2017).

[43] E. L. Pollock and D. M. Ceperley. “Path-integral computation of superfluid densities.” In: *Phys. Rev. B* 36 (1987), p. 8343. DOI: 10.1103/PhysRevB.36.8343.

[44] Debasish Banerjee, Shailesh Chandrasekharan, and Domenico Orlando. “Conformal dimensions via large charge expansion.” In: *Phys. Rev. Lett.* 120 (2018), p. 061603. DOI: 10.1103/PhysRevLett.120.061603.

[45] Wanwan Xu et al. “High-precision Monte Carlo study of several models in the three-dimensional U(1) universality class.” In: *Phys. Rev. B* 100 (2019), p. 064525. DOI: 10.1103/PhysRevB.100.064525.

[46] Nikolay Prokof’ev and Boris Svistunov. “Worm algorithms for classical statistical models.” In: *Phys. Rev. Lett.* 87 (2001), p. 160601. DOI: 10.1103/PhysRevLett.87.160601.

[47] Hidemaro Suwa. “Geometric allocation approach to accelerating directed worm algorithm.” In: *Phys. Rev. E* 103 (2021), p. 013308. DOI: 10.1103/PhysRevE.103.013308.

[48] M.E.J. Newman. “Computational Physics.” In: *CreateSpace Independent Publishing Platform* (2013).

[49] J. -C. Walter and G. T. Barkema. “An introduction to Monte Carlo methods.” In: *Physica A: Statistical Mechanics and its Applications* 418 (2015), pp. 78–87. DOI: 10.1016/j.physa.2014.06.014.

[50] Jiaxin Zhang. “Modern Monte Carlo Methods for Efficient Uncertainty Quantification and Propagation: A Survey.” In: (2020). arXiv: 2011.00680 [stat.ME].

[51] K. Binder. *Monte Carlo Simulation in Statistical Physics: An Introduction*. 2010.

[52] Linda E. Reichl. “A modern course in statistical physics.” In: *Springer* (2016). DOI: 10.1007/s10955-010-0062-1.

[53] Prof. João Manuel Viana Parente Lopes. *Notas da cadeira de Física Estatística*.

[54] N. V Prokof’ev, B. V Svistunov, and I. S Tupitsyn. “”Worm” algorithm in quantum Monte Carlo simulations.” In: *Physics Letters A* 238 (1998), pp. 253–257. DOI: 10.1016/S0375-9601(97)00957-2.

[55] N. V. Prokof’ev, B. V. Svistunov, and I. S. Tupitsyn. “Exact, Complete, and Universal Continuous-Time Worldline Monte Carlo Approach to the Statistics of Discrete Quantum Systems.” In: *J. Exp. Theor. Phys.* 114 (1998), pp. 570–590. DOI: 10.1134/1.558661.

[56] N. Prokof’ev and B. Svistunov. “Worm Algorithm for Problems of Quantum and Classical Statistics.” In: (2010). arXiv: 0910.1393 [cond-mat.stat-mech].

[57] H. G. Ballesteros et al. “Finite size effects on measures of critical exponents in d = 3 O(N) models.” In: *Physics Letters B* 387 (1996), pp. 125–131. DOI: 10.1016/0370-2693(96)00984-7.

[58] Gabriel Cuomo et al. “Numerical tests of the large charge expansion.” In: (2023). arXiv: 2305.00499 [hep-lat].

[59] Martin Hasenbusch and Ettore Vicari. “Anisotropic perturbations in three-dimensional O(N)-symmetric vector models.” In: *Phys. Rev. B* 84 (2011), p. 125136. DOI: 10.1103/PhysRevB.84.125136.

[60] Martin Hasenbusch. “Monte Carlo study of an improved clock model in three dimensions.” In: *Phys. Rev. B* 100 (2019), p. 224517. DOI: 10.1103/PhysRevB.100.224517.

[61] Gabriel Cuomo et al. “Rotating superfluids and spinning charged operators in conformal field theory.” In: *Phys. Rev. D* 97 (2018), p. 045012. DOI: 10.1103/PhysRevD.97.045012.

[62] Gabriel Cuomo and Zohar Komargodski. “Giant Vortices and the Regge Limit.” In: *J. High Energ. Phys.* 2023 (2023), p. 6. DOI: 10.1007/JHEP01(2023)006.

[63] Alexander Monin. “Partition function on spheres: How to use zeta function regularization.” In: *Phys. Rev. D* 94 (2016), p. 085013. DOI: 10.1103/PhysRevD.94.085013.

Appendix A

Coset Construction Examples

A.1 Example of the coset construction for the spacetime symmetries Conformal $\rightarrow$ Poincaré

In this section, we will be exemplifying the use of the coset construction for spacetime symmetries. At the end of the calculations we will have arrived at a Lagrangian with conformal symmetry spontaneously broken to Poincaré symmetry.

The non-trivial commutators corresponding to the conformal algebra are

$$\begin{aligned}
[L^{\mu\nu}, L^{\rho\sigma}] &= -i\left(\eta^{\mu\rho}L^{\nu\sigma} - \eta^{\mu\sigma}L^{\nu\rho} - \eta^{\nu\rho}L^{\mu\sigma} + \eta^{\nu\sigma}L^{\mu\rho}\right), \\
\left[L^{\mu\nu}, P^{\lambda}\right] &= -i\left(\eta^{\mu\lambda}P^{\nu} - \eta^{\nu\lambda}P^{\mu}\right), \\
\left[L^{\mu\nu}, K^{\lambda}\right] &= -i\left(\eta^{\mu\lambda}K^{\nu} - \eta^{\nu\lambda}K^{\mu}\right), \\
[D, P^{\mu}] &= iP^{\mu}, \\
[D, K^{\mu}] &= -iK^{\mu}, \\
[K^{\mu}, P^{\nu}] &= -2i\left(L^{\mu\nu} - \eta^{\mu\nu}D\right),
\end{aligned} \tag{A.1.1}$$

where $L^{\mu\nu}$ are the rotation generators, P^{μ} are the translation generators, D is the dilation generators and K^{μ} are the SCT generators. The broken pattern conformal to Poincaré implies that the D and K^{μ} will be the broken. Notice that the generators K and D are related via a commutator $[K, P] \sim D$, therefore not all the Goldstone fields associated with K and D will be independent. The coset prescription requires that we compute the Maurer-Cartan 1-form from the coset representative

$$\Omega\left(\pi_1, \pi_2, x\right) = e^{ix^{\mu}P_{\mu}} e^{i\pi_1 D} e^{i\pi_2^{\mu}K_{\mu}}. \tag{A.1.2}$$

The Maurer-Cartan 1-form reads

$$\begin{aligned}
\omega =& -i\Omega^{\dagger}d\Omega \\
=& \Omega^{\dagger}\left(d\left(x^{\mu}P_{\mu}\right)e^{ix^{\mu}P_{\mu}}e^{i\pi_1 D}e^{i\pi_2^{\mu}K_{\mu}} + e^{ix^{\mu}P_{\mu}}d\left(\pi_1 D\right)e^{i\pi_1 D}e^{i\pi_2^{\mu}K_{\mu}} + e^{ix^{\mu}P_{\mu}}e^{i\pi_1 D}e^{i\pi_2^{\mu}K_{\mu}}d\left(\pi_2^{\mu}K_{\mu}\right)\right) \\
=& dx^{\nu}e^{-i\pi_2^{\mu}K_{\mu}}e^{-i\pi_1 D}P_{\nu}e^{i\pi_1 D}e^{i\pi_2^{\mu}K_{\mu}} + dx^{\nu}\partial_{\nu}\pi_1 e^{-i\pi_2^{\mu}K_{\mu}}De^{i\pi_2^{\mu}K_{\mu}} + dx^{\nu}\partial_{\nu}\pi_2^{\mu}K_{\mu}.
\end{aligned} \tag{A.1.3}$$

The trick to simplify quantities of the form $e^A B e^{-A}$ is to use the Hausdorff formula,

$$e^A B e^{-A} = B + \frac{1}{1!}[A,B] + \frac{1}{2!}[A,[A,B]] + \frac{1}{3!}[A,[A,[A,B]]] + ... \tag{A.1.4}$$

Applying the Hausdorff formula to each term on Eq. A.1.3 yields

$$e^{-i\pi_1 D} P_\nu e^{i\pi_1 D} = e^{\pi_1} P_\nu,$$

$$\begin{aligned} e^{-i\pi_2^\mu K_\mu} e^{-i\pi_1 D} P_\nu e^{i\pi_1 D} e^{i\pi_2^\mu K_\mu} &= e^{\pi_1}\left(-2L^{\nu\mu}\pi_{2\mu} + P_\nu + 2\pi_{2\nu} D + 2\pi_{2\nu}\pi^{2\mu} K_\mu - \pi_2^2 K_\nu\right), \\ e^{-i\pi_2^\mu K_\mu} D e^{i\pi_2^\mu K_\mu} &= D + \frac{\pi_2^\mu}{1!} K_\mu. \end{aligned} \tag{A.1.5}$$

After gathering the terms by generators, one can write the Maurer-Cartan 1-form as

$$\omega = \omega_P^\nu P_\nu + \frac{1}{2}\omega_L^{\mu\nu} L_{\mu\nu} + \omega_D D + \omega_K^\nu K_\nu, \tag{A.1.6}$$

where

$$\begin{aligned} \omega_P^\nu &= dx^\nu e^{\pi_1}, \\ \omega_L^{\mu\nu} &= -2e^{\pi_1}\left(dx^\nu \pi_2^\mu - \pi_2^\nu dx^\mu\right), \\ \omega_D &= 2e^{\pi_1}\pi_{2\nu} dx^\nu + d\pi_1, \\ \omega_K^\nu &= d\pi_2^\nu + \pi_2^\nu d\pi_1 + e^{\pi_1}\left(2\pi^{2\nu}\pi_{2\lambda} - \pi_2^2\delta_\lambda^\mu\right) dx^\lambda. \end{aligned} \tag{A.1.7}$$

Now comes the part where the coset construction for spacetime symmetries differs from the internal symmetries, recall that commutator $[K,P] \sim D$ meaning that the Goldstone boson for broken K and D will mix. To prevent overcounting modes we will apply the inverse Higgs constraint $\omega_D = 0$, which results in

$$\pi_2^\mu = -\frac{1}{2} e^{-\pi_1}\partial^\mu \pi_1. \tag{A.1.8}$$

The Lagrangian can be built from covariant quantities ω_P^ν, ω_K^ν. The zeroth order term in $\partial\pi_1$ will be given by

$$S_0 = \int \omega_P^0 \wedge \omega_P^1 \wedge \omega_P^2 \wedge \omega_P^3 = \int e^{4\pi_1} dx^0 \wedge dx^1 \wedge dx^2 \wedge dx^3. \tag{A.1.9}$$

The first term containing derivatives of π_1, will be the kinetic term

$$S_1 = \int \omega_K^0 \wedge \omega_P^1 \wedge \omega_P^2 \wedge \omega_P^3 = \int e^{2\pi_1} dx^0 \wedge dx^1 \wedge dx^2 \wedge dx^3 \left(\partial_\mu \pi_1\right)^2. \tag{A.1.10}$$

Looking at the equation above we are able to identify $e^{2\pi_1} dx^0 \wedge dx^1 \wedge dx^2 \wedge dx^3$ as a volume form and therefore associate $e^{2\pi_1}$ as the square root of the determinant of the metric. A simple metric that would satisfy such condition would be $g_{\mu\nu} = e^{4\pi_1}\eta_{\mu\nu}$. A neat shortcut to avoid computing a lot of wedge products is to use this metric to build diffeomorphism invariant quantities[1] and used them to construct the Lagrangian. From general relativity we already know that that such quantities will the curvature tensor $R^\rho_{\mu\nu\sigma}$ and contractions.[2].

[1] Invariant under change in coordinates

[2] The beauty of the argument is that despite not being a gravitational theory, the Conformal to Poincaré symmetry breaking, a theory of a scalar field π_1, shares a similar formulation to general relativity.

A.2 Coset Construction for the Large Charge

$$SO\left(4,1\right)\times U\left(1\right)\rightarrow SO\left(3\right)\times\left(D+\mu Q\right)$$

The non-trivial commutators corresponding to the conformal algebra, $SO\left(4,1\right)\times U\left(1\right)$, are

$$\begin{aligned}
\left[L^{AB},L^{CD}\right] &= -i\left(\delta^{AC}L^{BD}-\delta^{AD}L^{BC}-\delta^{BC}L^{AD}+\delta^{BD}L^{AC}\right),\\
\left[P^{C},L^{AB}\right] &= +i\left(\delta^{BC}P^{A}-\delta^{AC}P^{B}\right),\\
\left[K^{C},L^{AB}\right] &= i\left(\delta^{BC}K^{A}-\delta^{AC}K^{B}\right),\\
\left[D,P^{A}\right] &= -iP^{A},\\
\left[D,K^{A}\right] &= +iK^{A},\\
\left[K^{A},P^{B}\right] &= -2i\left(L^{AB}+\delta^{AB}D\right),\\
\left[\bar{P}_{A},L_{0B}\right] &= i\delta_{AB}\left(\mu Q-\bar{P}_{0}\right),\\
\left[\bar{P}_{0},D\right] &= -i\left(\bar{P}_{0}+\mu Q\right).
\end{aligned}\tag{A.2.1}$$

For the symmetry breaking pattern in Eq. 3.6.6, we are able to write the representative for the coset as

$$\Omega=e^{iy^{A}(x)P_{A}}e^{i\pi_{1}(x)D}e^{i\eta^{B}(x)L_{0B}}e^{i\chi(x)Q}\equiv e^{iy^{A}P_{A}}e^{i\pi_{1}D}\tilde{\Omega}.\tag{A.2.2}$$

According to the gauging of translations, rotations and dilations, the covariant derivative, D_μ is defined by introducing the connection $\tilde{e}_{\mu}^{A}$, $\tilde{\omega}_{\mu}^{AB}$ and $\tilde{W}_{\mu}$

$$D_{\mu}=\partial_{\mu}+i\tilde{e}_{\mu}^{A}P_{A}+\frac{i}{2}\tilde{\omega}_{\mu}^{AB}L_{AB}+i\tilde{W}_{\mu}D.\tag{A.2.3}$$

Before computing the full Maurer-Cartan 1-form, it is convenient to start by

$$e^{-i\pi_{1}D}e^{-iy^{A}P_{A}}D_{\mu}e^{iy^{A}P_{A}}e^{i\pi_{1}D},\tag{A.2.4}$$

using

$$\begin{aligned}
e^{iy^{A}P_{A}}De^{iy^{A}P_{A}} &= D+y^{A}P_{A},\\
e^{-i\pi_{1}D}P_{A}e^{i\pi_{1}D} &= e^{-\pi_{1}}P_{A}\text{ and}\\
e^{-iy^{A}P_{A}}L_{AB}e^{iy^{A}P_{A}} &= L_{AB}-y^{A}\omega^{BA}P_{B},
\end{aligned}\tag{A.2.5}$$

one can simplify Eq. A.2.4 to

$$e^{-i\pi_{1}D}e^{-iy^{A}P_{A}}D_{\mu}e^{iy^{A}P_{A}}e^{i\pi_{1}D}=ie^{\pi_{1}}e_{\mu}^{A}P_{A}+iW_{\mu}D+\frac{i}{2}\omega_{\mu}^{AB}L_{AB},\tag{A.2.6}$$

where $e_{\mu}^{A}=\tilde{e}_{\mu}^{A}+\partial_{\mu}y^{A}+y^{A}e^{\pi_{1}}\tilde{W}_{\mu}-y^{B}\tilde{\omega}_{\mu}^{AB}$, $W_{\mu}=\tilde{W}_{\mu}+\partial_{\mu}\pi_{1}$ and $\omega_{\mu}^{AB}=\tilde{\omega}_{\mu}^{AB}$. Because Q commutes with all the generators

$$\begin{aligned}
\tilde{\Omega}^{-1}e^{-i\pi_{1}D}e^{-iy^{A}P_{A}}D_{\mu}e^{iy^{A}P_{A}}e^{i\pi_{1}D}\tilde{\Omega}=e^{-i\eta^{B}(x)L_{0B}}\Big[&\partial_{\mu}+ie^{-\pi_{1}}e_{\mu}^{A}P_{A}+iW_{\mu}D+\\
&+\frac{i}{2}\omega_{\mu}^{AB}L_{AB}+\partial_{\mu}\chi Q\Big]e^{i\eta^{B}(x)L_{0B}}
\end{aligned}\tag{A.2.7}$$

From now on the lower letter represent the indices associated with the spatial dimensions. Dividing the generator L into boosts, L_{0A}, and rotations, L_{ab},

$$e^{-i\eta^B(x)L_{0B}}\left(\partial_\mu + ie^{-\pi_1}e^A_\mu P_A + iW_\mu D + \frac{i}{2}\omega^{ab}_\mu L_{ab} + \omega^{0A}_\mu L_{0A} + \partial_\mu\chi Q\right)e^{i\eta^B(x)L_{0B}} \tag{A.2.8}$$

In matrix representation of $e^{i\eta^B(x)L_{0B}}$ are the Lorentz matrices, $\Lambda(\eta)$, associated with the boosts η

$$\left(e^{i\eta^B(x)L_{0B}}\right)^A_B = \Lambda^A_B. \tag{A.2.9}$$

Using the following properties,

$$\begin{aligned}
e^{-i\eta^B(x)L_{0B}}\partial_\mu e^{i\eta^B(x)L_{0B}} &= \frac{i}{2}\left(\Lambda^{-1}\partial_\mu\Lambda\right)^{ab}L_{ab} + i\left(\Lambda^{-1}\partial_\mu\Lambda\right)^{0a}L_{0a},\\
e^{-i\eta^B(x)L_{0B}}P_A e^{i\eta^B(x)L_{0B}} &= i\Lambda^B_A P_B,\\
e^{-i\eta^B(x)L_{0B}}L_{AB}e^{i\eta^B(x)L_{0B}} &= \frac{i}{2}\Lambda^c_a\Lambda^d_b L_{ab} + i\Lambda^C_0\Lambda^d_b L_{0b},
\end{aligned} \tag{A.2.10}$$

it is possible to simplify the Eq. A.2.8 and arrive at the simplified version of the Maurer-Cartan 1-Form,

$$\begin{aligned}
-i\Omega D\Omega =& dx^\mu\Big\{e^{-\pi_1}e^A_\mu\Lambda^B_A P_B + W_\mu D + \partial_\mu\chi Q + \mu e^{-\pi_1}e^A_\mu\Lambda^B_A Q\delta^0_B - \mu e^{-\pi_1}e^A_\mu\Lambda^B_A Q\delta^0_B +\\
&+\frac{1}{2}\left(\Lambda^c_a\Lambda^d_b\omega^{ab}_\mu + \left(\Lambda^{-1}\partial_\mu\Lambda\right)^{ab}\right)L_{ab} + \left(\Lambda^0_c\Lambda^a_d\omega^{cd}_\mu + \left(\Lambda^{-1}\partial_\mu\Lambda\right)^{0a}\right)L_{0a}\Big\}
\end{aligned} \tag{A.2.11}$$

To simplify, we will rename some quantities such that

$$-i\Omega D\Omega = dx^\mu E^A_\mu\left(\bar{P}_A + \nabla_A\pi_1 D + \nabla_A\chi Q + \nabla_A\eta^a L_{0a} + \frac{1}{2}\Omega^{ij}_A L_{ij}\right), \tag{A.2.12}$$

where

$$\begin{aligned}
E^A_\mu &= e^{-\pi_1}e^B_\mu\Lambda^A_B, \quad \nabla_A\chi = e^{\pi_1}e^\nu_C\Lambda^C_A\partial_\nu\chi - \mu\delta^0_A, \quad \nabla_A\pi_1 = e^{\pi_1}e^\nu_C\Lambda^C_A\left(\partial_\nu\pi_1 + \tilde{W}_\nu\right),\\
\nabla_A\eta^a &= e^{\pi_1}e^\nu_C\Lambda^C_A\left(\Lambda^0_c\Lambda^a_d\omega^{cd}_\nu + \left(\Lambda^{-1}\partial_\nu\Lambda\right)^{0a}\right),\\
\Omega^{ab}_A &= e^{\pi_1}e^\nu_C\Lambda^C_A\left(\Lambda^c_a\Lambda^d_b\omega^{ab}_\nu + \left(\Lambda^{-1}\partial_\mu\Lambda\right)^{ab}\right).
\end{aligned} \tag{A.2.13}$$

Applying the constraint to deal with redundant fields. First, the geometrical constraints

$$W_\mu = 0 \to \tilde{W}_\mu = -\partial_\mu\pi_1 \quad \text{and } T^C_{AB} = 0. \tag{A.2.14}$$

Then, the inverse Higgs constraints [3], $\nabla_A\chi = 0$ and $\nabla_A\sigma = 0$, which lead into

$$\mu e^{-\pi_1} = \left(\delta^{ab}e^\mu_b e^\nu_a\partial_\mu\chi\partial_\nu\chi\right)^{\frac{1}{2}} \quad \text{and } \beta_i = \frac{e^\mu_i\partial_\mu\chi}{e^\nu_0\partial_\nu\chi}. \tag{A.2.15}$$

[3] Lorentz matrix has the following elements $\Lambda^0_0 = \gamma$, $\Lambda^a_0 = \gamma\beta^a$, $\Lambda^0_a = \gamma\beta_a$ and $\Lambda^a_b = \delta^a_b + (\gamma - 1)\frac{\beta^a\beta_b}{\beta^2}$. Where $\beta_i = \frac{\eta_i}{\eta}\tanh\eta$, $\eta = \sqrt{\eta_i\eta^i}$ and $\gamma = \frac{1}{\sqrt{1-\beta^2}}$

A.3 Casimir Energy

The goal is to compute the quantum correction to the vaccum energy which are given by the determinant of the fluctuations

$$\Delta E = -\frac{1}{2}\log\det\left(-\partial_t^2 - \triangle_{S^2}\right), \tag{A.3.1}$$

where $\triangle_{S^2}$ is the laplacian operator of the 2D sphere with radius R. Because the determinant is invariant under the change of basis, we will compute it in the basis span by the eigenvectors, were

$$\det\left(-\partial_t^2 - \triangle_{S^2}\right) = \prod_n \lambda_n. \tag{A.3.2}$$

Plugging the equation above on Eq. A.3.1, we get

$$\Delta E = -\frac{1}{2}\sum_n \log\lambda_n, \tag{A.3.3}$$

as it will become clear when we specify the eigenvalues, in Eq. A.3.3, does not converge, therefore it will need to be regularized. It is convenient to introduce a new parameter, s, an define a new function

$$\Delta E\left(s\right) = -\frac{1}{2}\sum_n \frac{\log\lambda_n}{\lambda_n^s}, \tag{A.3.4}$$

such that when $s = 0$ we recover the energy of the summation in Eq. A.3.3. Although not trivial, $\Delta E\left(s\right)$ is the derivative of the generalized zeta function

$$\frac{d}{ds}\zeta\left(s\right) = \frac{d}{ds}\sum_n \frac{1}{\lambda_n^s} = \frac{d}{ds}\left(\sum \exp\left(-s\log\lambda_n\right)\right) = -\sum_n \frac{\log\lambda_n}{\lambda_n^s}. \tag{A.3.5}$$

Meaning that ΔE will be given by

$$\Delta E = \frac{1}{2}\frac{d}{ds}\zeta\left(s\right)\Big|_{s=0}, \text{where } \zeta\left(s\right) = \sum_n \lambda_n^{-s}. \tag{A.3.6}$$

The eigenvalues of $\left(-\partial_t^2 - \triangle_{S^2}\right)$ are given in terms of a natural number l and a real number ω

$$\lambda\left(l,\omega\right) = \omega^2 + \frac{l\left(l+1\right)}{2R^2}, \tag{A.3.7}$$

furthermore each eigenvalue has multiplicity, n_l, given by

$$n_l = \left(2l+1\right). \tag{A.3.8}$$

Our goal is to evaluate $\zeta\left(s\right)$ for an arbitrary s and regularize it for $s = 0$. For a finite time interval, $-\frac{T}{2} < t < \frac{T}{2}$, ζ can be written as [4]

$$\zeta\left(s\right) = T\int_{-\infty}^{+\infty}\frac{d\omega}{2\pi}\sum_{l=1}^{+\infty}\left(2l+1\right)\left(\omega^2 + \frac{1}{2}\frac{l\left(l+1\right)}{R^2}\right)^{-s}. \tag{A.3.9}$$

Following the method presented in [35, 63], the integral in ω can be solved directly in Mathematica and yields

[4] At the end we are interested in the limit where $T \to +\infty$ and therefore we are allowed to use $-\infty$ and $+\infty$ in the limits of integration.

$$\zeta(s) = T\left(R^2\right)^{s-\frac{1}{2}} \frac{2^{s-\frac{1}{2}}\Gamma\left(s-\frac{1}{2}\right)}{2\sqrt{\pi}\Gamma(s)} \sum_{l=1}^{+\infty} \left\{(2l+1)\left(l\left(l+1\right)\right)^{\frac{1}{2}-s}\right\}$$
$$\equiv \frac{F(s)}{\Gamma(s)}. \tag{A.3.10}$$

Recall that the goal is to evaluate the derivative of the $\zeta(s)$,

$$\frac{d}{ds}\zeta(s) = \frac{1}{\Gamma(s)}\frac{dF(s)}{ds} + \frac{d\Gamma(s)}{ds}F(s), \tag{A.3.11}$$

assuming $F(s)$ is already regular at $s=0$, we will verify that this is true later on, and using the fact that

$$\left.\frac{1}{\Gamma(s)}\right|_{s=0} = 0 \text{ and } \frac{d}{ds}\left(\frac{1}{\Gamma(s)}\right)_{s=0} = 1, \tag{A.3.12}$$

one can simplify the task of computing ζ to evaluating

$$\Delta E(s) = \frac{1}{2}T\left(R^2\right)^s \frac{2^s\Gamma(s)}{2\sqrt{\pi}} \sum_{l=1}^{+\infty} \frac{2l+1}{\left(l\left(l+1\right)\right)^s}, \tag{A.3.13}$$

when $s=-\frac{1}{2}$. The non-trivial part of $\Delta E(s)$ corresponds to the sum

$$\Sigma(s) = \sum_{l=1}^{+\infty} \frac{2l+1}{\left(l\left(l+1\right)\right)^s}. \tag{A.3.14}$$

For starters, let us introduce a function $f(s;a,b,c)$ defined as

$$f(s;a,b,c) \equiv \sum_{l=1}^{+\infty} l^{-s+b}\left(l+a\right)^{-s+c}. \tag{A.3.15}$$

One can verify that $\Sigma(s)$ can be written as a sum of two f fuctions,

$$\Sigma(s) = f(s;1,0,1) + f(s;1,1,0). \tag{A.3.16}$$

Through the rest of the derivation we will assume that a is an integer. The next step we divide $f(s;a,b,c)$ into two sums

$$f(s;a,b,c) = \sum_{l=1}^{a} l^{-2s+b+c}\left(1+\frac{a}{l}\right)^{-s+c} + \sum_{l=a+1}^{\infty} l^{-2s+b+c}\left(1+\frac{a}{l}\right)^{-s+c} \tag{A.3.17}$$

and apply the binomial expansion to the second term

$$f(s;a,b,c) = \sum_{l=1}^{a} l^{-2s+b+c}\left(1+\frac{a}{l}\right)^{-s+c} + \sum_{l=a+1}^{\infty} l^{-2s+b+c}\sum_{k=0}^{-s+c}\frac{\Gamma(1-s+c)}{k!\Gamma(1-s-k+c)}\left(\frac{a^k}{l^k}\right). \tag{A.3.18}$$

In Fig. A.3.1, we plot $\frac{\Gamma(1-s+c)}{k!\Gamma(1-s-k+c)}\left(\frac{a^k}{l^k}\right)$ as a function of k, notice that for k greater than $c-s$, $\frac{\Gamma(1-s+c)}{k!\Gamma(1-s-k+c)}\left(\frac{a^k}{l^k}\right)$ is zero. Allowing us to extend the sum in k to $+\infty$. Furthermore, we will substitute $\sum_{l=a+1}^{\infty}$ by $\sum_{l=1}^{\infty} - \sum_{l=1}^{a}$. Having done all the above mention, we get that f can be expressed as

$$f(s;a,b,c)=\sum_{l=1}^{a} l^{-2s+b+c}\left(1+\frac{a}{l}\right)^{-s+c}+ \\ +\sum_{k=0}^{\infty}\left(\zeta_R(-2s+b+c-k)-a^k\sum_{l=1}^{a} l^{-2s+b+c}\frac{\Gamma(1-s+c)}{k!\Gamma(1-s-k+c)}\right), \tag{A.3.19}$$

where $\zeta_R(2s+k-b-c)=\sum_{l=1}^{\infty} l^{-2s+b+c-k}$.

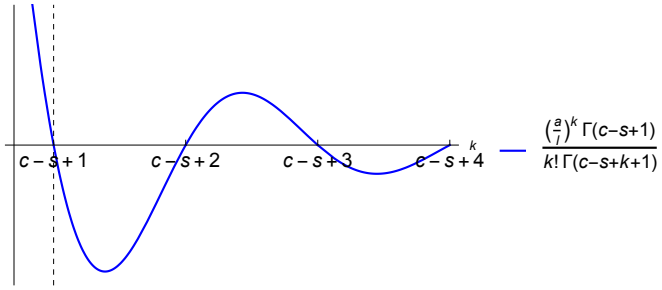

Figure A.3.1: $\frac{\Gamma(1-s+c)}{k!\Gamma(1-s-k+c)}\left(\frac{a^k}{l^k}\right)$ as a function of k for $k>-s+c$

Plugging Eq. A.3.19 into Eq.A.3.16 we get

$$\Sigma(s)=2^{-s+1}+2^{-s}+\sum_{k=0}^{\infty}\left\{\frac{\Gamma(1-s)}{k!\Gamma(1-s-k)}\left[\zeta_R(2s+k-1)-1\right]+\frac{\Gamma(2-s)}{k!\Gamma(2-s-k)}\left[\zeta_R(2s+k-1)-1\right]\right\}. \tag{A.3.20}$$

For $s=-\frac{1}{2}$,

$$\sum\left(-\frac{1}{2}\right)=2^{3/2}+2^{1/2}+\sum_{k=0}^{+\infty}\left\{\frac{\Gamma(3/2)}{k!\Gamma(3/2-k)}\left[\zeta_R(k-2)-1\right]+\frac{\Gamma(5/2)}{k!\Gamma(5/2-k)}\left[\zeta_R(k-2)-1\right]\right\}. \tag{A.3.21}$$

Looking at the above formula we may expect that the expression diverges, since the $\zeta(k-2)$ diverges for $k\to 3$, Fig. A.3.2. Turns out that, when summed, the infinities cancel giving a finite result, see Fig. A.3.3.

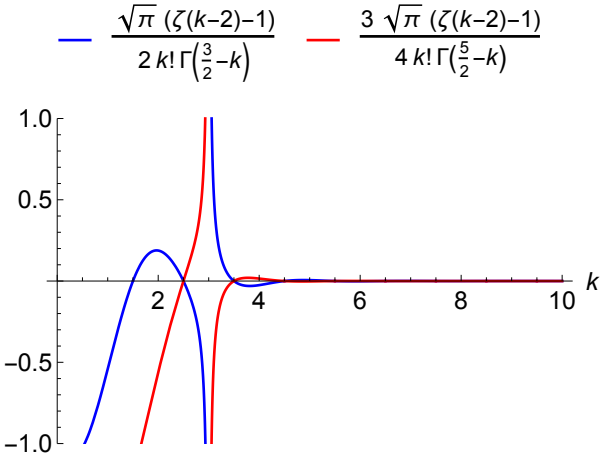

Figure A.3.2: Zeta functions multiplied by their prefactors, Eq. A.3.21, before being sum as a function of k.

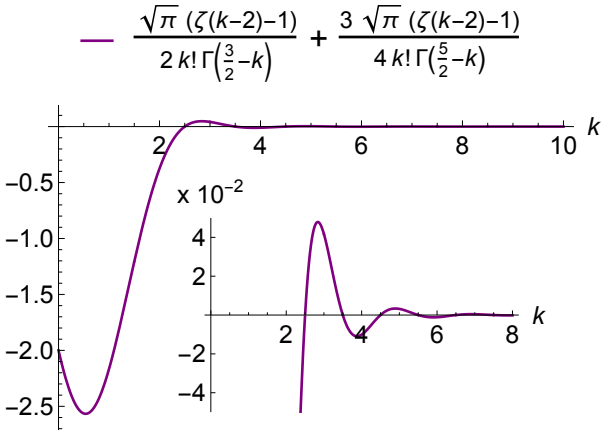

Figure A.3.3: Sum of the zeta function and their prefactor, Eq. A.3.21, as a function of k.

As shown in Fig. A.3.3, the values we are summing over are all finite. Expression A.3.21 is as far as the analytical arguments will take us, however, using Mathematica, we can find that a good numerical approximation would be

$$\sum_{k=0}^{+\infty}\left\{\frac{\Gamma\left(3/2\right)}{k!\Gamma\left(3/2-k\right)}\left[\zeta_R\left(k-2\right)-1\right]+\frac{\Gamma\left(5/2\right)}{k!\Gamma\left(5/2-k\right)}\left[\zeta_R\left(k-2\right)-1\right]\right\}\approx-4.50774 \tag{A.3.22}$$

Plugging all into Eq. A.3.21 and substituting the result into Eq. A.3.13 one arrives at the quantum corrections to the vacuum correction given by

$$\Delta E=-0.0937254\frac{T}{R}. \tag{A.3.23}$$

Appendix B

Numerical Data

B.1 Numerical Data for $\Delta_Q - \Delta_{Q-1}$ and Δ_Q

$U(1)$ Charge - Q	$\Delta_Q - \Delta_{Q-1}$	Δ_Q
1	0.5201 (9)	0.5201 (9)
2	0.716 (1)	1.236 (1)
3	0.874 (2)	2.111 (2)
4	1.009 (4)	3.120 (4)
5	1.130 (5)	4.250 (6)
6	1.234 (6)	5.484 (9)
7	1.34 (1)	6.82 (1)
8	1.43 (1)	8.28 (2)
9	1.53 (1)	9.80 (2)
10	1.60 (2)	11.39 (3)
11	1.68 (2)	13.07 (4)
12	1.76 (4)	14.82 (6)
13	1.84 (6)	16.7 (1)
14	1.94 (6)	18.6 (2)
15	2.03 (16)	20.6 (3)
16	2.02(9)	22.6 (3)
17	2.10(24)	24.6 (6)
18	2.08(22)	26.8 (9)
19	2.2 (1)	29 (1)

Table B.1.1: Numerical data for the difference in conformal dimensions, $\Delta_Q - \Delta_{Q-1}$, and for the conformal dimensions Δ_Q.